SPARK PLUG BASED DIAGNOSTICS FOR FUEL-AIR RATIO DETERMINATION

by

Yongping Han

A thesis submitted in conformity with the requirements for the
degree of Master of Applied Science
Graduate Department of Mechanical & Industrial Engineering
University of Toronto

National Library of Canada
Acquisitions and Bibliographic Services
395 Wellington Street
Ottawa ON K1A 0N4
Canada

Bibliothèque nationale du Canada
Acquisitions et services bibliographiques
395, rue Wellington
Ottawa ON K1A 0N4
Canada

Your file Votre référence

Our file Notre référence

0-612-33969-6

Canada

ABSTRACT

Experiments were performed in a simulated combustion chamber with non-combustible and combustible mixtures to study the feasibility of spark plug based diagnostics for fuel-air ratio determination in the spark plug gap of a Spark Ignition (SI) engine at ignition. During the experiments, the breakdown voltage (V_s) as well as the spark light emission were measured to correlate to the characteristics of the gas mixture. A simulated combustion chamber was used rather than an actual engine to obtain better control of mixture composition and other experimental parameters.

The dependence of V_s on the pressure, the temperature, the gas composition and the gap size was tested in non-combustible mixtures by measuring the true values of V_s and the agreement between the experimental results and Paschen's Law was studied. In addition, the correlation between V_s and the fuel-air equivalence ratio (ϕ), as well as the residual gas fraction (RGF) was tested in combustible mixtures.

In the measurements of spark light intensities, relative intensity (the spectral intensity of a particular molecule normalized by the shot or broadband intensity) was studied to reduce the effect of the variations of orientation of the spark initiation. The relative intensity of the CN radical, centered at 385 nm, was tested to have the strongest intensity 5 μs after the spark ignition compared to those of the other radicals, such as CH and NH. It has also been found that the relative intensity of CN has great dependence on ϕ as well as RGF.

The study of this spark plug based diagnostics provides a feasible method for determination of mixture composition in the spark plug gap at ignition.

ACKNOWLEDGMENTS

I would like to express my most sincere appreciation to Professor J. S. Wallace for his invaluable guidance and support, encouragement and patience throughout this project. Thanks to Professor M. Lowen for his generosity in allowing me to use his laboratory equipment. My special thanks are given to Hannu Jääskeläinen and Paul Salanki for their help in the completion of my experiments. Finally, I would like to thank all of my colleagues in the ERDL for their advise, support, and most of all, their friendship.

Table of Contents

List of Tables

List of Figures

Chapter 2

Chapter 3

Chapter 5

Chapter 6

Appendices

List of Appendices

Nomenclature

θ	crank angle
μ	current amplification of a PMT
ϕ	fuel-air equivalence ratio
δ	gain factor of the dual-channel amplifier (constant), V/A
κ	gas compressibility
α	number of ionizing collisions per cm of path in the direction of the field
γ	probability of electron emission per ion striking the cathode
χ	transmittance factor of the neutral density filter (constant)
λ	wavelength
$\alpha(\lambda)$	transmittance of the monochromator, a function of λ
$\beta(\lambda)$	response of the photomultiplier, a function of λ
$\lambda_{\theta i}$	center wavelength of a narrow bandpass filter at θ_i° angle of incidence
λ_0	center wavelength of a narrow bandpass filter at 0° angle of incidence
θ_i	angle of incidence light from normal
γ_s	specific heat (1.32)
$[CH_4]$	concentration of CH_4 by volume
$[CO_2]$	concentration of CO_2 by volume
9% CO_2	a gas mixture of 9% CO_2 and 91% N_2 by volume
a	crank radius (L/2)
A/F	air-fuel ratio
BC	bottom center
BTDC	before top dead center

B_x	a constant for gas x in the Paschen's Law
$C_{\%}$	concentration in percent by volume
CCD	charge coupled device
CFR	co-oporative fuel research
CH_4	methane
CN	cyanogen radical
CP	constant pressure
CRT	cathode ray tube
d	gap size of a spark plug
E	electric field strength
EGR	exhaust gas recirculation
EX	exhaust valve
FFID	fast flame ionization detector
FID	flame ionization detector
HC	hydrocarbon
$I(\lambda)$	spark light intensity, a function of the wavelength λ
i_a	electron current collected by the anode
i_c	electron current emitted by the cathode
ID	inner diameter
IN	intake valve
K	a constant for a specified PMT for the calculation of current amplification
k	view factor of the optical probe to the spark
l	connecting rod length
L	stroke
l/a	the ratio of the connecting rod length to crank radius

m.f.p.	mean free path
n	gas number density
n_θ	effective index, specified as a numerical value derived for the indices of the thin film layers of the bandpass filter
N_0	Avogadro's number (6.024×10^{23} molecules/mole)
NG	natural gas
OD	outer diameter
OLLRC	Ontario laser and lightwave research center
PMT	photomultiplier
P_n	contributing partial pressure
R	universal constant (8.314 J/mol.K)
r_c	compression ratio
rfi	radio-frequency interference
RG	residual gas
RGF	residual gas fraction
rpm	revolution per minute
SI	spark ignition
TC	top center
UV	ultraviolet
V	supplied voltage between the cathode and the anode for a PMT
V_c	clearance volume
V_d	displacement volume
VIS	visible
V_{ix}	effective ionization potential for electron collisions of gas x
V_s	experimental breakdown voltage

$V_s^{\cdot}$	predicted breakdown voltage
$V_{s\ 150\ psig}^{\cdot}$	predicted breakdown voltage at 150 psig
$V_{s\ 180\ psig}^{\cdot}$	predicted breakdown voltage at 180 psig
V_{shot}	shot or total intensity of spark light emission
V_{spec}	spectral light intensity of spark light emission

CHAPTER 1 INTRODUCTION

1.1 Introduction

Spark ignition (SI) engines experience cyclic variations which result in poor drivability that also precludes the optimization of fuel efficiency and emission control. During the last 40 to 45 years, a great deal of research has been done with the aim of elucidating the mechanism causing cyclic variability. It has been suggested that if the cyclic variability could have been eliminated, there would be a 10% increase in the power output for the same fuel consumption for weak mixtures [Soltau, 1960]. Today, in order to address various environmental issues and promote energy conservation, there are still strong demands to study the cyclic variability of SI engines.

The cyclic variations of SI engines are the result of variations in the combustion process. The combustion process in an SI engine consists of the spark discharge, inflammation, initial flame development, and propagation of the flame in the combustion chamber [Heywood, 1988]. It is generally accepted that, the cyclic variation in the combustion process is caused by variations in the mixture motion, in the amounts of air and fuel fed into the cylinder and their mixing, and in mixing with residual gas (RG) and exhaust gas recirculation (EGR), especially in the vicinity of the spark plug. Clearly, the mixture formation is one of the most important factors causing the cyclic variations. Hence, it is of great interest to study the air-fuel ratio in-cylinder, especially in the vicinity of the spark plug gap in order to understand the cyclic variability.

Due to the difficulties of in-situ time and space resolved measurement of the air-fuel ratio, the understanding of the physical process of fuel and air mixing, and its

distribution in the combustion chamber is still not very clear. During the past few decades, many studies have been done in different ways to determine air-fuel ratio in order to study the cyclic variability. With the help of laser-based diagnostics, it is possible to probe into the combustion chamber without perturbation to the flow and remotely detect the physical properties of the system under investigation with high spatial and temporal resolution by using spectroscopic methods. Laser-assisted Raman spectroscopy has been applied to investigate the process of the fuel-air mixing and the distribution in a motored Direct Injection Stratified Charge engine [Johnston, 1979]. As well, laser Rayleigh scattering measurement has been used to determine time and space resolved fuel/air concentration in a propane and air mixture [Dyer, 1979]. However, these laser assisted techniques need modification of the combustion chamber to provide optical windows for the access of the excitation light source. Since any modification of the combustion chamber will cause the combustion process to be distorted, it is desirable to keep the combustion chamber as close to original as possible. Therefore, it is still necessary to develop a more efficient technique for measuring air-fuel ratio which can be applied to the study of production engines under various conditions.

Merer and Wallace [1995] have investigated the use of spark spectroscopy for measuring the mixture compositions in-cylinder. Instead of an auxiliary light source, spark spectroscopy uses the energy delivered to the gas by the electric spark discharge as excitation for the spectroscopic measurements. A modified spark plug with an optical fiber inserted through the center electrode was used to detect the light emission from the spark discharge. The output of the optical fiber was guided to a monochromator for spectral

analysis. To evaluate this method, a series of experiments were carried out, not only in a combustion bomb for non-combustible mixtures, but also in an SIngle-cylinder research engine fueled by natural gas. The spectral light emission centered at 385 nm from CN (cyanogen radical) formed in the spark discharge plasma was observed to correlate with the fuel-air equivalence ratio in the spark gap for well-scavenged cycles (without residual gas). However, when the engine was fired every cycle, the presence of residual gas weakened the correlation.

On the basis of this previous research, additional work has been designed to characterize the effect of residual gas on the light emissions during the spark discharge. Since the spark discharge is the energy source of the spark light emission, during the spark discharge, the breakdown phase is the most important stage which decides the energy of the spark emission. Also, the breakdown voltage is a widely dependable combustion parameter. Hence, along with the measurements of the light emission, the spark breakdown voltage has been measured to help reduce the effect of the variations of the spark occurrence in order to clarify the correlation between the light emission and the air-fuel ratio when residual gas is present.

1.2 Objective

The objective of the present work is to use the spark plug based diagnostics (both the breakdown voltage and the spark light emission were tested) in determining the mixture composition in the spark plug gap before ignition. In order to better control the mixture composition in-cylinder before combustion, the present work has been carried out in a well

simulated combustion bomb under various conditions, e.g. non-combustible, combustible, lean and rich mixtures, with simulated EGR and with simulated RG in addition to EGR. Through the investigation of the spectral light emission centered at 385 nm from the CN radical, as well as the measurements of the spark breakdown voltage under the different conditions, the effect of the residual gas in-cylinder each cycle on light emission can be characterized more clearly. In addition, the light emission and breakdown voltage can be correlated with the mixture composition more accurately even under actual combustion conditions with residual gas. Finally, the spark plug based diagnostics was evaluated for the use of measuring the air-fuel ratio in the vicinity of the spark plug gap in-cylinder.

CHAPTER 2 LITERATURE REVIEW

2.1 Spark Evolution

In a Spark Ignition (SI) engine, the combustion process is a very important and complicated process. However, it can be divided into four stages — spark discharge, inflammation, flame propagation, and flame termination. All these stages have significant characteristics and play different roles in supporting the combustion process in an SI engine. Among those four stages, the first one — spark discharge — is a relatively dominant stage because it determines the initiation of the combustion process. Hence, further study of spark discharge will help understand the whole combustion process more comprehensively. During the past decades, many researches have been carried out in this area. Hereafter is a review of the relevant studies which will help elucidate the foundation of the present work.

Basically, the evolution of a spark discharge can be characterized into four phases — pre-breakdown, breakdown, arc, and glow discharge according to the significant variations of the voltage and current [Maly, 1984]. Figure 2-1 gives a detailed schematic of spark evolution which shows the voltage and current variations with time for a conventional coil SI system.

2.1.1 Pre-Breakdown

Basically, the pre-breakdown phase is an electron-accumulating process which happens after the spark pulse is applied and usually lasts for a few nanoseconds. It starts

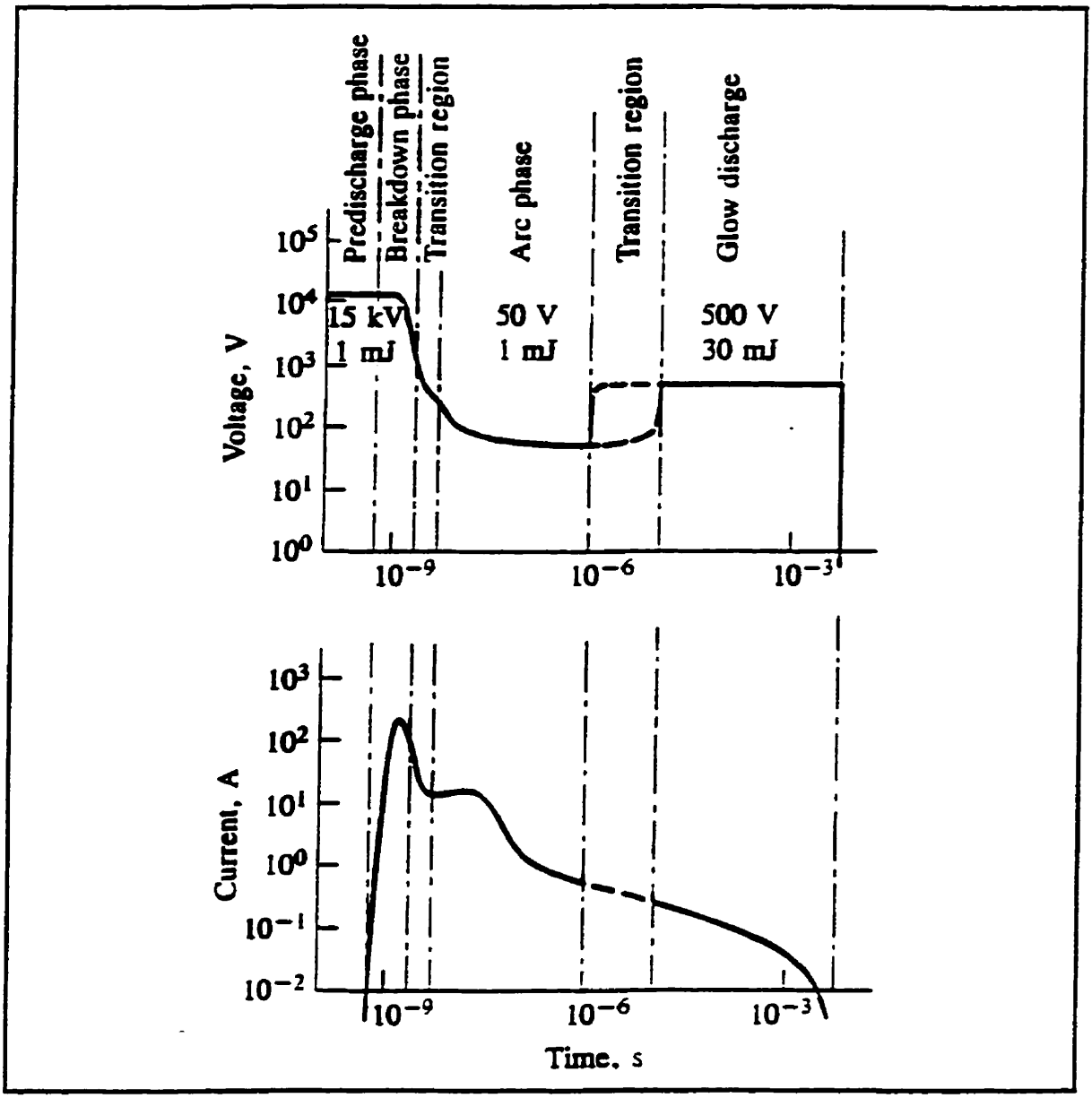

Fig. 2-1 Variations of Voltage and Current with Time for a Conventional Coil SI System [Maly, 1976]

from a small electron current, continues with more and more electrons and ions (generated by collisions between the accelerated electrons and the gas molecules) adding into the current flux. As the voltage supplied to electrodes of the spark plug increases to a very high level (50-100kv/cm), the number of electrons and ions increases rapidly like in

an avalanche which results in a sharp increase of the electron flow. The pre-breakdown phase ends before the current rises to levels greater than 10mA. During this phase, the gas temperature is still close to its initial value and the mean electron density is less than 10^{15} e/cm^3, while in the individual ionizing channels (streamers) the density may reach up to 10^{18} e/cm^3.

2.1.2 Breakdown

As soon as enough electrons are produced by the collisions between the moving electrons and the gas molecules or by the UV radiation from the excited ions, the current rises exponentially up to hundreds or thousands of amperes within nanoseconds, and is effectively assisted by a self-created charge within the electron channel. The current increase will be limited by the impedance of the discharge and the external circuit close to the gap (i.e., the spark plug). The significant feature of this phase is the peak voltage of the center electrode (rises up to 50kV) which lasts for less than 10 nanoseconds (Fig. 2-2). At the moment of breakdown, the electric current rises rapidly to approximate 100A. The minimum energy required to initiate a complete breakdown at 1 bar and 1.0mm gap is 0.3mJ.

During the breakdown phase, the temperature of the plasma increases up to 60,000K and the electron density is as high as 10^{19} e/cm^3.

The breakdown phase ends at the point when the ignition voltage has dropped below 10% of its initial value or at the point from which a hot cathode spot exists and turns the discharge into an arc.

The breakdown phase has a high efficiency (around 90%) in transferring energy from the electrical system to the medium. Although this phase accounts for only 10% of the total energy delivered by the electrical system, this energy is very effective because it is mainly stored in the plasma as potential energy (dissociation, excitation, and multiple ionization) and feeds the expanding spark channel at later times [Albrecht, et al., 1977].

2.1.3 Arc Phase

Following the breakdown phase is the arc phase with a hot cathode which results from the high current of the breakdown phase, causing severe erosion of the electrode surface. For the arc phase, the voltage is relatively low and the electric current is greater than 100mA.

The arc phase lasts for a few microseconds. During this period, the stationary value of the electron density is 10^{17} e/cm^3, and the center temperature of the electrons decreases to 5000 - 6000 K.

During this phase, the prolonged and intense contact of the arc plasma with the electrodes leads to serious heat losses via conduction. At the same time, radiation losses also occur from the plasma surfaces. The energy transfer efficiency of the arc phase is around 50% [Maly, 1984].

2.1.4 Glow Discharge

The glow discharge is known as an inductive phase of the spark which lasts for up to several milliseconds. It starts from the beginning of the small increase of voltage shown in Fig. 2-1. The current during this phase is lower than 50mA.

The steady-state value of the electron density is $10^{14}e/cm^3$ and the temperature of the kernel is 3,000K. Although the glow discharge phase has an energy transfer efficiency as low as 30%, it can release most of its energy because of its long duration.

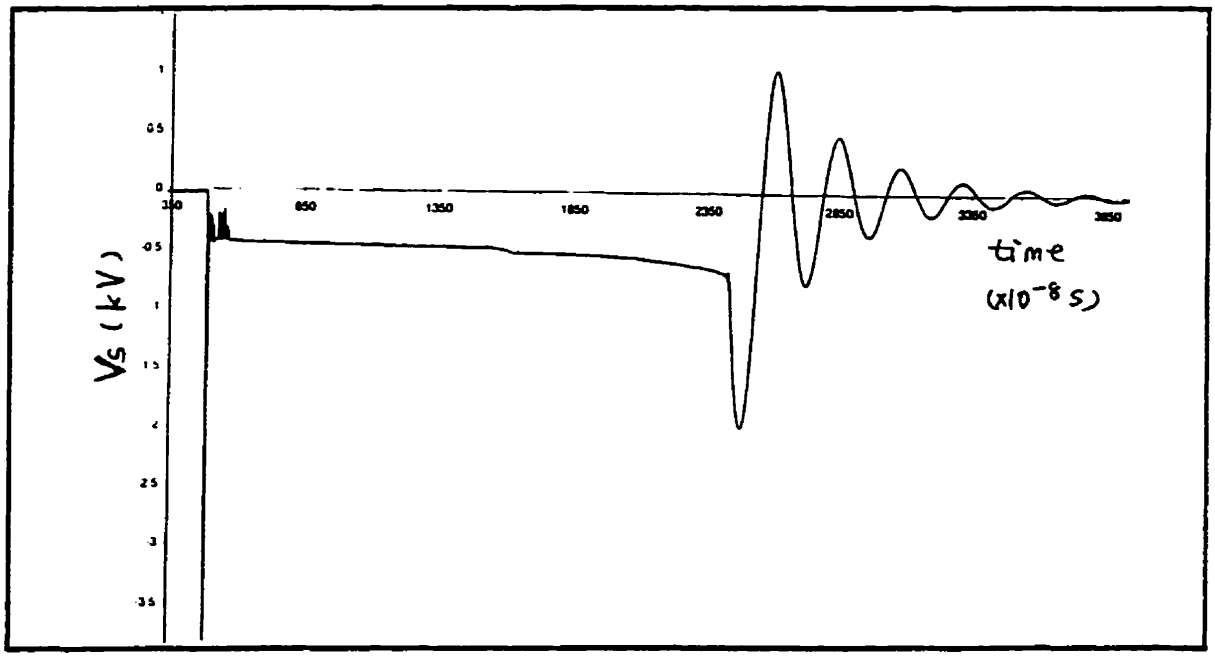

Fig. 2-2 Typical Breakdown Voltage Signal Captured in the Non-Combustible Mixtures Tests

2.2 Breakdown Voltage

Overall, among the spark evolution, the second phase — breakdown — is of the most interest because it has a high efficiency (approximate 90%) in transferring energy from the electrical system to the medium, accounting for 10% of the total energy of the spark transfered from the electrical system. Hence, it is necessary to get further understanding of the breakdown phase as well as its effects on the other engine parameters. In part of present work, the focus is on the peak breakdown voltage (in non-

combustible mixtures) which has a very high value (up to 30kV) and a very short duration (less than10ns).

The breakdown phase has been studied for many years. Most of the work has been summarized by Meek and Craggs [1976]. It is quite commonly accepted that the breakdown voltage depends on many other parameters in the combustion process, such as the pressure, the temperature, the gas composition, the gap size, the gap orientation, and the electrode material. The most important principle of breakdown voltage is Paschen's Law which gives the correlation between the breakdown voltage and gas number density, as well as the spark plug gap size within limited ranges (limited temperature and pressure, especially limited pressure). Paschen's Law can be written as follows:

$$\mathbf{V_s} = f(\mathbf{nd})_s$$

where $\mathbf{V_s}$ is the breakdown voltage (in kV), **n** is the number density of the gas, **d** is the gap size, and f represents some function of $(nd)_s$ which is the value of nd at which a spark occurs. From Paschen's Law, it can be seen clearly that the breakdown voltage is essentially proportional to the number of molecules per unit electrode face area between the electrodes of the spark plug.

Since the breakdown voltage is an important parameter which correlates with the mixture concentration, pressure, temperature, and other combustion parameters, in order to better understand the combustion process in an SI engine, it is necessary to further study the spark discharge phase by measuring the breakdown voltage. It has been known that the breakdown happens within 10 ns with a very high breakdown voltage value. Therefore, a very high temporal resolution high voltage probe and a recording system

with a high sampling rate are required as to capture the breakdown voltage pulse accurately.

Since the breakdown voltage has a strong correlation with the other combustion parameters, it has always been measured along with other parameters to help further understand the combustion process. Recently, some researches have been carried out in the measurements of breakdown voltage. Klimstra and Overmars [1991] used a Tektronix P6015 high voltage probe and digital Nicolet 450 oscilloscope to measure the spark voltage to help measure the on-line gap sizes of spark plugs. The result was used for condition monitoring for maintenance purposes, indicating that a necessary replacement of the spark plug will be near. In addition, Shimasaki et al. [1993] applied spark voltage sensors which were installed (non-contact) on the high voltage zone, in the vicinity of the spark plugs to measure the spark plug voltage and used spark plug voltage analysis for monitoring the combustion process in an internal combustion engine. Also, Verhoeven [1995] studied the spark heat transfer in flowing gases. In his experiments, the same Tektronic P6015 high voltage probe was used to measure the breakdown voltage which helps to study the efficiency of the heat transfer.

In the present work, the breakdown voltage was studied to correlate with the fuel-air ratio in-cylinder as well as with the fraction of residual gas. Since high accuracy of the breakdown voltage measurements under various engine conditions is desirable, both the same high resolution Tektronix P6015 high voltage probe and a Hewlett Packard high resolution 54503A digitizing oscilloscope have been used in the present work. Later on, a

higher temporal resolution Hewlett Packard 500 MHz 54615B oscilloscope was purchased for the tests.

2.3 Cycle-to-Cycle Variations in SI Engines

Spark ignition engines experience cyclic variations which results in poor driveability that also precludes the optimization of fuel efficiency and emission control. Cyclic variability has been studied for 40 to 45 years. It has been suggested that if cyclic variability could have been eliminated, there would be a 10% increase in the power output for the same fuel consumption.

It is well known that the cycle-by-cycle variations are the result of variations in the combustion process. The early flame development time (0~2% mass burned duration) is an SIgnificant fraction (~30%) of the total burn duration [Young, 1981]. Hence, the early flame development period is an important contributor to the cycle-by-cycle variations in the engine performance. The work done by Gatowski, Heywood and Deleplace [1984] for two different cycles in the same cylinder gives an evidence that the variations at the start of combustion result from randomness of cylinder turbulence and cycle-to-cycle inconsistencies in swirl, squish, and tumble, hence, causing totally different combustion processes for the two cycles. The variations of the start of combustion were observed in Schlieren photographs which are shown in Fig. 2-3.

The early flame kernel development has lots of dependencies, but mainly can be characterized into two steps. Firstly, the formation of the flame kernel depends on: the local fuel-air ratio, the mixture motion, and the amount of exhaust gas residual in the spark plug gap **at the time of ignition**. Secondly, the development of the flame kernel

depends on: the local fuel-air ratio, the mixture motion, and the amount of exhaust gas residuals in the vicinity of the spark plug **immediately after ignition**. Obviously, the spark ignition stage plays a very significant role in the combustion process. Hence, it is very important to the further study of cyclic variations in SI engines.

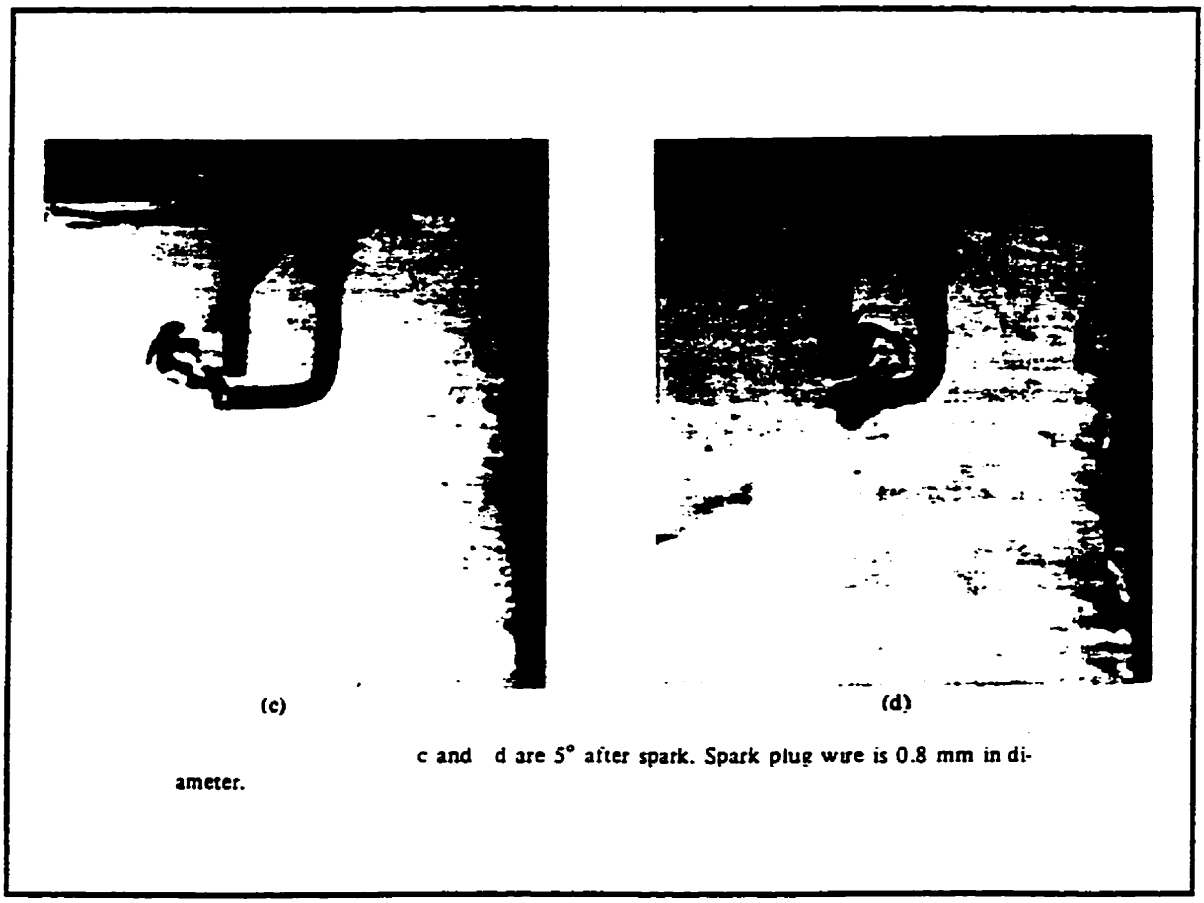

Fig. 2-3 Schlieren Photographs of the Start of Combustion for Two Different Cycles in the Same Test Engine Cylinder, Showing the Variations at the Start of Combustion between the Two Cycles [Deleplace, C. 1984]

2.4 Cyclic Variability Measurements

In order to improve engines efficiency, as well as to control the pollution, it is necessary to better understand the cyclic variability. It is clear that, in SI engines, the air-fuel ratio in-cylinder, especially in the vicinity of the spark plug, is of great interest

because it is an important factor which affects the cyclic variation of the combustion process.

Hydrocarbon concentration and residual gas fraction in-cylinder are two key factors in the measurement of the fuel-air ratio. To get the information of the fuel-air ratio, these two factors needed to be measured simultaneously. During the past few decades, a large amount of research has been done to investigate these parameters in order to study the cyclic variability. In general, most of the research can be characterized into two groups: One is the FFID group, which uses a probe sampling method, and the other one is the spectroscopy group which analyzes the detected spectrum of light emission from the different stages of the combustion process.

2.4.1 Sampling — Fast-response Flame Ionization Detector

The Fast-response Flame Ionization Detector (FFID) has been widely used for several years to investigate hydrocarbon emissions from internal combustion engines. The FFID device is shown schematically in Fig. 2-4. In a common application the exhaust gas is sampled from the exhaust system relatively close to the exhaust valve over a cycle. Different from the conventional Flame Ionization Detector (FID), FFID allows the concentration of hydrocarbons to be resolved within the engine cycle. As well, this FFID device has been used to sample gases from within the combustion chamber.

Many researchers have used the FFID for exhaust port work but fewer have attempted to sample directly from the cylinder. Sleighthholme [1990] applied an early version of the FFID to study charge inhomogeneity by sampling from within the combustion chamber via the auxiliary spark plug port of a single cylinder engine. With

the slow transit time of the entire sampling system, the study was not very precise. Later, with some success, Peckham and Collings [1992] used the software supplied with the FFID to estimate the transit time of in-cylinder sampling. Some other related work has been summarized by Summers and Collings [1995].

Besides the hydrocarbon concentration, the FFID method is also applied to measure the residual gas fraction in-cylinder. Galliot et al. [1990] measured the hydrocarbon concentrations at the vicinity of the spark plug of an SIngle cylinder, two-valve spark ignition engine using propane fuel premixed with air under two different conditions — motoring and firing. The use of the premixed gaseous fuel separated the issues associated with the evaporative process of a liquid fuel so that there is an unambiguous interpretation of the signal. From the difference of the measured hydrocarbon concentration between motoring and firing conditions, the residual gas (or burned gas) fraction just before flame arrival can be obtained.

Since the residual gas always exists in the engine cylinder each cycle from the previous engine cycle in addition to the fuel and air mixture, the hydrocarbon concentration and the fuel-air ratio are two separate pieces of information. Although FFID measures HC volume fraction, not fuel-air ratio, its results can be indicative of the fuel-air ratio behavior by calibration. Recently, Crawford and Wallace [1996] sampled the mixture in-cylinder in two opposite sampling positions — NEAR (the spark plug) and FAR (from the spark plug) in a CFR engine under comparatively more representative conditions of a production engine. The tests showed good agreement between the HC volume fractions determined at the near sampling location, and the "true" value at the far

location. Therefore, this experiment quantifies the cyclic variations of in-cylinder composition in the vicinity of the spark gap. In addition, the fuel-air ratio behavior is indicated through the actual measurements of the fuel concentration in-cylinder.

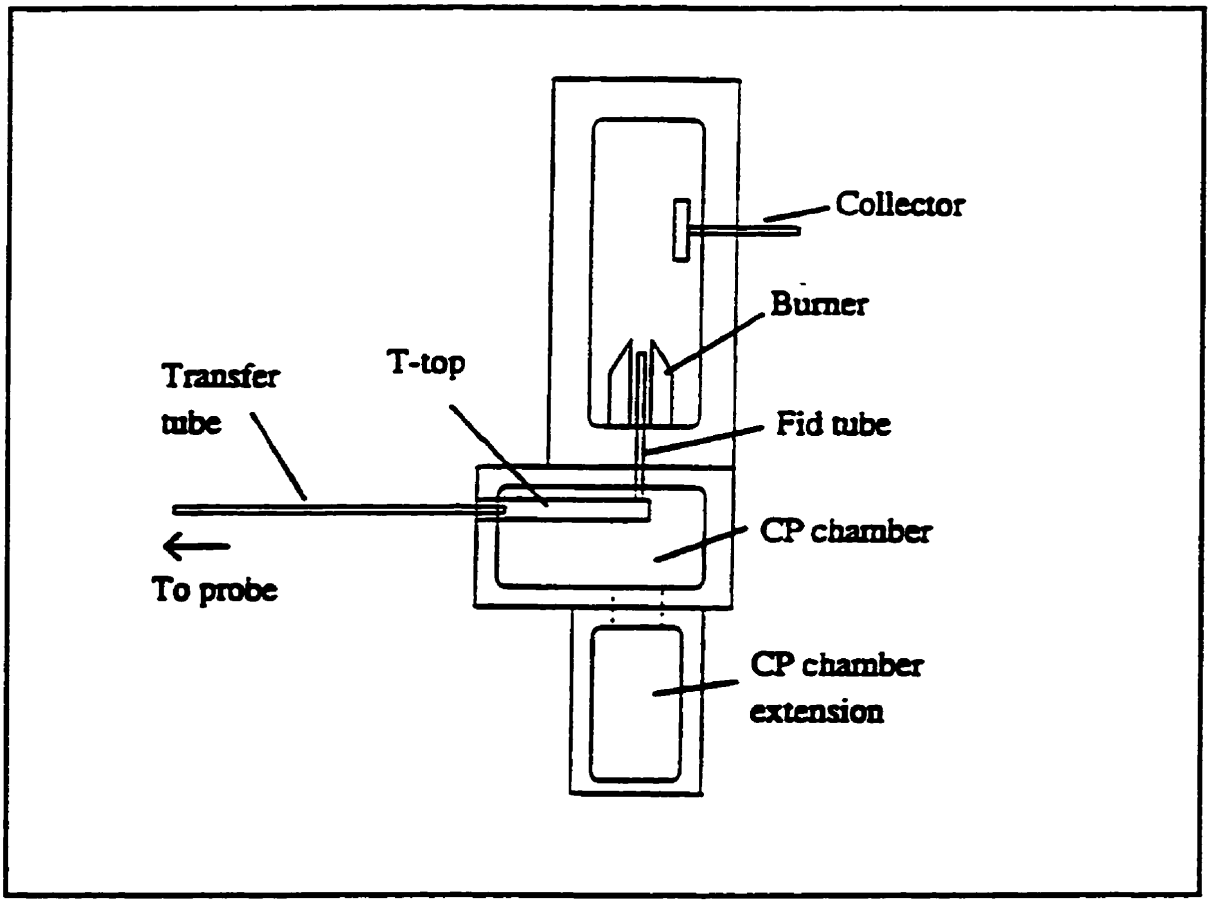

Fig. 2-4 Schematic of Fast-Response Flame Ionization Detector [Cambustion Catalogue]

Overall, the FFID method has been proved to be a valid technique in testing either hydrocarbon concentration or residual gas fraction under some condition. As well, it can be used to investigate the fuel-air ratio behavior. However, it is necessary to achieve good calibration for the indication.

2.4.2 Spectroscopy

Besides the FFID sampling method. the spectroscopy technique has been developed and widely applied in the study of the cyclic variability in an SI engine.

Basically, molecules can be excited by a variety of processes, and in returning to their normal states they will emit radiation. During the combustion process, because of the collisions between particles with high energy (the energy provided by combustion, or as a result of electronic excitation), the molecules can be excited easily. Hence, the spectroscopy of the light emission from the different stages of the combustion process can be recorded as to characterize the information of the combustion.

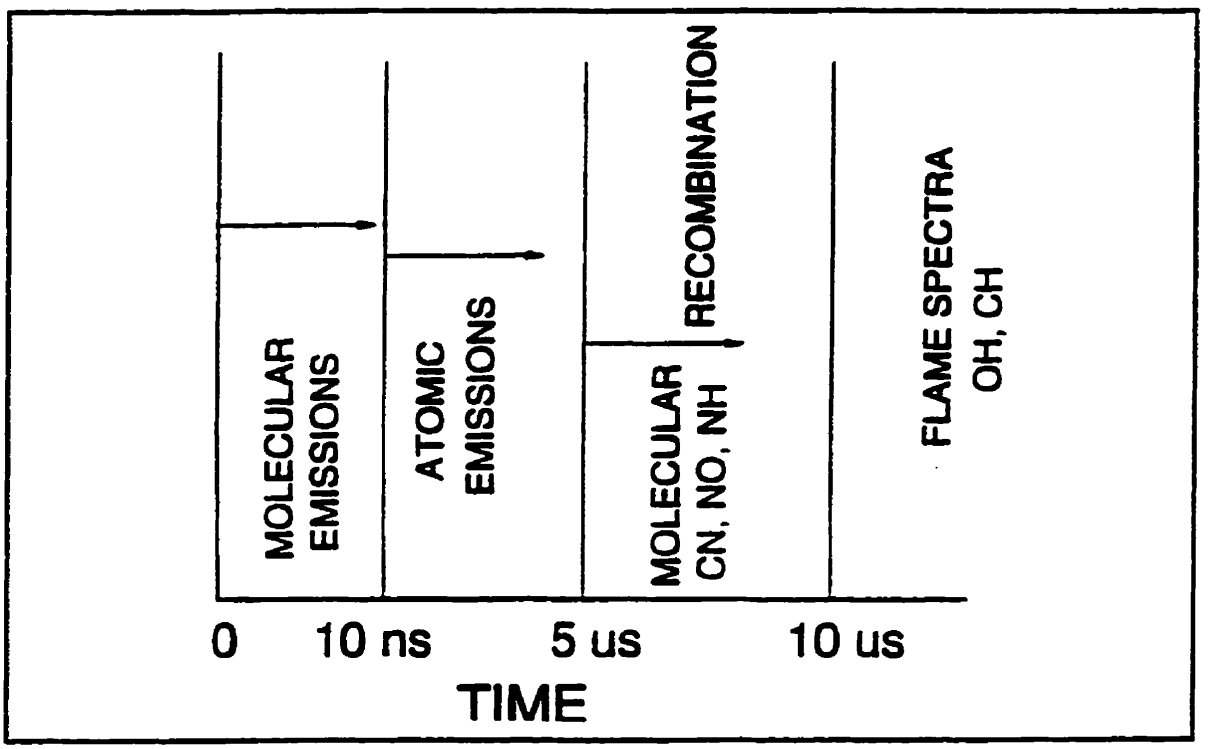

Fig. 2-5 Evolution of Spark Light Emission

In spark ignition engines, spark discharge is the initiation of the combustion. The spark discharge causes the complete dissociation of the gas molecules in its path. The dissociation induces the self-sustained chemical reactions and results in successful

combustion. This process can be divided into several stages and each stage has significant light emission characteristics. Figure 2-5 presents the evolution of spark light emission.

Theoretically, it is possible to apply the spectroscopic method to test the spectrum of the atomic light emission in the period of 10 ns to 5 μs after initiation of spark discharge. Hence, the concentration of the gas compositions can be interpreted through the analysis of the spectrum. Because of the requirements of a very high temporal resolution equipment, the difficulties of the optical access to the limited combustion chamber, and the influence of the strong molecular light emission 5 μs after initiation of spark discharge, the theoretical method has not been validated. However, a number of research projects have been performed in this area.

2.4.2.1 History of Spectroscopy

Spectroscopic measurement techniques have been used to study combustion in engines for more than 70 years. During the long history of the development of the spectroscopy techniques, numerous work has been carried out. Some important work has been reviewed by Merer [1994]. The following is a brief review of the related work which will help get an insight to the present work.

In the past, spectroscopic measurement techniques were quite commonly applied to flames [Gaydon, 1974], but were rarely applied to engines because of optical and mechanical problems. Based on the development of optical access to engines and the high temporal resolution data acquisition systems, the spectroscopic measurement techniques have achieved great improvement.

Briefly speaking, most of the previous work with assisted optical sensors has concentrated on luminous intensity relating to pressure, knock, flame growth, temperature and compositions. The earliest investigation was done by Clark and Henne [1927]. In the experiments, the ultra-violet spectroscopy was used to assess detonation and the effect of knock suppressers — octane improvers. The results of ultraviolet spectra show that all substances which act as knock suppressers have precisely the same effect, in that in their presence there is no emission in the far ultraviolet, such as occurs in detonation.

It has been shown that each explosion in an engine consists of a flame front movement through the charge accompanied by the emission of light and that, after the passage of each flame front, the combustion gases continue for some time to radiate light which is called the afterglow. In order to study them separately, Rassweiler and Withrow [1932] developed an optical apparatus, including a stroboscopic disk which rotates at crank shaft speed, resulting in separate spectra of flame fronts and the afterglow. Through those experiments, it was found that CH and C_2 bands decrease if the engine is knocking, and conversely, if the engine is not knocking, the densities of these bands increase. This examination shows the relationship between knock and flame temperature providing the foundation from which modern optical combustion analysis has developed.

In recent years, Nagase et al. [1985] inserted some optical fibers into a combustion chamber to detect the spectroscopic characteristics of the light for several wavelengths from the visible to the neighboring infra-red range through which the spectrum of the flame image was obtained. The results show the relation between the rate of heat release and the spectrum of the flame, as well as the estimation of the combustion

temperature. In addition, Pinnock, Extance and Cockshott [1987] used fiber-optics sensors to detect knock and poor burns in the cylinder of a spark-ignition engine.

From the study of the flame, the emission spectra of the most important gas components in the flame [Gaydon, 1974] is given. Figure 2-6 shows that the range of wavelengths from about 300nm to 600nm is the most important range for detecting the radiation of the gas components which are highly responsible for the combustion. Based on it, Spicher et al. [1988] detected the flame radiation by using a multi-optical fiber measurement technique, including a specially developed non-contacting optical transmission system, to determine the spatial flame propagation. With a high temporal resolution and the non-contacting transmission system, this method could be applied in different engines (both research and production engines) under various conditions. Also in this measurement, instead of the conventional photodiodes, a photomultiplier (PMT) was used because of its good advantage of internal amplification of the signal.

As well, Hancock, Belmont and Buckingham [1988] measured the light emission from the early stages of combustion near the spark plug and described a correlation between the quality of the cycle and the light emission from this region. In the meantime, Witze, Hall and Wallace [1988] installed a series of eight optical-fiber probes in a ring around the spark plug to sense flame speed and direction relative to the spark plug during the early stages of combustion. The measuring system used in this experiment has been widely applied by other researchers. Later, Shoji et al. [1995] used absorption spectroscopy and emission spectroscopy to reveal behavior thought to correspond to the passage of a cool flame and a blue flame respectively to obtain a better understanding of

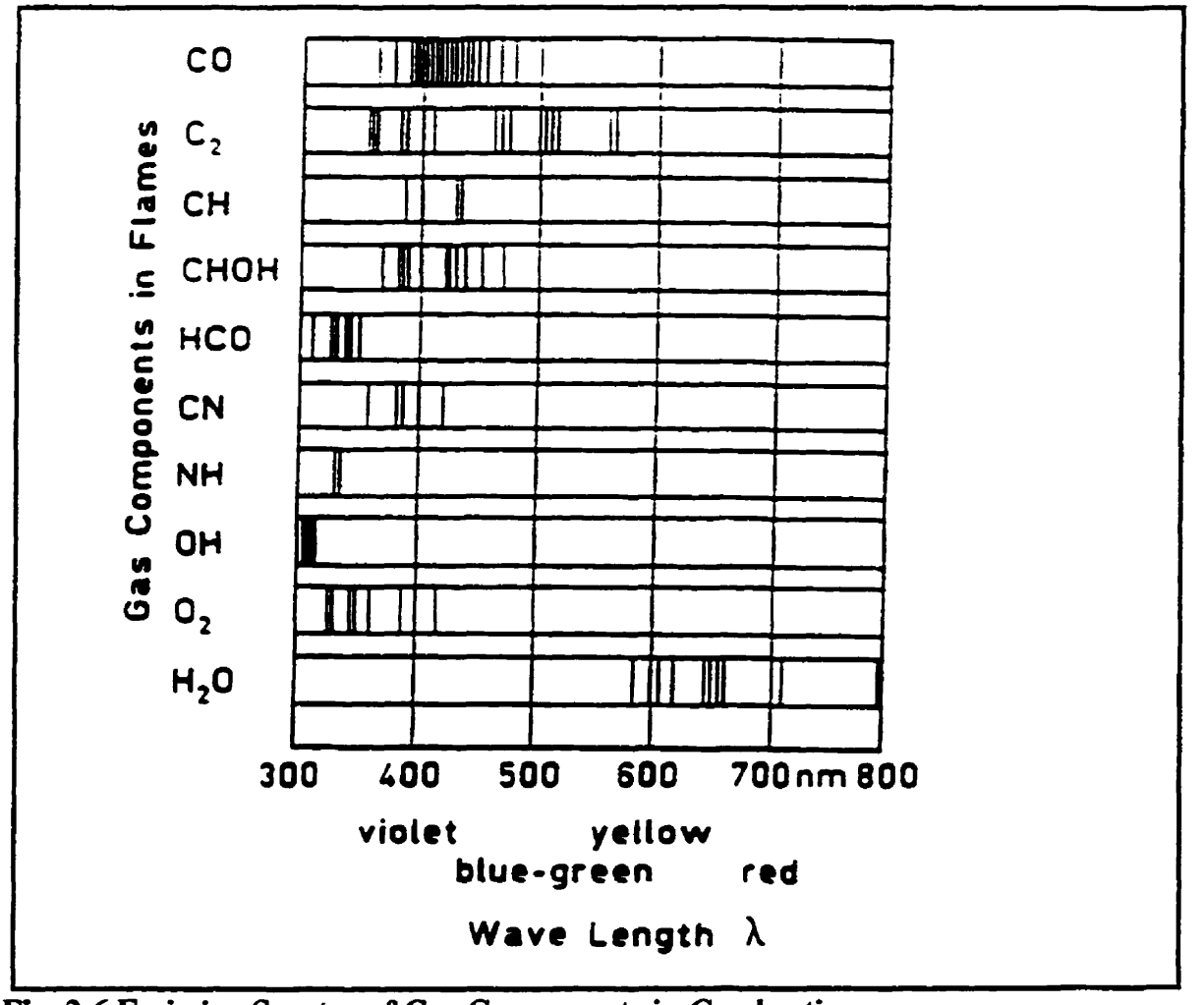

Fig. 2-6 Emission Spectra of Gas Components in Combustion

engine knocking phenomena. Also, Pendlebury and Nwagboso [1996] mounted an optical sensor which consists of a fused silica rod in a cylinder head. The results show the effective detection of the start of combustion and 50% mass burned angles, as well as the correlation to heat release profiles. In addition, Moeser and Hentsche [1996] combined a CCD-camera with a streak-mode operation and optical fibers to record UV/VIS emission spectra from inside the combustion chamber with temporal resolution in the μs range. The appearance of the light emissions of intermediate combustion products, molecule formation processes or particle emissions indicate the different stages of the combustion

process, e.g. the time of ignition, the active combustion phase and the CO-oxidation phase. Hence, the cycle-by-cycle variations can be investigated through the highly resolved spectral and temporal images.

2.4.2.2 Application of Spectroscopy Technique in the Fuel - Air Ratio Measurements

Due to the difficulties of in-situ time and space resolved measurement of the air-fuel ratio, there is only limited understanding of the physical process of fuel and air mixing, and its distribution in the combustion chamber. On the basis of the development of laser-based diagnostics, it is possible to probe into the combustion chamber without any perturbation to the flow and remotely detect the physical properties of the system under investigation with high spatial and temporal resolution. During the last two decades, researchers have started to apply the spectroscopy techniques in the investigation of the fuel-air ratio behavior in spark ignition engines and have achieved improvements. One important method that has been used is the Raman spectroscopy technique. The Raman effect was demonstrated by Raman in 1928. A Raman spectra is observed when visible light is scattered inelastically by molecules in solid, gases or liquids. The Raman range includes the middle-to-far infra-red which is between 2.50 μm to 1000 μm. The Raman spectra of a particular compound depends on the compound itself, no matter what the incident light is. Hence, the Raman spectroscopy can be used to interpret the mixture compositions. In addition, Johnston [1980] applied the laser Raman spectroscopy technique, utilizing a continuous-wave laser, to measure fuel/air ratio as a function of

crank angle at a single spatial location — the spark plug electrode gap. Figure 2-7 presents the configuration of the simplified spark plug and the laser beam used in this experiment. The experiment was performed in a single-cylinder direct-injected stratified charge engine. Under the unthrottled condition, the fuel-air ratio altered when the amounts of the injecting fuel differs.

In addition, the laser Rayleigh scattering measurement has been used to determine time and space resolved fuel/air concentration in a propane and air mixture [Dyer, 1979], as well as the mixture fluctuations in the vicinity of the spark plug gap for both homogeneous and inhomogeneous mixture preparations in an SI engine [Lee and Foster, 1995]. In those experiments, since the combustion chamber needs to be modified to provide optical access ports for the laser beams and receiving optics and since the narrow laser beams focus on a small volume, the measurements may suffer some variation caused by the variations of the spark initiation.

Lately, on the basis of the development of various fiber optics techniques, more research has been carried out to study the fuel-air mixing behavior in-cylinder and has contributed greatly to the progress in this field. Nishimura [1987] used a single fiber-optic probe for the detection of poor air-fuel mixing. Remboski et al. [1989] developed and tested an in-cylinder optical sensor for use in spark-ignition engine combustion analysis and control to measure the luminous emission in the near infra-red region. The results show good correlation between the measured luminosity and engine combustion parameters, such as location and magnitude of maximum cylinder pressure, location and magnitude of maximum heat release and the in-cylinder air-fuel ratio. In addition,

Ohyama, Ohsuga and Kuroiwa [1990] combined fiber optics with a conventional spark plug to detect the light emitted by the spark discharge (V_w) between spark electrodes and the combustion flames in the cylinders (the fuel is gasoline*). In this experiment, the breakdown voltage (V_0) was also measured to correlate with the mixture compositions. The ratio of the light intensities of CH and C2 radicals appearing after the spark discharge indicates the cycle-by-cycle air-fuel ratio of the mixture near the spark plug. Figure 2-8 shows the relation between the air-fuel-ratio and the intensity of the light emission as well as the breakdown voltage. Subsequently, Sphoma et al. [1991] measured the fluctuations of excess air ratios and temperatures in the combustion chamber of a spark ignition engine with an optical diagnostic technique by the ratios of the light emission intensities of 431nm and 517nm, 502nm and 797nm respectively.

Recently, Koenig and Hall [1997] modified an optical spark plug to detect the radiation from an infrared source and measured the attenuation of the infrared radiation transmitted through a region in the vicinity of the spark gap. The experiment measured in-cylinder concentrations of hydrocarbons in the precombustion regions of the engine cycle and gave qualitative results for unburned hydrocarbons in the post-combustion regions.

2.4.2.3 Spark Spectroscopy Technique

Overall, the fiber optics assisted spectroscopy techniques have been validated in studying the combustion process in spark ignition engines. To further understand the cyclic variations, based on the high technology of the optical science and high speed data acquisition equipment, the spark spectroscopy technique has been applied to study the

* For gasoline, $(A/F_s) = 14.6$.

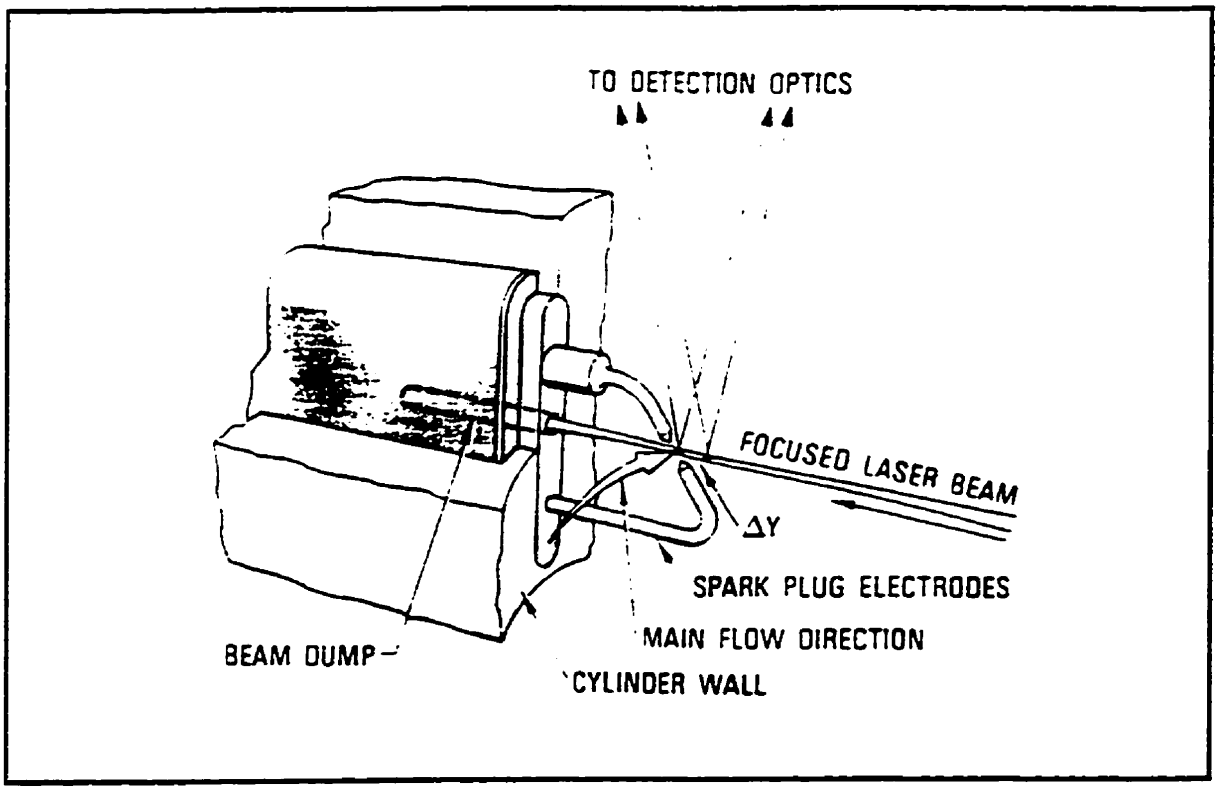

Fig. 2-7 Raman Spark Plug — Showing Focused Laser Beam and Collected Raman Scattered Radiation

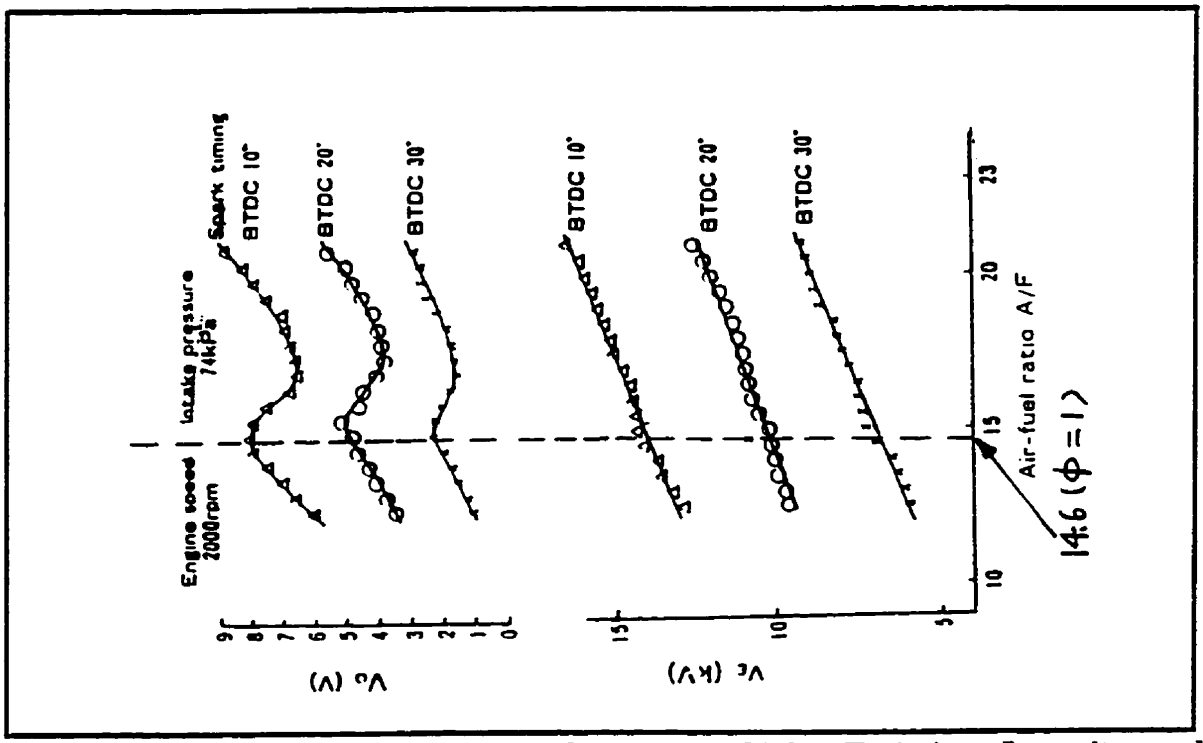

Fig. 2-8 Relation between Air-Fuel-Ratio and Light Emission Intensity and Breakdown Voltage

fuel-air ratio in the spark gap through the analysis of the light emission from the spark which initiates combustion. Different from laser spectroscopy, this measurement technique uses the energy delivered to a gas by an electric spark discharge as a source of excitation. To evaluate this method, Merer and Wallace [1995] conducted a series of experiments in a single cylinder research engine under different conditions. In those experiments, a modified spark plug with a fiber optic cable inserted through the center electrode was developed to observe the light emission from a spark discharge before combustion in order to investigate the possibility of determining the fuel-air ratio in the spark gap. The experiments focused on the light emission during the first 10 μs after initiation of the spark (before combustion) and studied the influence of the strong molecular emission from CN (centered at 385 nm) after a few micro-seconds as well as the correlation between the intensity of the CN emissions and some combustion parameters, such as gas concentration, breakdown voltage, spark plug gap size, etc.. The results show a correlation between the ratio of the spectral intensity of CN to the shot intensity (broad banded) and the fuel-air equivalent ratio ϕ.

Merer's work showed the good potential of the new spark spectroscopy technique in measuring air-fuel ratio in an SI engine. To further evaluate the usefulness of spark spectroscopy as an engine diagnostic tool for determining cycle resolved fuel-air ratio in the spark gap at the time of ignition, additional work is required to characterize the effect of residual gas on the light emission during the spark discharge.

The basic problem is that two pieces of information are needed simultaneously to determined fuel-air ratio: (1) hydrocarbon concentration, and (2) residual gas fraction.

The objective of the present work is to extract the second piece of information — the residual gas concentration. from the measurement, either by measuring the breakdown voltage or by an additional measurement of light intensity of another specific wavelength.

CHAPTER 3 APPARATUS

3.1 Breakdown Voltage Measurements In Non-Combustible Mixture

3.1.1 Spark Discharge System

The discharge system is the basic component in this project, especially in the preliminary breakdown voltage tests. In order to get a homogenous mixture before spark discharge, it is desirable to achieve discontinuous spark discharge to allow enough time for the stabilization of the post-mixing gases inside the combustion chamber. Hence, an easy manually controlled experimental discharge system was designed in this project, as shown in Fig. 3-1.

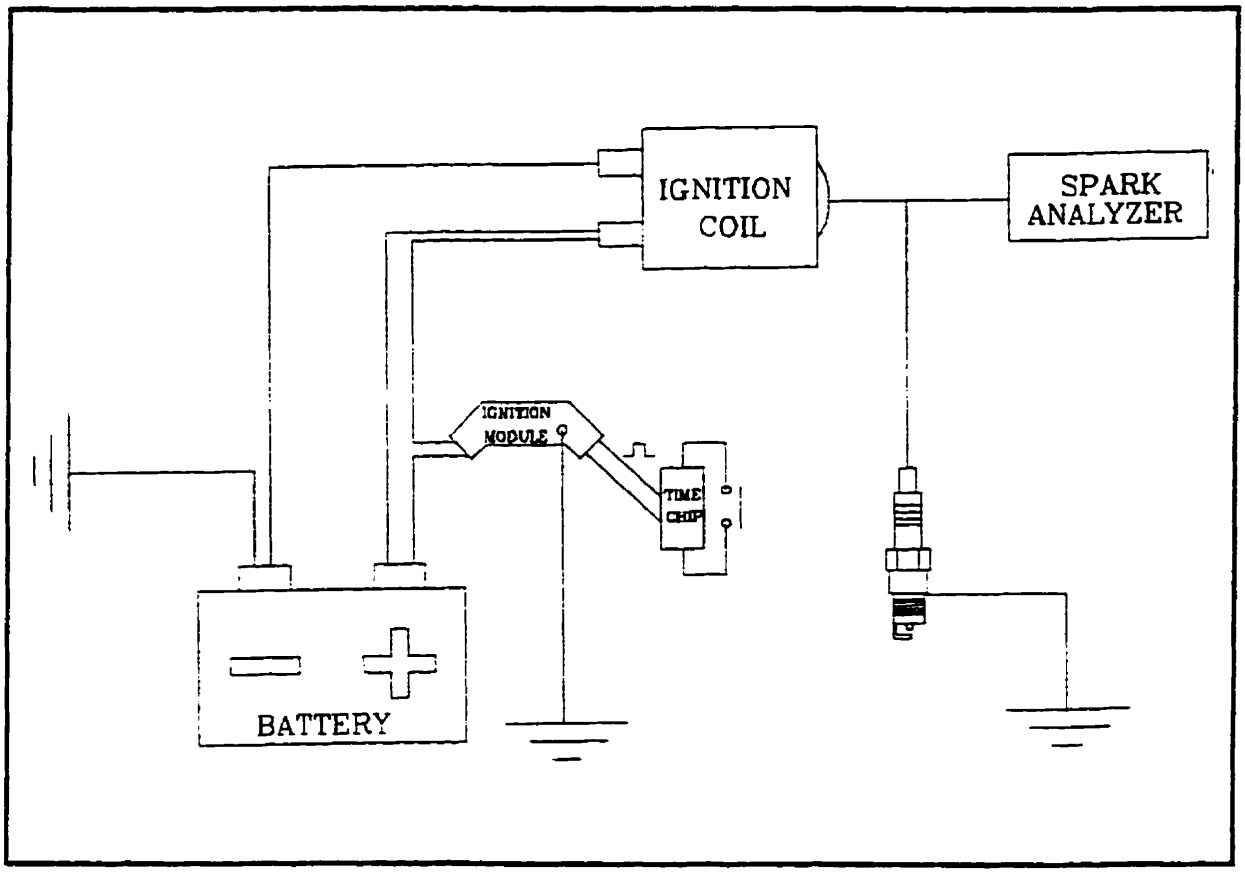

Fig. 3-1 Discharge System

The power supply of the discharge system is a standard 12V automotive battery which can be recharged. In order to control the spark occurrence and to get a stable and repeatable spark, an adjustable time-control-switch is used to connect directly to a Delco Remy (1977 GM Chevette) ignition module. The time-control-switch consists of a time chip with an adjustable "on" time from 1 ms to 10 ms. This duration is a good period for charging the ignition coil. Based on the result of the preliminary experiments of discharging time setting, a fixed period of 8.5 ms was chosen which is not only good for the experiments but also reasonable for the combustion process in a production engine [Appendix A]. So, each time the time-control-switch is switched on & off (by hand), a 8.5 ms long square wave signal is sent to the ignition module which provides a 8.5 ms long current flow to the ignition coil (40 kV Delco Remy). Thus, a high voltage is induced in the secondary circuit of the ignition coil. As soon as the voltage developed by the circuit reaches the level of the breakdown voltage for the gases contained between the spark gap, a spark will be discharged between the central and ground electrodes of the spark plug. As well, the same discharge system was used in later combustible tests.

3.1.2 Combustion Chamber

In order to well simulate the combustion process in an production engine, a real combustion chamber is required with as little modification as possible. Since the period between the end of the compression stroke and the beginning of combustion process is of the most interest, a simplified combustion chamber was designed for both non-combustible and combustible tests (Fig. 3-2). Compared to a production engine, the advantage of this simulated combustion chamber is in the ease for controlling the mixture

compositions inside the chamber before spark discharge. This combustion chamber consists of a Chev-V8 5.0 Liters (GM 1977-1993) cylinder head with only one combustion chamber being used. Instead of the cylinder block and piston, a 1" thick steel plate was screwed to the cylinder head for simplification. High strength bolts (17 SB Chevrolet Brodix -8, -11, -11XB head bolts — 170,000 psi, torqued to 85ft-lb=115N-m) were used to fasten the cylinder head to the plate. To avoid gas leakage from the intake and exhaust valves, Metal-Set epoxy was used to glue the intake and exhaust valves to their seats tightly. On the steel plate, within the designed combustion chamber area, two holes were drilled and tapped to 1/8" NPT. In the tests with non-combustible mixtures, each hole is connected to a stainless steel Street Tee Fitting. One "T" was connected to a SS-2C4-10 Whitey Poppet Check Valve for inducting mixture gases and a 2-way "on-off" SS-83TF2 Cajon Ball Valve for discharging the exhaust gas after firing. The working pressure of the check valve is at least 2000 psi (103 bar) and working temperature is up to 232°C (450°F). The working pressure of the ball valve is up to 3000 psig (206 bar) while the working temperature is up to 191°C (375°F). The other "T" was connected to a Bordon tube pressure gauge** and a thermocouple to monitor the pressure and temperature inside the combustion chamber before spark discharge. For the sake of safety, a hydrostatic test was done in the simulated chamber before conducting any combustible tests inside. The result shows that the simplified combustion chamber can stand as high as **2300** psig pressure while in a real engine, the peak pressure (calculated by Stanjan software) after combustion will not exceed 2300 psig. To characterize the effects of the

** In the combustible mixtures tests, this pressure gauge was replaced by other pressure transducers (see Section 3.2.1)

temperature on the breakdown voltage, a Polytemp Constant Temperature Control Bath was used to circulate distilled water through the cooling passage of the whole cylinder head, controlling the coolant temperature approximately from 25°C to as high as 95°C. Later, a steam generator was applied to increase the chamber temperature up to 285°F to prevent H_2O (product of the combustion) from condensing and remaining inside the chamber.

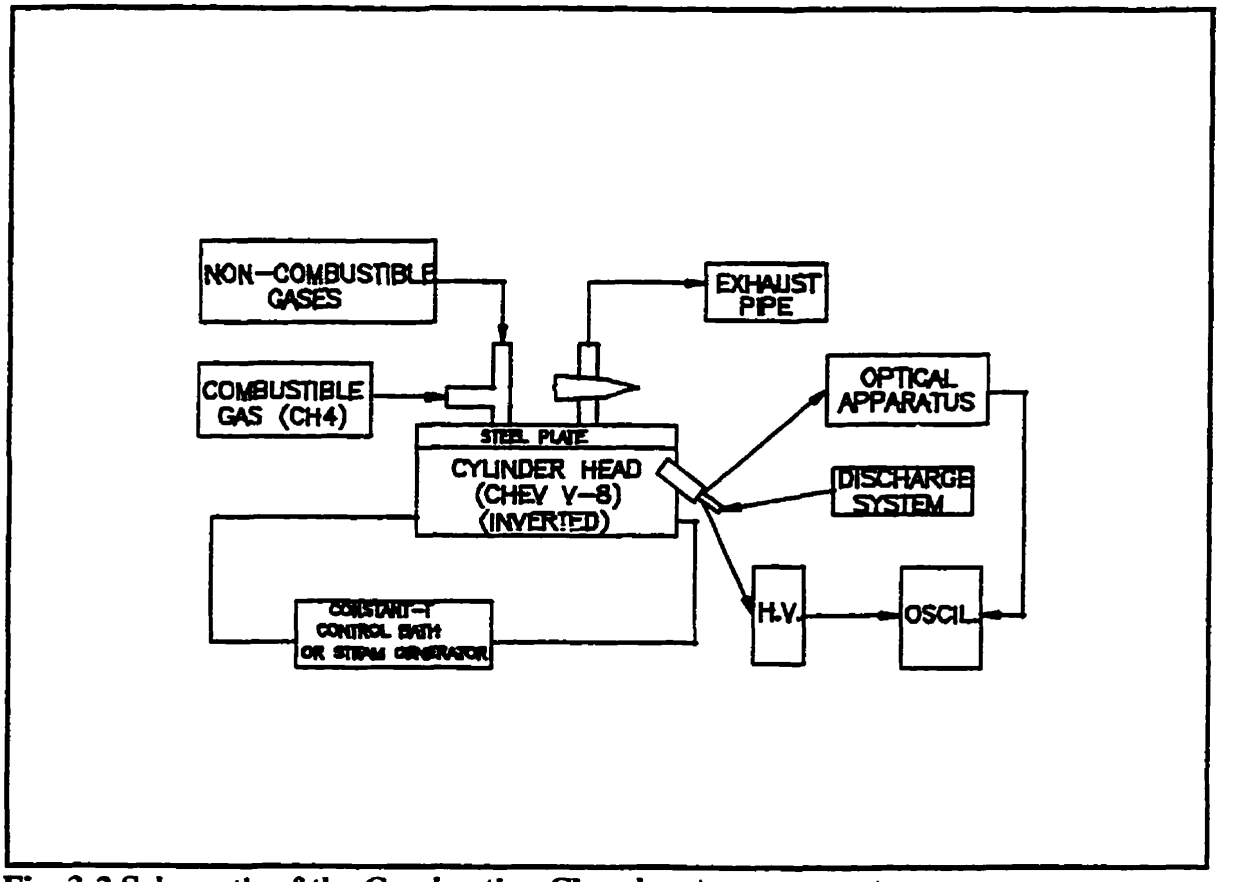

Fig. 3-2 Schematic of the Combustion Chamber Arrangement

In the breakdown voltage measurements, an unmodified taper seated AC R43TS (GM) spark plug with a 3/4" reach and 14 mm thread diameter was used. Also, a standard ignition cable was modified with a "T" connector (just beyond the normal contact point

of the cable and the central electrode of the spark plug) from which the High Voltage Probe and spark plug were assembled together.

3.1.3 Instruments with High Temporal Resolution

In order to capture the breakdown voltage signal which happens within nanoseconds, a Tektronix P6015A 1000X High Voltage Probe was purchased. The maximum input voltage is 20 kV (DC + Peak AC), with maximum peak pulse of 40 kV. This probe has as high as 75 MHz bandwidth which is fast enough to capture the breakdown voltage signal (approximate 35 MHz). For recording, a Hewlett Packard 54503A Digitizing Oscilloscope was used to readout the output from the high voltage probe. The bandwidth of this oscilloscope is as high as 500 MHz with sample rate of 1 MSa/s and the vertical resolution is 8 bits.

3.2 Mixing Control

3.2.1 High Accuracy Pressure Transducers — Producing the Combustible Mixtures

During the tests of breakdown voltages in non-combustible mixtures, the composition of the species inside the combustion chamber were roughly controlled by filling with each gas to a level mixtures by a standard Bordon tube pressure gauge. For the tests with combustible mixtures, a more accurate measurement of pressure was necessary. Since a small amount change of the air and fuel will affect the equivalence ratio dramatically, it is desirable to achieve high accuracy mixing of fuel and air in the

combustible mixtures tests. In the present work, the partial pressure method was applied (Appendix C) and three pressure transducers with high accuracy were used to help control the mixing ratio of fuel and air as well as the fraction of residual gas such as CO_2, H_2O and CO, etc.. To control the amount of CH_4 (regarded as a fuel equivalent to natural gas), a Schaevitz P-3061 0-15 psia pressure sensor with an accuracy of 0.5% has been applied. It requires a 10-32 V DC power supply and has an output from 0-5 V DC. It was calibrated by adjusting "Zero and Span" under vacuum (evacuated to 0.8497 psia by a vacuum pump), and atmospheric pressure (14.51 psia). To adjust the amount of air, a Schaevitz P1081 220 psig pressure transducer with accuracy of +/- 0.14% has been used. It also requires a 10-36 V DC power supply and has a full range output from 4-20 mA. Hence, a 250Ω resistor was connected to convert the output current to voltage. The transducer was calibrated by a Dead Weight Tester from 0 psig to 200 psig under 14.76 psi atmospheric pressure (Appendix D). Both of these pressure sensors are powered by a dual 14 V DC power supply. The outputs of these two sensors were monitored directly by a Fluke 87 true RMS multimeter.

In order to study the effect of the residual gas, it is necessary to know the amount of residual gas inside the combustion chamber before combustion at different fuel-air equivalence ratios. Hence, each time after combustion, a certain amount of the exhaust gas was kept inside the combustion chamber and then was mixed with the freshly charged fuel and air at the same fuel-air equivalence ratio before the next combustion. To simulate the general combustion condition, 10% residual gas (when compression ratio $r_c = 10$) was chosen in the present work. Therefore, a Viatran model 118 0-75 psia pressure transducer

with an accuracy of 0.4% was used to keep the 10% residual gas inside the combustion chamber by discharging the unwanted amount of exhaust gas to the exhaust pipe through a metering valve. Thereafter, the same Viatran 75 psia pressure transducer was used to help control the amount of freshly charged CH_4 at different fuel-air equivalence ratios. The unamplified milivolts output of the Viatran 75 psia pressure transducer was amplified by a bridge amplifier and also monitored by the same Fluke multimeter. As well, this pressure transducer was calibrated by the same Dead Weight Tester from 0 psig to 60 psig under 14.803 psia atmospheric pressure (Appendix E).

3.2.2 HFR400 Fast FID — Testing the Homogeneity of the Combustible Mixtures inside the Combustion Chamber

Inside the simulated combustion chamber, since there is no strong turbulence, the mixing of the fuel and air was achieved mostly by diffusion. In order to study the fuel-air ratio in-cylinder, especially between the spark plug gap by using this simulated chamber, it is important to have a homogeneous fuel-air mixture inside the chamber. Hence, a Cambustion HER400 Fast FID was used to test the homogeneity of the mixture before the combustible mixtures tests.

As pointed before, the FFID sampling system is designed to enable measurements of hydrocarbon concentration on a very short timebase (of order milliseconds) in internal combustion engines. By connecting the sample tube directly to the simulated chamber, the FFID system measured the HC concentration of the experimental mixture at different fuel-air ratios (after mixing without combustion). The result of the test shows very good

homogeneity of the mixtures inside the chamber (Appendix F) after high speed air injection (which promotes mixing) and 160 seconds of diffusion.

3.3 Apparatus of the Spark Light Emission Test in Combustible Mixtures

3.3.1 Optical Probe

Spark light emission is of the most interest in the present research on the SI engine combustion process. In order to detect the spark light emission, it is necessary to modify the engine combustion chamber to provide the optical access for light emission detection. Since any modification of the combustion chamber may cause some change in the combustion process, it is desirable to make as little modification as possible. Hence, many previous research projects have concentrated on modifying the spark plug only [Witze, Hall, Wallace and Bennett, 1988 & 1990]. The most important modification is inserting an optical fibre into the center electrode (central view) to detect the spark emission before combustion, e.g. in Merer's work [Merer, 1995]. This central view of the spark emission guarantees strong detection of light, but it needs more calibration because of the carbon deposit on the optical fiber end, and also because of the changes of the spark plug gap caused by degradation after firing a while. On the basis of the previous work, three feasible methods have been studied. Instead of the central view of the spark, these three optical probes all provide an SIde view of the spark emission. The following paragraphs present the method which was used mostly in the present work and the other

two methods considered are described in Appendix G in detail. This optical probe is not the optimal but the simplest and the most economical.

This optical probe consists of a 750 μm diameter stripped Diaguide ST-U600F-FV optical fiber with enhanced UV characteristics enclosed in a stainless steel hypodermic tube (0.042" OD, 0.032" ID) which maintains the strength of the stripped optical fiber. The optical probe was inserted inside another wider hypodermic tube (0.058" OD, 0.042" ID) which is shown in Fig. 3-3 with a drilled out screw soldered on it. The stripped optical fiber and the two hypodermic steel tubes were fixed together by Metal-set epoxy (which can stand high temperature and pressure). Since a tiny scratch on the end of the optical fiber may cause much loss of light emission, the end of the optical fiber has been polished very carefully under a microscope by a series of polishing papers of increasing fineness before being assembled to the spark plug to keep the fiber end well polished without any tiny scratches on it*.

Instead of modifying the spark plug, a small modification on the steel plate has been made. Perpendicular to the position of the spark plug, the optical probe was threaded through the plate with the end of the fiber optics exposed to the spark plug gap. In order to avoid the blockage of the spark light emission caused by the ground electrode, several spark plugs were tried before doing experiments and only those which have their ground

* Small tricks to facilitate this: inserting the optical fiber into the small size hypodermic tube → coarse polishing → inserting the optical fiber and the small tube into the big size hypodermic tube → polishing → pulling back the optical fiber and the small size tube until the end of fiber is inside the big tube → threading inside the plug → pushing the fiber and small tube until the end of fiber exposed to the spark gap and then using epoxy to glue the fiber and the tubes together.

electrode far away from the end of the optical probe have been chosen for the light emission tests. The position of the optical probe and the field of view was shown in Fig.3-3 schematically. Different from the other two side view designs, this one can detect much more light emission from the spark. The same as the other two optical probes, this design was also susceptible to be contaminated by the combustion. However, after sets of experiments, the optical probe was taken out for checking the cleanness and it shows surprisingly good condition — no soot formation and dirt on it.

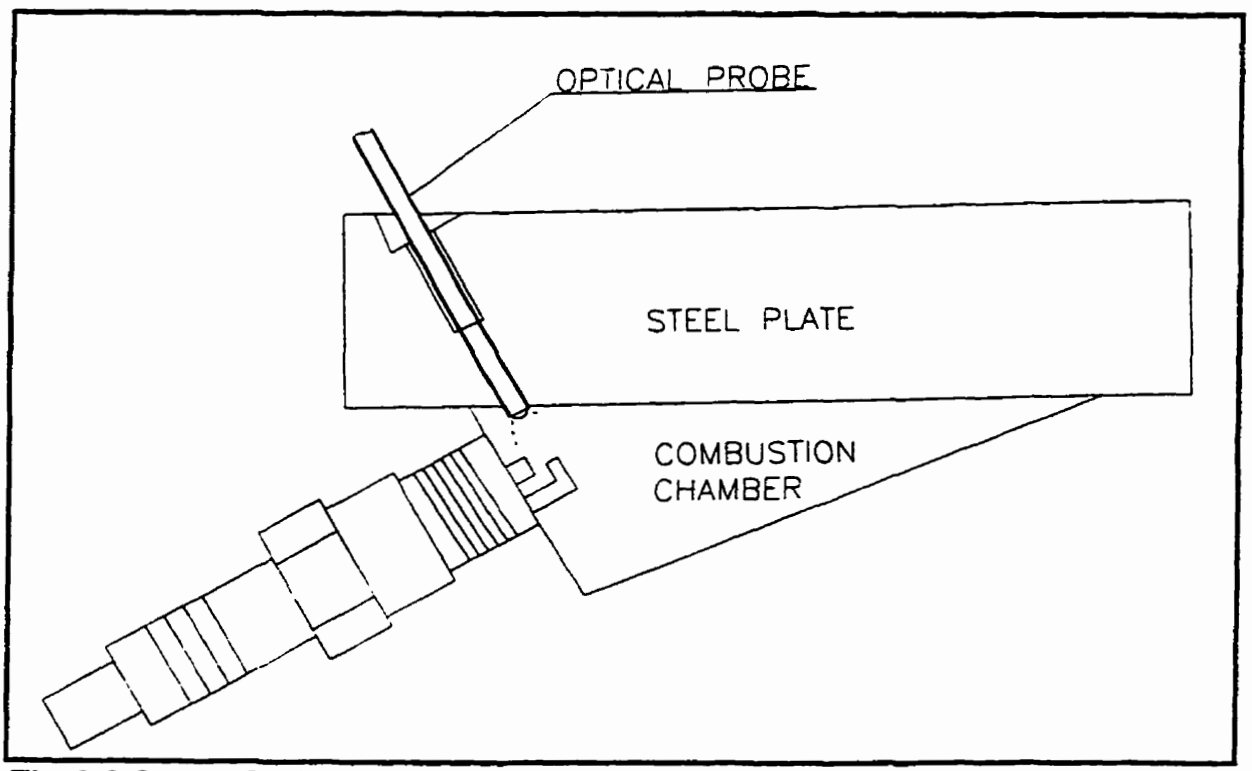

Fig. 3-3 Optical Probe Position and Field of View

3.3.2 Beam Splitter

In order to measure the broadband (shot) intensity of the spark emission and the spectral intensity centered at 385nm simultaneously, the light is channeled out through

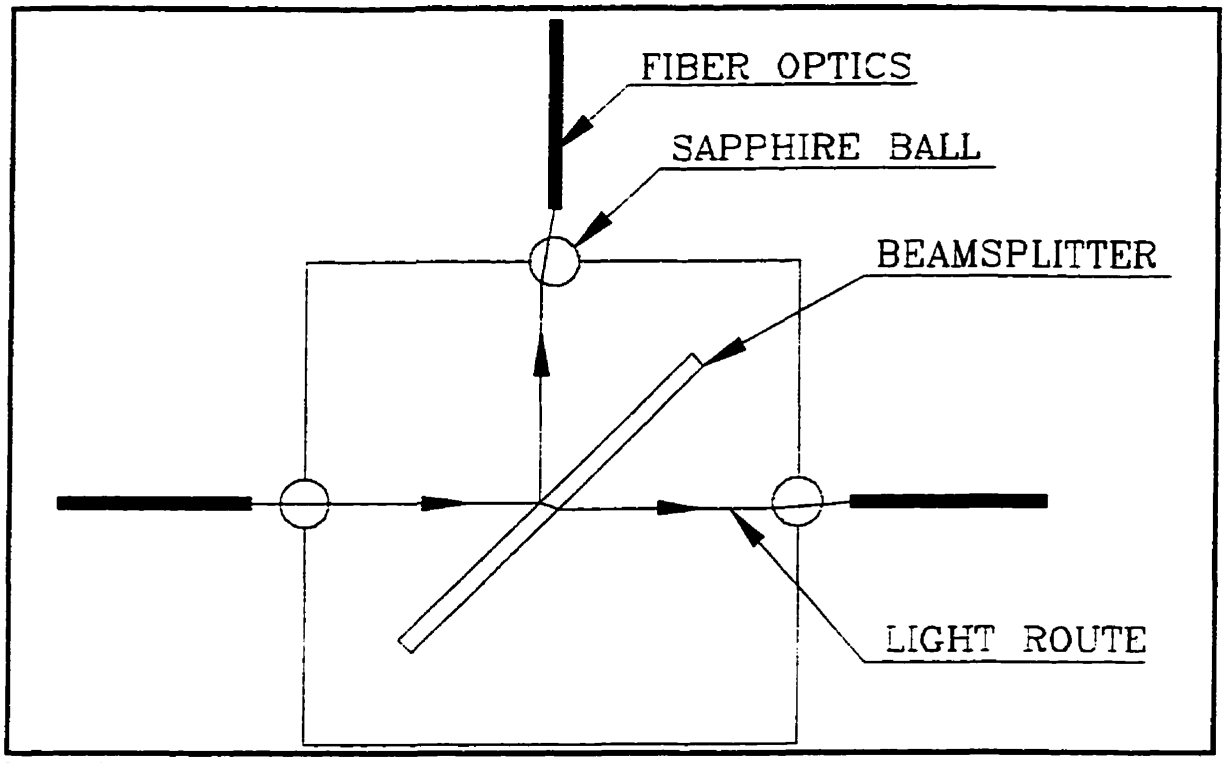

Fig. 3-4 Beam Splitter

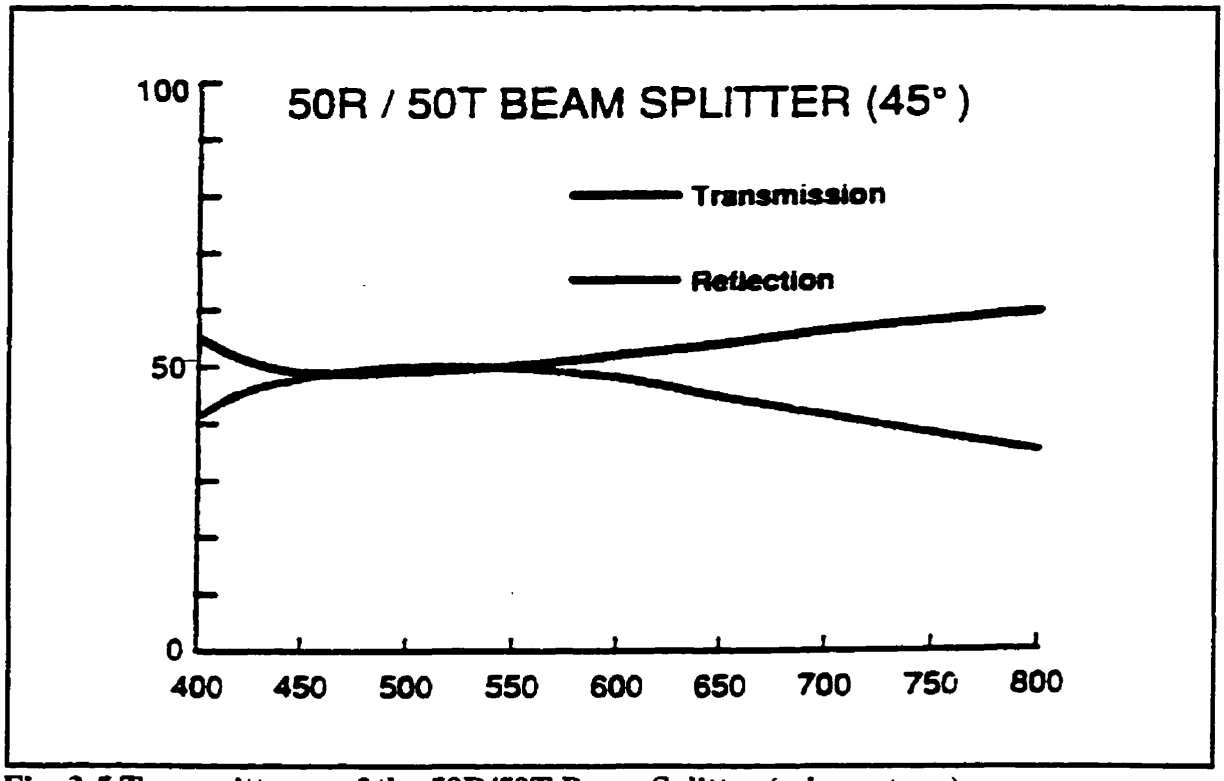

Fig. 3-5 Transmittance of the 50R/50T Beam Splitter (mirror type)

the optical probe from the combustion chamber and then is divided into two roughly equal channels by a beam splitter which is shown as Fig. 3-4.

The beam splitter assembly was made by mounting an EfstonScience A32269 50R/50T beam splitter (mirror) in a fitted slot machined in a hollow split steel cube at 45°. Half of the incident light is transmitted through the mirror and half of it is reflected. The measured transmittance plot of the beam splitter is shown in Fig. 3-5. To collimate the light beams of the three channels (incident, reflection and transmission), three sapphire balls were used as collimators before the light arrives at the mirror face and before the light goes into the optical fibers to efficiently guide the reflected and transmitted light beams into two optical fibers. Since the intensity of the spark emission from the side view is weaker than that from the central view, a simpler arrangement was used for the second design optical probe to avoid the light emission loss caused by the collimators and optical fiber connectors. Instead, two simple adapters were designed to mount the detectors (photomultipliers) directly to the beam splitter outputs.

3.3.3 Grating Monochromator

The beam splitter divides the light from the spark emission into two light beams with roughly equal intensity. To measure the broadband intensity (the total or shot intensity), one beam was guided through a neutral density filter directly into a photomultiplier tube. In order to measure the spectral intensity (CN emission at 385 nm), the other beam should go through a narrow band pass optical apparatus before entering the second photomultiplier tube. For simplification, it had been suggested to use a high resolution band pass filter. Hence, a Newport (Klinger) P10-390-A, 0.5" diameter

bandpass filter was purchased, which has 10 nm bandwidth with its center wavelength at 390 nm.* Although the filter has been tilted as to shift the centre wavelength to 385 nm (discussed in Appendix H), its undesirable transmittance is still very high, being unable to filter several other wavelengths which are close to 385 nm because of its relatively wide 10 nm bandwidth. The results from several sets of experiments showed that the spectral intensity (measured after the filter, regarded as the emission from CN at 385 nm) sometimes had excessive variation which was susceptible to be caused by the unavoidable effect of other radicals (e.g. CH). In order to improve the precision of the measurements of the spectral light intensity of CN, high resolution equipment was

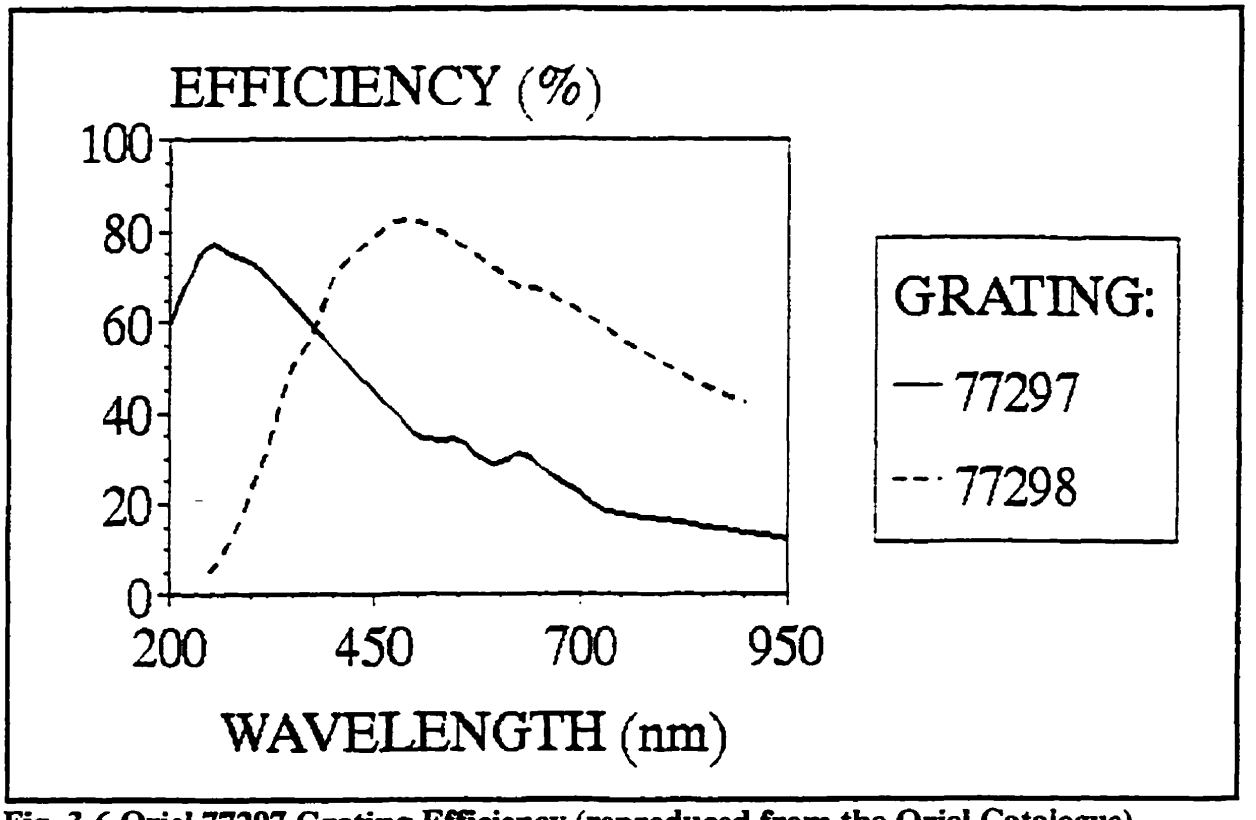

Fig. 3-6 Oriel 77297 Grating Efficiency (reproduced from the Oriel Catalogue)

* Several optics companies have been checked and it is difficult to find a very high resolution bandpass filter (with bandwidth less than 10 nm) which has the center wavelength down to UV (around 385 nm). Hence, this filter was chosen.

required. To satisfy this demand, an Oriel Model 77250 1/8 m Monochromator was used with an Oriel Model 77297 grating. Figure 3-6 shows the efficiency of the this grating. Since the amount of throughput and the degree of resolution provided by the monochromator mostly depends on the width of the entrance and exit slits, it is important to choose appropriate slits to get an optimum resolution as well as a detectable throughput. Based on the spectral power distribution of the monochromator (shown in Fig. 3-7), two 760 μm (microns) fixed slits were purchased which provide 5 nanometers bandpass with approximate 5% transmittance efficiency. The monochromator was calibrated by a 0.5 mW Helium-Neon laser which has a red laser beam at wavelength λ = 632.8 nm with a beam diameter of 0.48 mm. In addition, the monochromator was calibrated by a convenient mercury lamp in the Lab (dark room) at the following wavelength (invisible light was not used for this calibration):

Wavelength	Colour
404.7 nm	Violet (Faintly)
407.8 nm	Violet
434.8 nm	Blue
435.8 nm	Blue (can't be resolved from the previous one)
546.1 nm	Green
577.0 nm	Yellow
579.1 nm	Yellow (can't be resolved from the previous one)

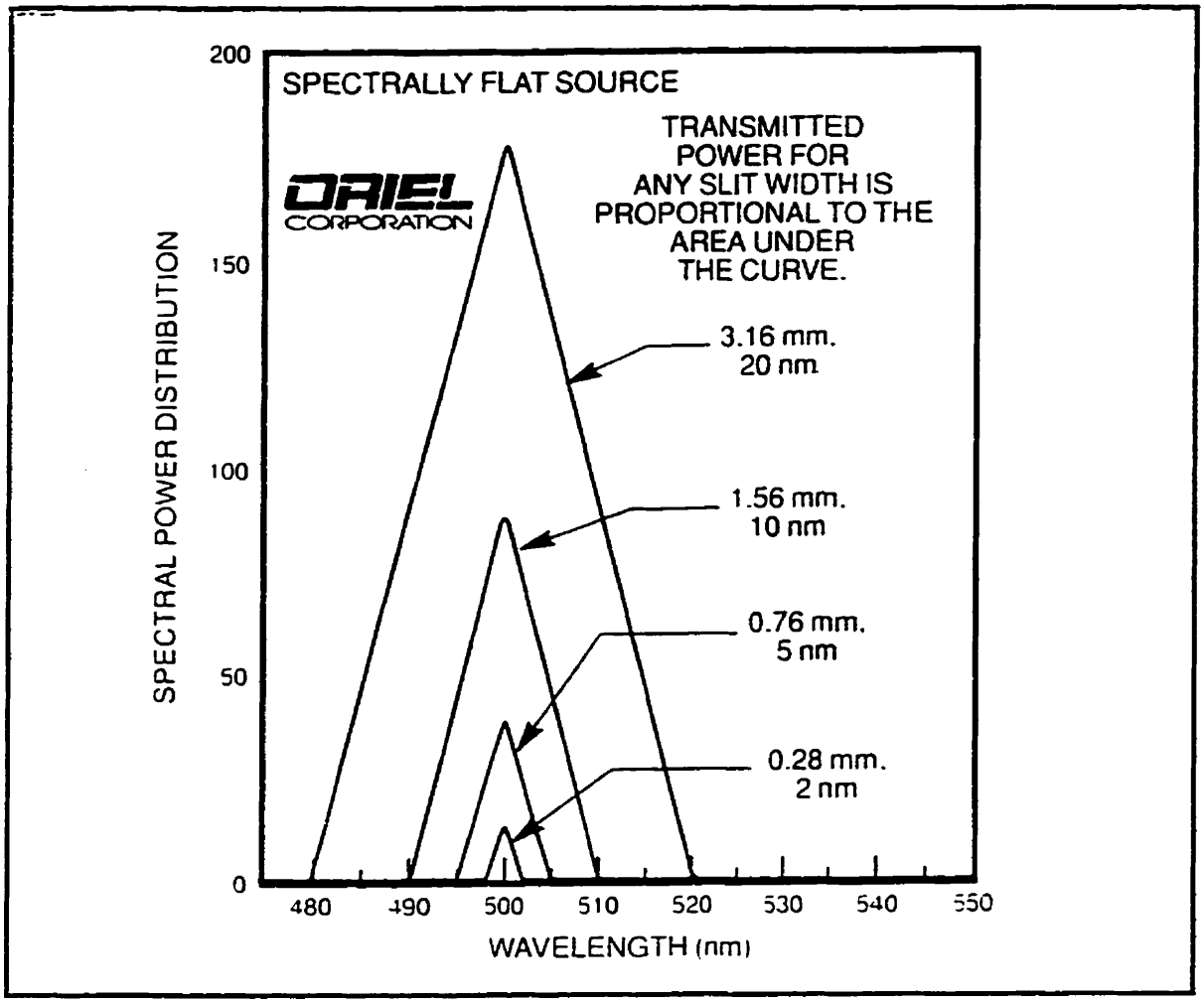

Fig. 3-7 Spectral Power Distribution of 77250 1/8 m Monochromator with Various Slits (Oriel Catalogue, 1995)

3.3.4 Detectors — Photomultipliers and Current Amplifier

In order to compare the two channels of spark light emission after the beam splitter (and a monochromator[‡] in the case of one channel), the best way is to convert the light signals to comparable electric signals. This was achieved by photomultiplier (PMT).

[‡] At the beginning, a narrow bandpass filter was used.

A PMT mainly consists of a photocathode followed by a focusing electrode, an electron multiplier and an electron collector (anode) (Fig. 3-8). When light enters the photocathode, the photocathode emits photoelectrons which are directed by focusing electrode voltage towards the electron multiplier where electrons are multiplied by the process of secondary emission. Finally, the multiplied electrons are collected by the anode as an output signal.

Since the wavelength range between 200 nm to 700 nm is of the most interest in spark light emission measurements, two side-on Hammamatsu R446 photomultipliers (9 dynode stages) were chosen because of their enhanced UV sensitivity. As shown in Fig. 3-9, this model PMT has relatively high quantum efficiencies between the wavelength range of 200 nm to 700 nm. Also, its high time response of 2.2 ns is sufficient for time resolution of spark discharge.

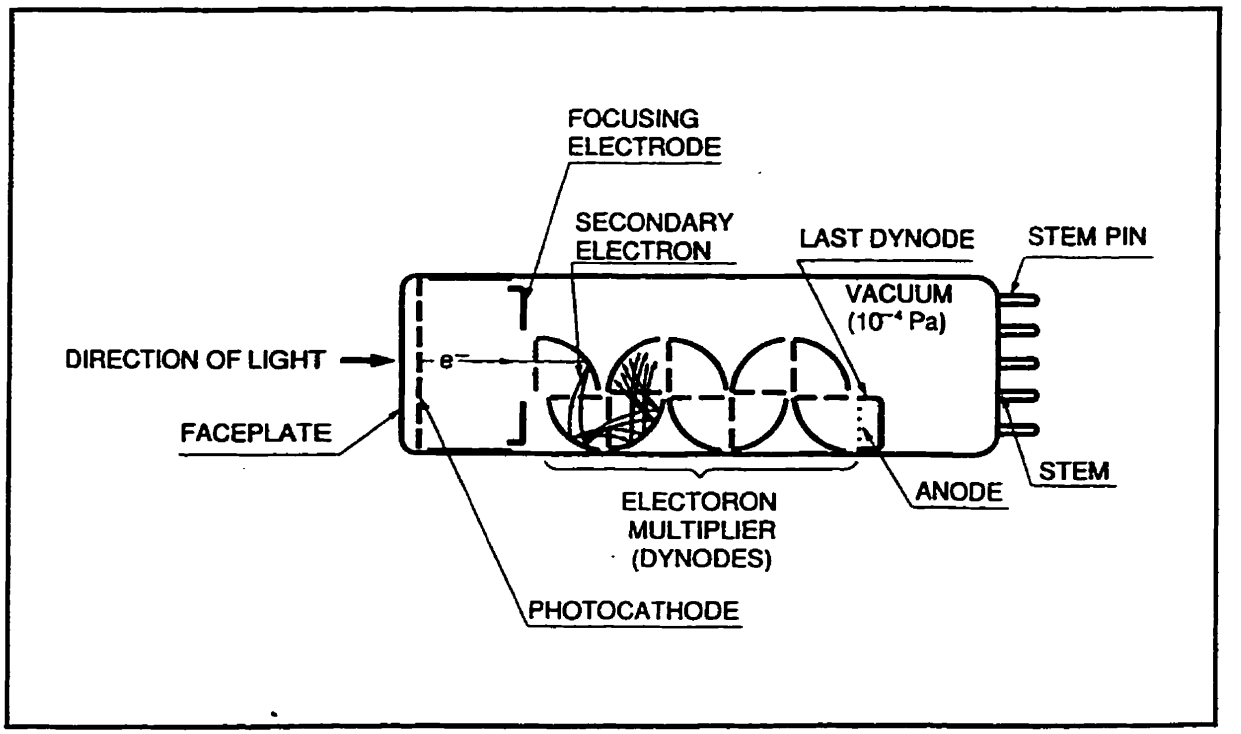

Fig. 3-8 Cross-Section of a PMT [Reproduced from Hammamatsu Catalogue]

For a PMT, the output signal is determined by the current amplification which can be expressed as $\mu = K \bullet V^{\alpha n}$, where K is a constant for a specified PMT, V is the supplied voltage between the cathode and the anode, α is a coefficient which usually has a value of 0.7 to 0.8 and n is the number of the dynode stage. This expression shows that the output signal of the PMT is extremely susceptible to fluctuations in the power supply voltage. Hence, a very stable power supply was required to provide minimum ripple, drift, etc. In this case, two C1309-04 Hammamatsu modular power supply were purchased for the two PMT's and assembled to provide a constant negative voltage at -1110V (tested by the high voltage probe).

Figure 3-10 shows the response of a PMT vs. light intensity. It shows that when the light intensity is strong (beyond a certain level), the PMT is saturated and the response of the PMT starts to be non-linear. Hence, in order to compare the two channels of light from the beamsplitter (one is shot , the other one is spectral), it is necessary to keep the responses of the PMTs' linear for both signals.

In the case of the second design of optical spark plug (described in Appendix G), the spark light emission is detected by an SIde-view optical probe. Therefore, the detected light intensity is relatively low and should not exceed the linear response range of the PMT. But the optical probe described in Section 3.3.1 has a larger view of the spark light emission. Hence, when it was used, the increasing intensity of the light emission caused the PMT to become saturated, resulting in non-linear response. In order to reduce the light emission, a Newport QD-40-F neutral density filter was purchased to reduce the total light transmittance to 39.8%.

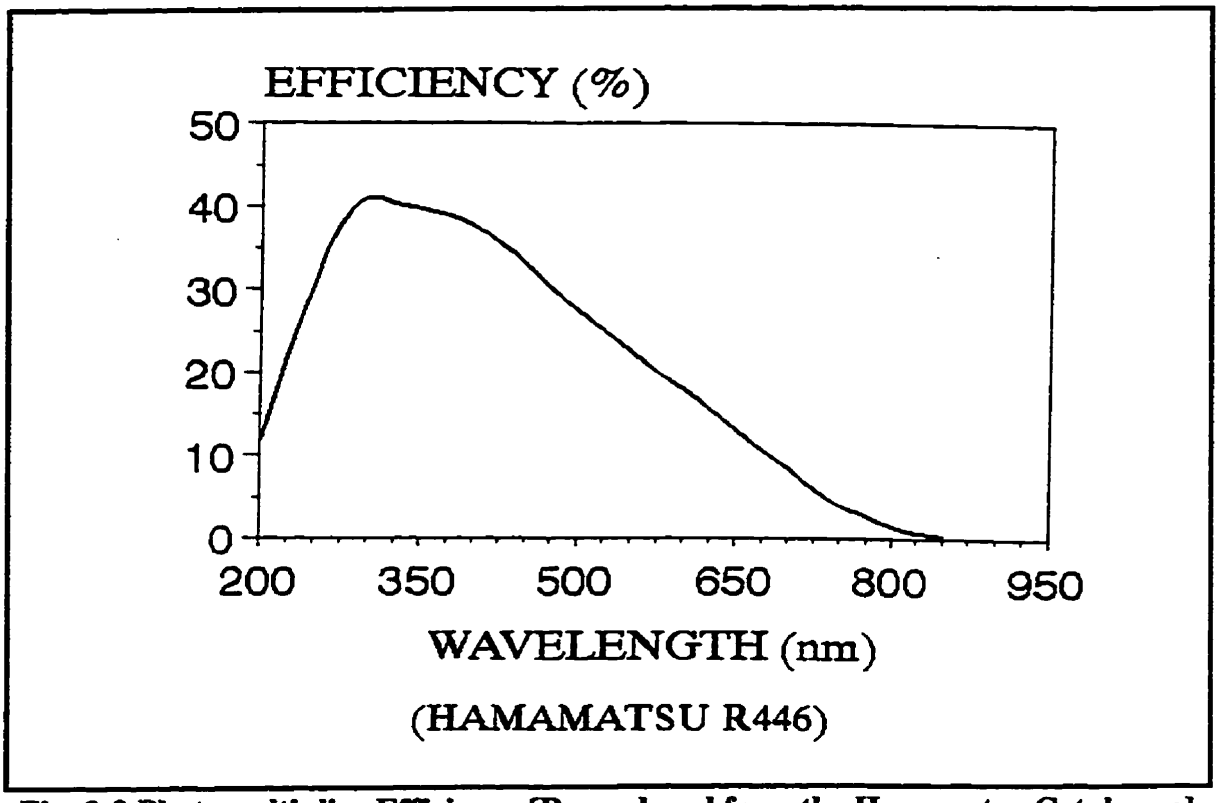

Fig. 3-9 Photomultiplier Efficiency [Reproduced from the Hamamatsu Catalogue]

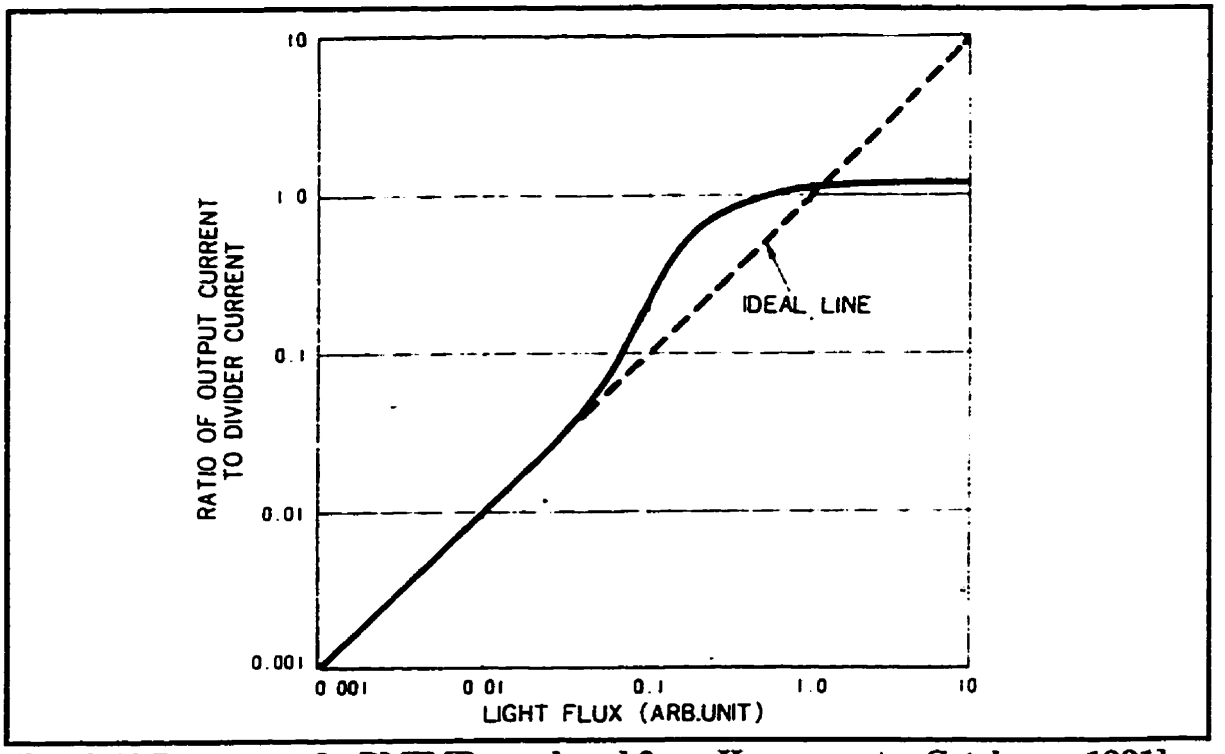

Fig. 3-10 Response of a PMT [Reproduced from Hammamatsu Catalogue, 1991]

After the PMTs, the output signals were converted to a voltage pulse through a current amplifier which has a lowest gain of 10^4 V/A and a rise time of approximate 1μs which is still sufficient for integration of the spark light intensity in the most interesting period — the initial 5-10 μs after spark initiation and before combustion.

3.3.5 Recording — Oscilloscopes

The converted and amplified PMT output was recorded on a Nicolet 4094 digital oscilloscope with model 4562 plug-ins. This oscilloscope has a maximum digitizing rate (sampling rate) of 500 ns/point which is fast compared to the current amplifier rise time and hence is more than sufficient for the integration of the light intensity in the initial 5-10 μs. As well, the data storage and analysis capabilities of this oscilloscope provided an easy way to analyze data during the experiments.

It has been shown that, the breakdown voltage decides the energy of the spark and hence determines the intensity of spark light emission. Therefore, it is more helpful to detect the breakdown voltage and the light emission simultaneously. Using both the shot intensity and the breakdown voltage to normalize the spectral intensity will reduce the influence caused by the position changes of sparks and also will eliminate other unexpected effects. This idea shows great potential for the study of combustion in the SI engine, helping to further understand the relation between the gas components and the light emission, especially the spectral light emission (CN), in order to determine the air-fuel ratio in the vicinity of the spark plug before combustion. In the previous measurements of breakdown voltage, an existing Hewlett Packard 54503A oscilloscope

was used. Although it has as high as 500 MHz bandwidth, the bandwidth for an SIngle shot is just as low as 2 MHz, and its maximum sampling rate is only 20 MSa/s. Also, its waveform record length is only 501 points. In order to get a less distorted breakdown signal, at least a higher sampling rate is required. In order to choose an appropriate oscilloscope, first the signal bandwidth needed must be determined. For the breakdown voltage signal, the bandwidth needed is: 0.35/ (10 ns rise time) = 35 MHz. In order to capture it, the bandwidth of the oscilloscope must be at least twice as the signal bandwidth of 35 MHZ or at least 70 MHz. Also, the sample rate should be fast enough to capture the 10 ns rise time signal. So the sample rate should be at least 100 MHz. For a digital oscilloscope,

$$\textbf{Sample Rate} = \frac{\text{WaveformMemory}}{(\text{Timebase})\text{x}(\#\text{CRT.Divisions})}$$

where CRT refers to Cathode-Ray Tube. Obviously, increasing memory will increase the sample rate at a fixed timebase setting. According to all these, a relatively inexpensive Hewlett Packard 500 MHz 54615B oscilloscope was chosen. It has 5,000 points of memory even for an SIngle shot and 1 ns peak detection. Also, the maximum sampling rate is 1 GSa/s while the bandwidth for an SIngle shot is up to 250 MHz which is sufficient for detecting the 10 ns breakdown signal.

By combining this high temporal resolution oscilloscope with the high resolution high voltage probe, more accurate breakdown voltage measurements were achieved.

3.3.6 Shielding

Theoretically, the high frequency fluctuation of current or charge in a conductor results in the radiation of part of the energy in the conductor in the form of an electromagnetic wave. This wave propagates through space at the speed of light and is called as radio-frequency interference (rfi) which is an unpleasant thing in testing. In this experiment, the ignition system is a source of this kind of interference. Since there are more than one earth paths in use when examining signals on an oscilloscope, an interference signal may develop and then appears superimposed on those acquired signals, resulting in deviation of the measurements. This interference can be reduced by effective shielding. A Faraday cage is the most effective one. For simplification, a kind of heavy duty aluminum foil was used to wrap all the ignition parts as well as the PMTs and amplifier, etc. All of the shielding was connected to the common reference ground. This simple aluminum shielding showed good effect in the preliminary tests.

CHAPTER 4 EXPERIMENTAL PROCEDURES

4.1 Breakdown Voltage Measurements in Non-combustible Mixtures

In the previous work done by Merer [Merer, 1995], a set of breakdown voltage (V_S) tests had been performed in non-combustible mixtures to identify the general trends over mixture concentrations, gap sizes, and pressure. However, those measurements were made with the Beckman spark analyzer which only outputs an uncalibrated analog signal proportional to breakdown voltage. To quantify the previous results and extend them over a wider range of conditions, a new set of experiments has been done which tested the effects of the pressure, the temperature and the gap size of the spark plug on V_S in different non-combustible mixtures. The test matrix #1 is shown in Table 4-1.

In SI engines, Exhaust Gas Recirculation (EGR) has been widely used to reduce NO_x emissions. As well, the residual gas inside the combustion chamber (left from the combustion of the previous cycle) is another important factor which will affect the combustion process of the next cycle very much. For a natural gas (here regarded as 100% CH_4 for simplification) fueled engine, CO_2, CO and H_2O are the main components of both EGR and residual gas. Before ignition, all of those components mix together with the freshly charged CH_4 and air. Since CO_2 is relatively important among the EGR and residual gas components, an additional set of experiments were conducted to test the effect of CO_2 in nitrogen with different concentrations of CH_4 on the breakdown voltage (shown in Table 4-2). The tests were carried out under 150 psig and 180 psig respectively. These conditions were chosen because they are similar to those in

Table 4-1: Breakdown Voltage (V_S) Test Matrix #1 (One and Two-Components Non-Combustible Mixtures)

Species *	Pressure Range (psig)	Gap Size (mm)	Temperature Range (C°)
N_2	20 - 180	1.0	25-85
N_2	60 - 140	0.584	25
Air	20 - 140	1.0	25
O_2	20 - 140	1.0	25
11.2% CO_2	20 - 160	1.0	25
14.3% CO_2	20 - 180	1.0	25- 85
100% CO_2	20 - 160	1.0	25
2% CO	20 - 140	1.0	25
2% CO	20 - 140	0.584	25
10% CH_4	20 - 160	1.0	25 - 85
10% CH_4	60 - 140	0.584	25
100% CH_4	20 - 140	1.0	25

Table 4-2: Breakdown Voltage Test Matrix #2: Effect of CO_2 & CH_4 (Balance is N_2) on Breakdown Voltage

CH_4 (%) \ CO_2(%)	0	5	10	15
0	*	*	*	*
5	*	*	*	*
10	*	*	*	*
15	*	*	*	*

* For all the mixtures, the balance is N_2.

production engines during the spark discharge period before combustion with compression ratio at $r_c = 9$, and 12 respectively (See Appendix B).

4.2 Combustible Mixtures Tests

It has been studied that the for an SI engine, the light emission from the spark discharge and the breakdown voltage has a strong correlation with the fuel-air ratio as well as the residual gas fraction and the percentage of EGR. For skipped fired combustion (without residual gas and EGR), the intensity of light emission and breakdown voltage decreases with the increase of the fuel-air ratio. But under normal combustion conditions (with residual gas) and conditions with additional EGR, the correlation changed [Ohyama, 1990 & Merer, 1994]. As well, it has been studied that the intensity of the light emitted by the CN radicals within 10 μs (before combustion) also has very strong correlation with the fuel-air ratio. In order to further study the correlation between the light emission (especially the light emission of the CN) and the fuel-air ratio in SI engines, it is necessary to study the effect of the residual gas on the light emission. In the combustible tests, several sets of experiments have been conducted on the same simulated combustion bomb which is easy to be used for controlling the fuel-air ratio and fraction of residual gas.

In order to simplify the composition of the fuel, the Ultra High Purity (UHP) methane (CH_4) was chosen in the combustible mixtures tests. For stoichiometric combustion (when $\phi = 1$), the chemical reaction equation can be written as follows:

$$CH_4 + 2\,(O_2 + 3.773\,N_2) \longrightarrow CO_2 + 2\,H_2O + 7.546\,N_2$$

In the combustible mixtures tests, the fuel-air equivalence ratio (ϕ) was changed from 0.7 to 1.1 with an increment of 0.1[†].

To control the mixing of the species inside the combustion bomb, three pressure transducers have been used (Table 4-3) and the mixing procedure can be shown as follows (see Appendix J for details):

without residual gas: methane ⟶ air
with residual gas: residual gases ⟶ methane ⟶ air

Table 4-3: List of the Pressure Transducers

Number	Company	Pressure range
#1	Vitran	15 psia
#2	Vitran	75 psia
#3	Durham	220 psig

4.2.1 Combustible Mixtures Tests without Residual Gas

The first set of experiments was done without residual gas. The percentage of methane and air at different fuel-air equivalence ratio is shown in Table 4-4.

4.2.2 Combustible Mixtures Tests with 10% Residual Gas

[†] In some experiments, the increment was chosen as 0.05.

In order to study the effect of the residual gas. an additional set of experiments has been conducted. Table 4-5 shows the percentage of different species at different fuel-air equivalence ratio with 10% residual gas inside.

Table 4-4: Combustible Mixtures Tests without Residual Gas

Fuel-air equivalence ratio (ϕ)	Fuel (Methane CH_4) (%)	Air (O_2 + 3.773 N_2) (%)
1.10	10.332	89.6675
1.00	9.482	90.518
0.90	8.616	91.384
0.80	7.733	92.267
0.70	6.832	93.168

The partial pressure and pressure sensor outputs of different species during the mixing procedures both with and without residual gas (with combustion bomb pressure at 150 psia) were detailed in Appendix J.

Table 4-5: Combustible Mixtures Tests with Residual Gas

Fuel-air equivalence ratio (ϕ)	Residual gases (xCO_2+ yH_2O+ zN_2) (%)	Fuel (Methane) (% CH_4)	Air (%)
1.10	10	9.299	80.701
1.00	10	8.534	81.466
0.90	10	7.754	82.246
0.80	10	6.959	83.041
0.70	10	6.149	83.851

4.2.3 Effect of Residual Gas in Combustible Mixtures Tests

The results of the breakdown voltage tests without and with 10% residual gas showed significant differences, implying that the residual gas has a strong effect on the breakdown voltage and therefore on the spark light emission. In order to further understand the correlation between the fraction of residual gas and the breakdown voltage and the intensity of the light emission, additional sets of experiments (in a stoichiometric mixture where $\phi = 1$) were carried out with the fraction of residual gas changing from 0% to 25% in 5% increments. Table 4-6 presents the compositions of the CH_4, CO_2, H_2O, O_2, and N_2 with different fractions of residual gas in the stoichiometric mixture, showing the fractional change of the important residual components CO_2 and H_2O. In addition, 9% CO_2 (the balance is N_2) was used instead of the residual gas in one set of experiments to isolate the influence of the H_2O vapor.

Table 4-6: Tests of Effect of Residual Gas in Combustible Mixtures

Residual gas (%)	CH_4 (%)	CO_2 (%)	H_2O (%)	O_2 (%)	N_2 (%)
0	9.482	0.000	0.000	18.965	71.553
5	9.008	0.474	0.948	18.016	71.553
10	8.534	0.948	1.896	17.068	71.553
15	8.060	1.422	2.845	16.120	71.553
20	7.586	1.896	3.793	15.172	71.553
25	7.112	2.371	4.741	14.223	71.553

CHAPTER 5 RESULTS AND DISCUSSION OF BREAKDOWN VOLTAGE MEASUREMENT

The breakdown voltage measurements were achieved by a Tektronix P6015A 1000X high voltage probe which was calibrated after purchasing. However, the breakdown voltage measurements showed some random variation, presumably due to variations in the discharges themselves. For this reason, each measurement was repeated about ten to twenty times and the breakdown voltage value was averaged.

5.1 Breakdown Voltage Measurements in Non-Combustible Mixtures

For the non-combustible mixtures, unmodified taper seated AC R43TS (GM) spark plugs* were used and the breakdown voltage was recorded by a HP 54503A digitizing oscilloscope. The aim of test matrix #1 (Table 4-1) was to achieve more accurate values of breakdown voltage (V_S) under different conditions in order to well understand the effects on the breakdown voltage of the other parameters related to combustion, such as the pressure, the temperature, the mixture composition (especially in the spark plug gap), and the gap size of the spark plug, etc.

5.1.1 Tests in Pure Gases

Figure 5-1 presents the results from the tests carried out in pure air, pure nitrogen, and pure oxygen respectively. As expected, the results agree with the previous work

* In these tests, the spark plugs were replaced from time to time. Although they are all the same model, having the same geometry, the electrodes surface conditions vary from each other, probably causing unexpected variations in the tests.

summarized by Meek and Craggs [1978]. As shown in Fig 5-1, under the experimental conditions (T = 298 K), the breakdown voltage measured in N_2, air and O_2 increases with the increase of the pressure. The correlations between the breakdown voltage and the pressure for the three gases are quite linear and are very similar to each other (the differences between the three trendlines are not statistically significant). However, when the pressure is very high, say above 10 atmospheres, the breakdown voltage in O_2 and air has a slightly higher value than that in N_2.

Initially, the gas volume within the electrodes gap acts as a perfect insulator. When the spark pulse is applied, the randomly existing electrons gain energy in the rising electric field and are accelerated towards the anode. When the applied electric field has reached sufficiently high values, the field-accelerated electrons ionize the gas molecules by the collisions, generating additional electrons and ions. These charge carriers gain energy from the electrical field as well and further contribute to the rising electron current. Finally, breakdown is achieved in the gap after the avalanche of the electrons and the current reaches a very high level (~100 A) [Maly, 1984].

When the pressure is low, the density of the electrons in the spark plug gap before the breakdown phase is relatively low and the electrons have less chance of colliding with molecules or ions. Hence, the electrons can gain much more energy from the rising electric field. This increases the number of effective collisions which in turn produce more and more electrons and ions to help breakdown. Also, even when the collisions are not effective, the molecules or ions can be excited to a multitude of electronic levels,

emitting UV radiation which reaches the cathode directly and easily at low pressure, to liberate with high efficiency photoelectrons at its surface. Hence, the breakdown is easily

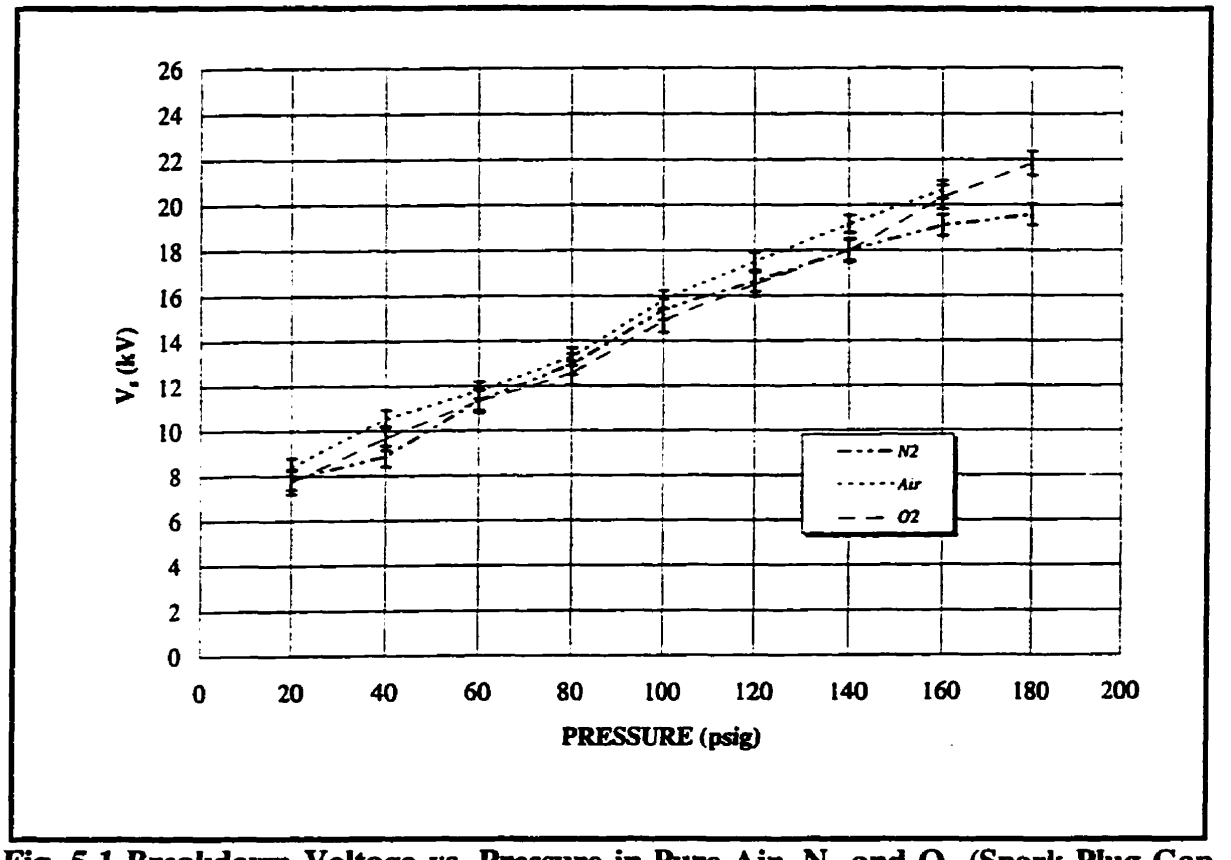

Fig. 5-1 Breakdown Voltage vs. Pressure in Pure Air, N_2 and O_2 (Spark Plug Gap Size d=1.0 mm, T=298 K)

achieved at low pressure. On the contrary, when the pressure is increased, the density of the electrons is higher and the chance of encountering an ionizing collision is increased as well. Mean free path of electrons go down, thus energy gained by electrons is not as much between collisions. Thus, the electrons can not acquire as much kinetic energy as that gained at a low pressure. Therefore, the collisions in the channel result in more excitation than ionization due to the low energy levels of the electrons. Also, a higher percentage of the UV radiation emitted by the excited ions is absorbed by the surrounding gas molecules rather than reaching the cathode and creating photoelectrons, causing a low

percentage of them to become radiation ionized in the cathode region. Therefore, the electron avalanche is inhibited, resulting in an increase in breakdown voltage.

When the pressure is high, the electrons gain less energy when they are accelerated towards the anode due to a higher collision frequency, Hence, the probability of the electron attachment to the neutral atoms or molecules increases.[†] Since the probability of the electron attachment also depends on the nature of the gas, O^-, O_2^- are readily formed but not N^-, N_2^- [Nasser, 1971]. Therefore, the electron avalanche is inhibited in O_2 and air when there is O present, resulting in an increase of the breakdown voltage in air and O_2 at high pressure (as shown in Fig. 5-1).

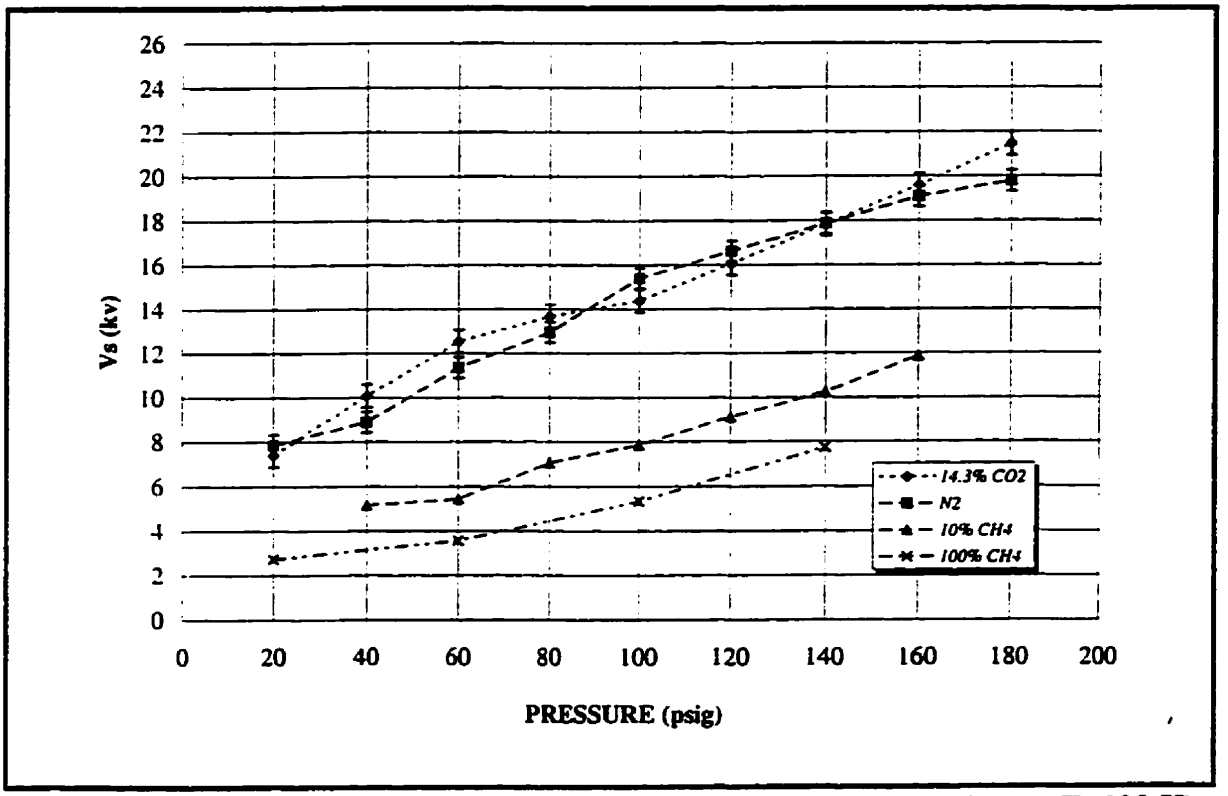

Fig. 5-2 Effects of CO_2 & CH_4 (in N_2) on Breakdown Voltage (d=1.0 mm, T=298 K)

In addition, when the pressure is high, say greater than a few atmospheres, the

[†] The probability of attachment increases as the electron energy decreases, because the electron remains within the sphere of influence of the atom for a longer time.

breakdown voltage starts to have a greater dependence on other factors, such as electrode material and electrode surface conditioning, resulting in unexpected variations in the breakdown voltage. The field emission may become a factor. In the present work, the effect of these other factors was not studied.

5.1.2 Tests in Binary Mixtures of Gases

5.1.2.1 Gas Composition

Previous studies have shown that the gas composition has a strong effect on the breakdown characteristics, however, the effect is not very straightforward, especially when the pressure is high.

For a natural gas fueled SI engine, the main components of the mixture in-cylinder are N_2, O_2, CH_4, CO_2 and H_2O. Since the concentrations of these gases vary cyclically before combustion even when the engine fires at a constant fuel-air ratio, it is important to study the influence on the breakdown voltage of the gas composition. In general, the gas mixture has a breakdown voltage between those of the individual components. However, when one constituent molecule is strongly electronegative[‡], the mixture can have a higher breakdown voltage than either of the constituents. Alternatively, the mixture can also have a lower breakdown voltage than that of either of the constituents as a result of the Penning effect [•] or an unclear reason [Meek and Craggs, 1978]. Since CO_2

[‡] When free electrons are available and attach themselves to neutral atoms or molecules, negative ions are formed. Not all gas atoms can form negative ions. Gases with one or two electrons deficient in their outer shell tend to easily attach one electron, thereby filling the outer shell of the atom and forming singly charged negative ion. These gases, such as oxygen, are therefore known as electronegative gases [Nasser, 1971].

[•] Penning effect: Excitation energy can be exchanged between neutral atoms. In particular, an excited atom can be ionized by virtue of its excitation energy, if the latter is larger than the required ionization energy.

and CH_4 are the most important components of the gas mixture in a NG fueled SI engine, sets of experiments were done in the mixtures of CO_2 and CH_4 (the balance of the two mixtures is N_2) respectively and the results were discussed as follows.

Figure 5-2 presents the effects of CO_2 and CH_4 on V_s. When the pressure is lower than 80 psig, V_s in a mixture of 14.3% CO_2 is slightly higher than that in pure N_2. After the pressure is above 80 psig, the breakdown voltage in 14.3% CO_2 starts to decrease a little in comparison to that in N_2, probably because of the high pressure effect which was related to the electrode surface conditioning as mentioned before. But with 10% CH_4 added to pure N_2, the V_s drops dramatically (compared to V_s in pure N_2), probably due to the lower ionization energy of CH_4 (299 kcal/mole for single ionization comparing to that of N_2 which is 360 kcal/mole), resulting in the decrease of V_s since the breakdown voltage represents the amount of energy transferred to molecules existing between the gap for ionization.

The effect of the concentration of CO_2 on V_s is shown in Fig. 5-3. In general, an increase of CO_2 concentration will increase V_s. This has been shown in the work conducted by Moruzzi and Lucas [1974] in the mixture of air/CO_2[§]. However, in the present experiments, the increase of CO_2 concentration doesn't affect the breakdown voltage very much, especially when the concentration of CO_2 is above a certain level. As

---

Such a process is made more probable if the excited atom is in a metastable state and has thus a longer lifetime in which to undergo a collision. The process is known as the Penning effect and can be an important ionizing agent for discharges in mixtures containing the rare gases, the atoms of which have metastable states of high energy [Howatson, 1976]. Air contains small amount of A_r, but there is no rare gases present in N_2/CO_2 mixture.

[§] In the tests, the gas number density was below the magnitude of 10^{18} cm^{-3}. At room temperature, it can be converted to pressure which was below atmospheric pressure.

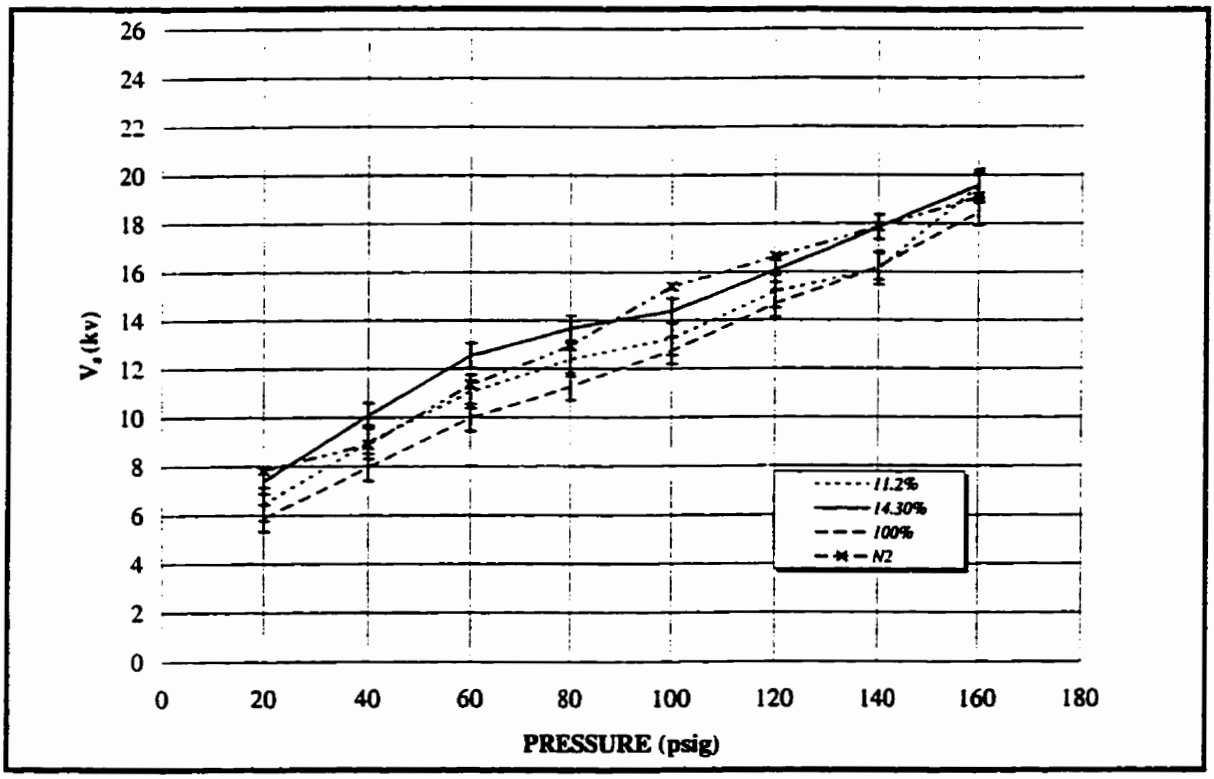

Fig. 5-3 Effects of CO_2 on Breakdown Voltage (d=1.0 mm, T=298 K)

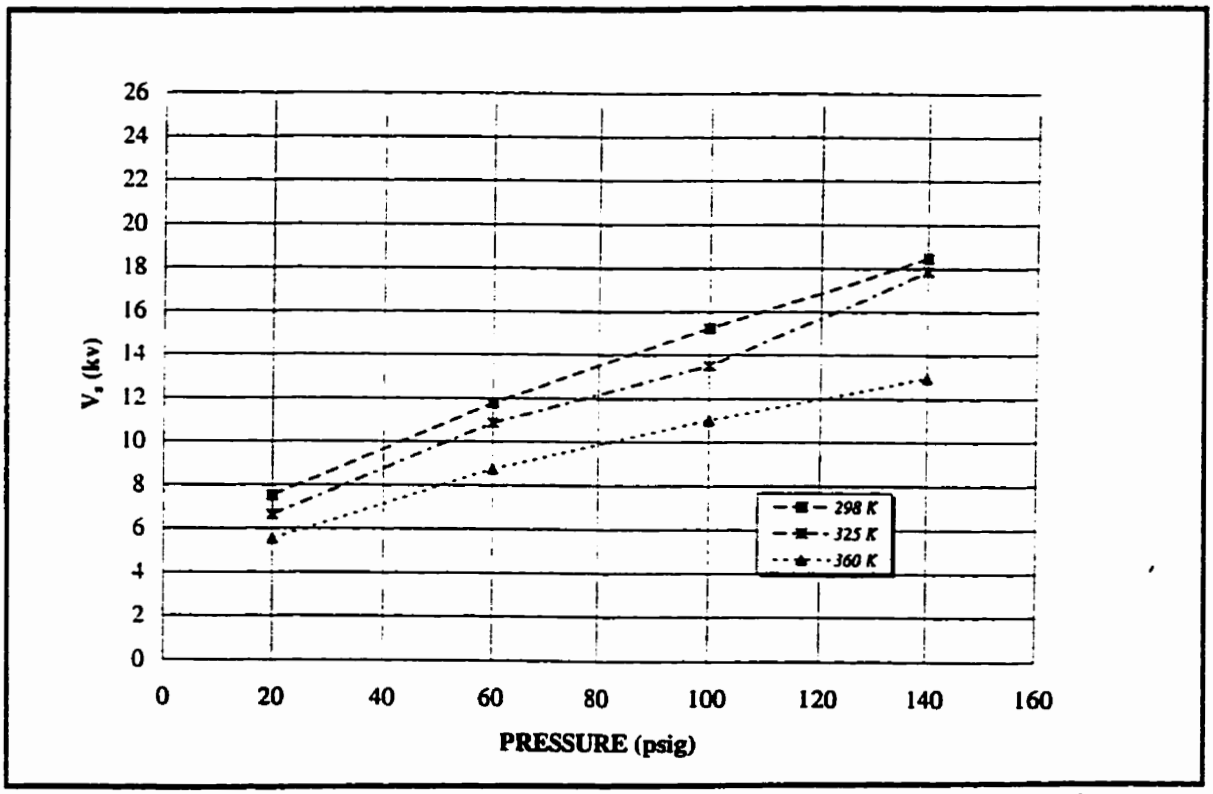

Fig. 5-4 Effect of Temperature on Breakdown Voltage in 14.3% CO_2 (d=1.0 mm)

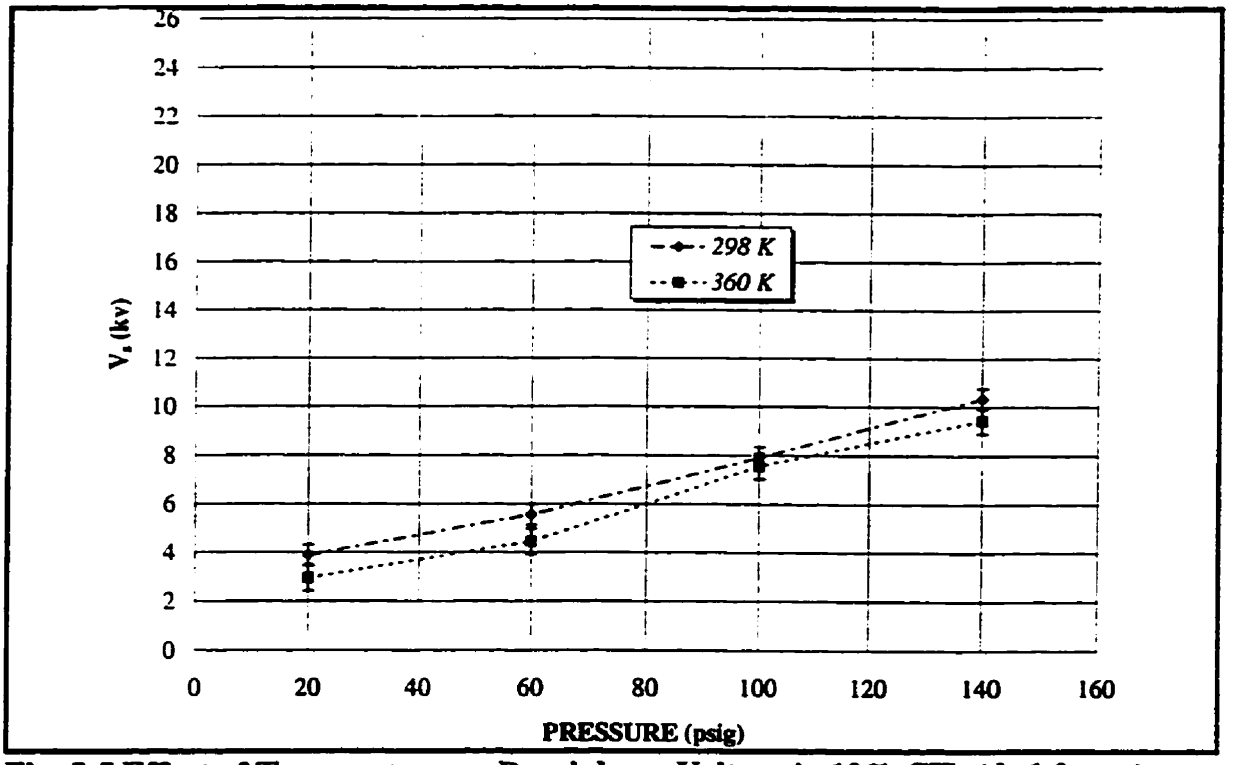

Fig. 5-5 Effect of Temperature on Breakdown Voltage in 10% CH_4 (d=1.0 mm)

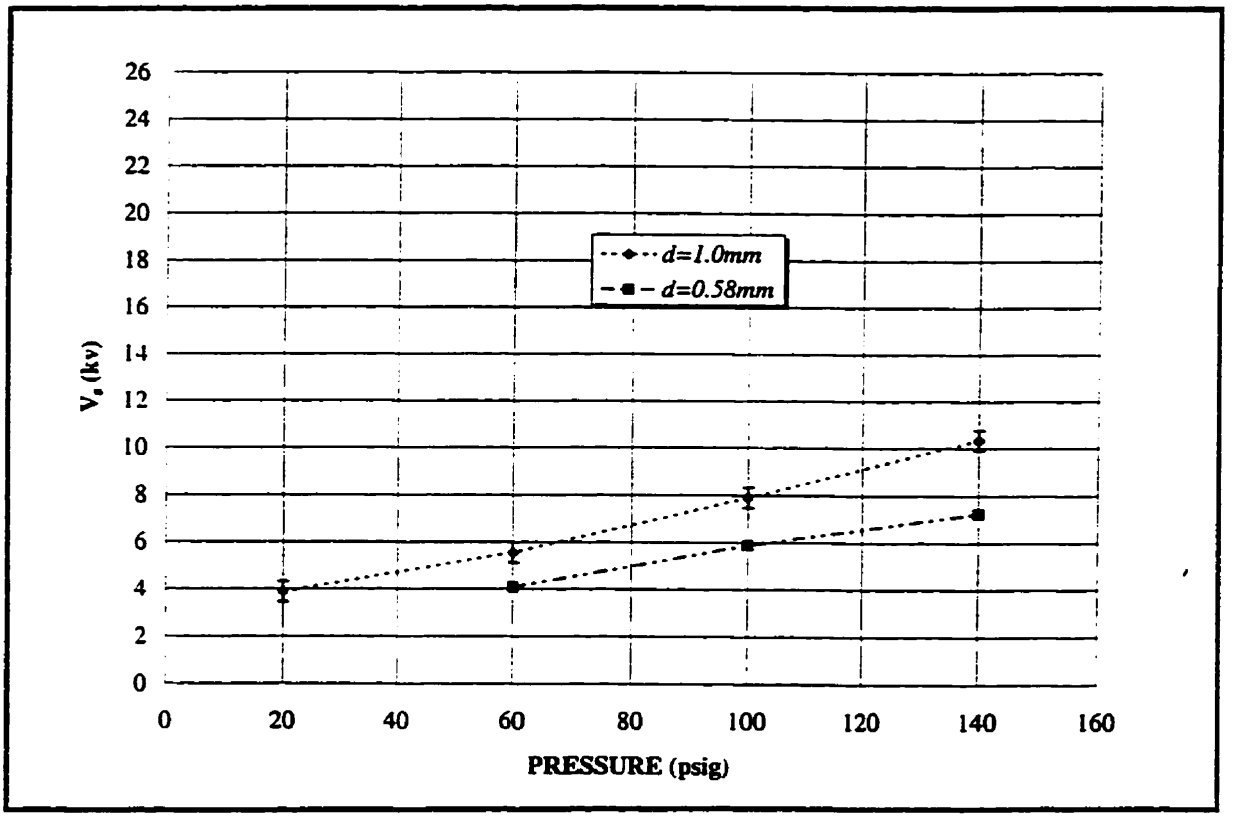

Fig. 5-6 Breakdown Voltage vs. Pressure in 10.0% CH_4 with Different Gap Size

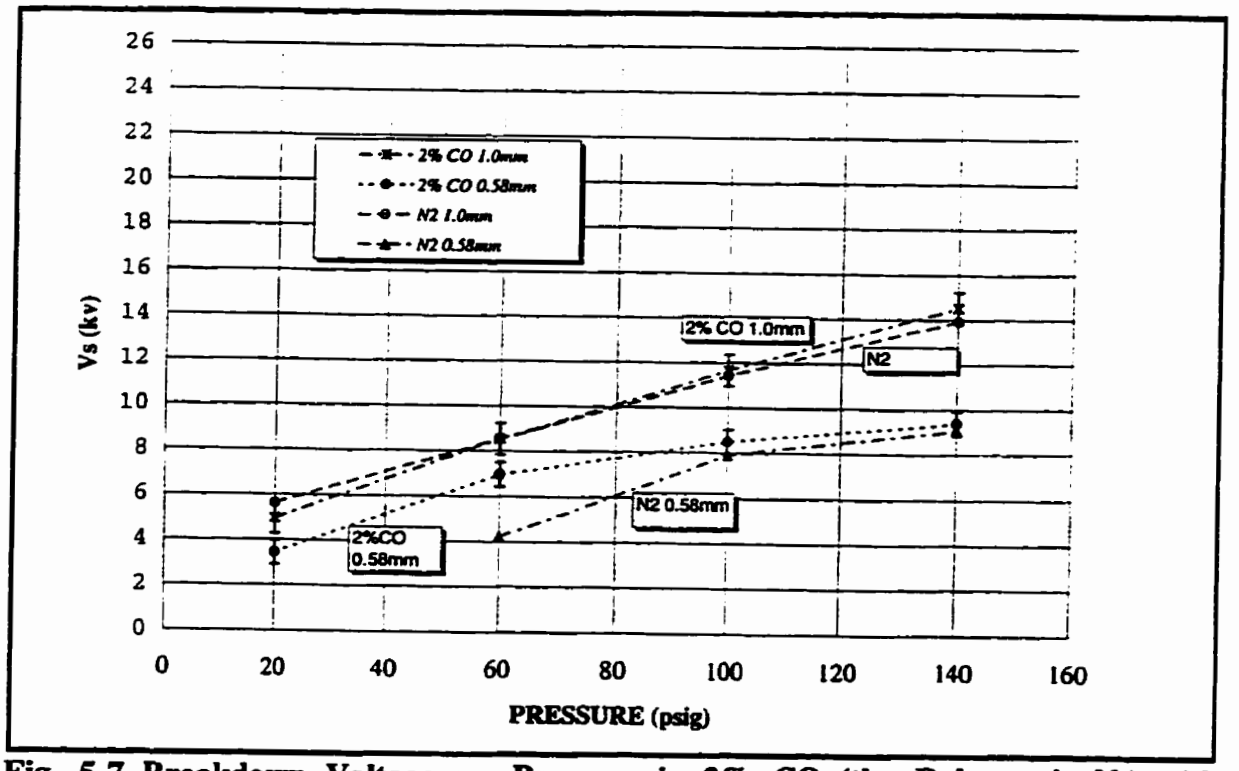

Fig. 5-7 Breakdown Voltage vs. Pressure in 2% CO (the Balance is N_2) with Different Gap Size (T= 298 K)

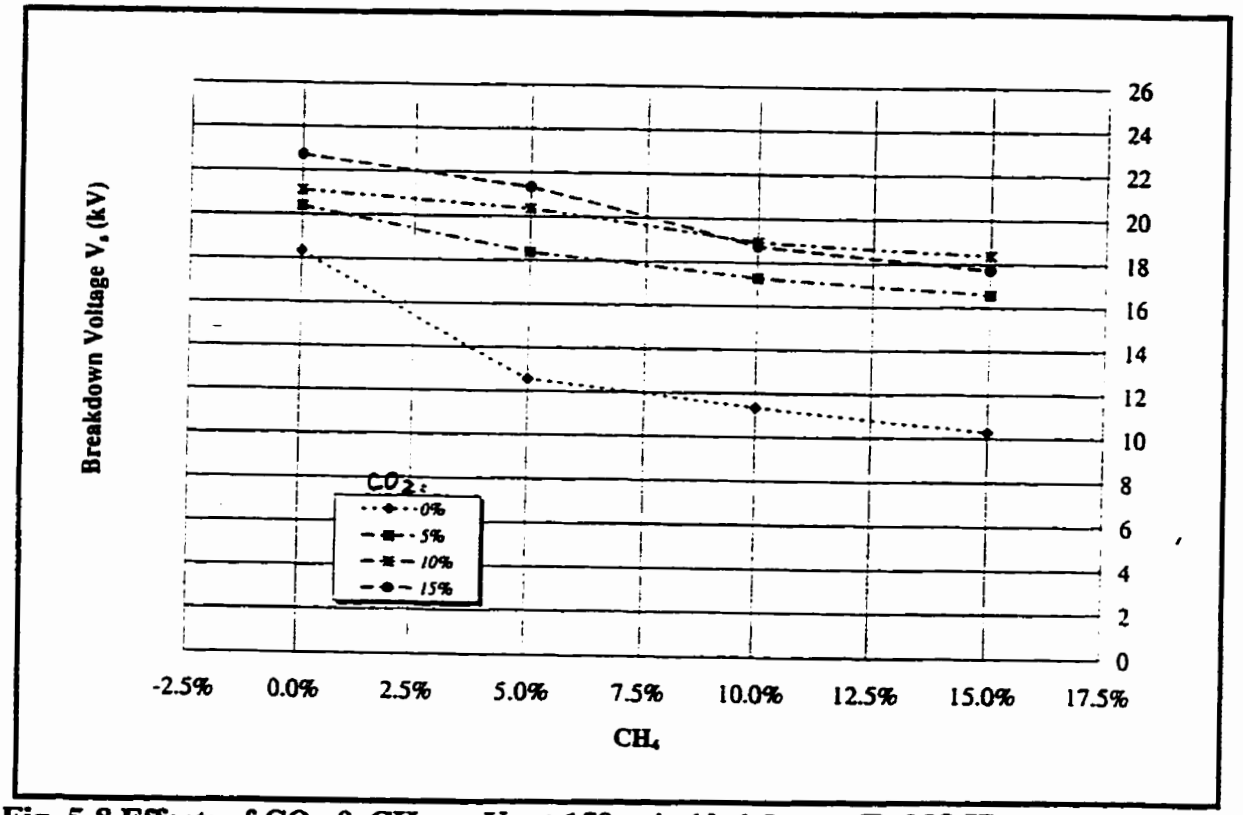

Fig. 5-8 Effects of CO_2 & CH_4 on V_s at 150 psig (d=1.0 mm, T=298 K)

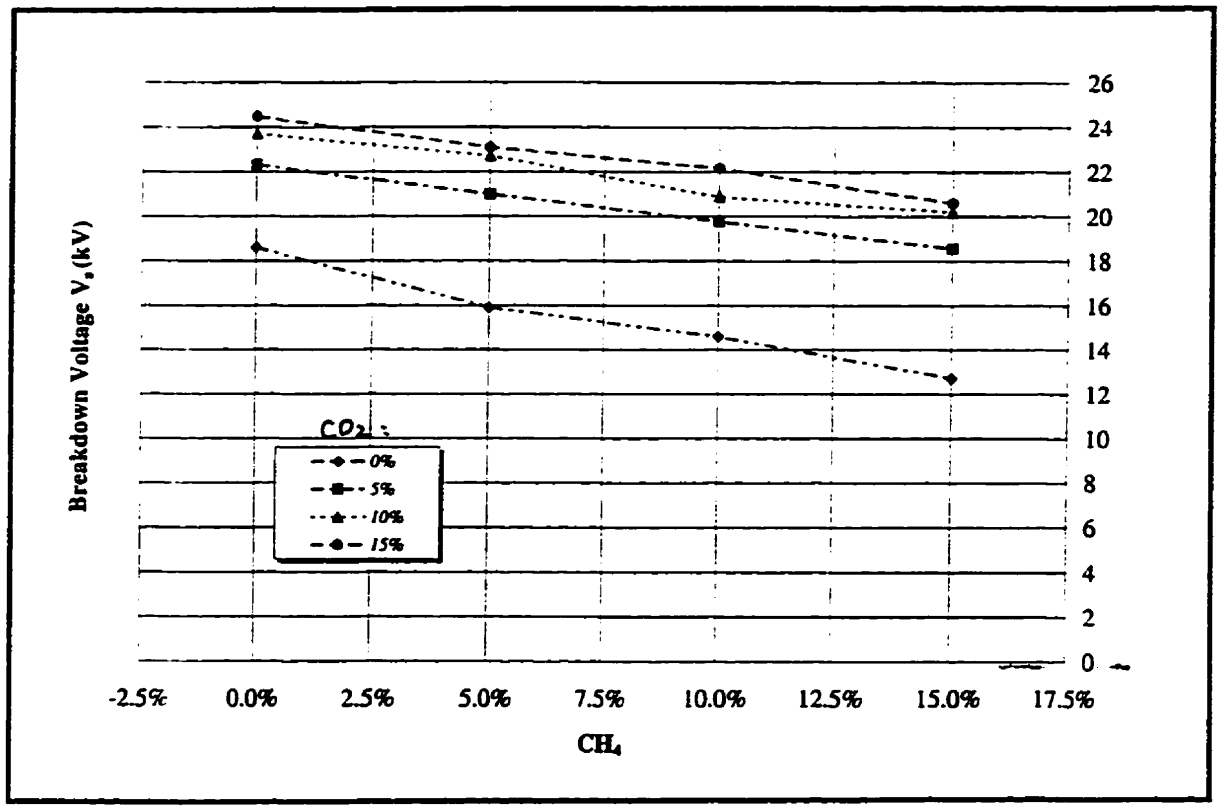

Fig. 5-9 Effects of CO_2 & CH_4 on V_s at 180 psig (d=1.0 mm, T=298 K)

shown in Fig 5-3, the breakdown voltages in 11.2% and 14.3% CO_2 are very close to that in N_2, and the breakdown voltage in 100% CO_2 is lower than that in 11.2% and 14.3%CO_2. The reason that causes these results is not very clear. It is suspected that the electrodes conditioning has a dominant influence in this case. However, the results give some indication that with only CO_2 added to the N_2, the breakdown voltage doesn't change significantly.

5.1.2.2 Temperature

In general, the temperature of the gas in the electrode gap has an effect on V_s as well. The density of the randomly existing electrons in the spark gap decreases with the increase of the temperature at a given pressure. As a result, the mean free path lengthens,

allowing more time for electrons to be accelerated before collision to gain more energy. The higher electron energy increases ionization which reduces V_S. This is shown in Fig. 5-4 and Fig. 5-5 which present the results of the experiments conducted in a 14.3% CO_2 mixture and a 10% CH_4 mixture (all the balance is N_2) respectively. From these two figures, comparing to CO_2 it can be seen that CH_4 is less sensitive to the temperature, probably due to its low ionization potential. Because of the limitation of the equipment** used, the further study of the effect on V_S of the temperature was not done. However, the general effect is quite straightforward.

5.1.2.3 Gap Size

It has also been shown that the electrode materials and conditioning have an influence on the breakdown voltage [Kuffel, E., 1959]. In the present work, only the effect of the gap size of the spark plug has been studied. Figure 5-6 and Fig. 5-7 present the results of the experiments which were carried out in two mixtures (10% CH_4 and 2% CO in N_2) and one pure gas (N_2) for two gap sizes (1.0 mm and 0.584 mm). Clearly, the smaller the gap size, the lower the breakdown voltage. Also as shown in Fig. 5-7, the addition of CO affects the breakdown voltage at the smaller gap size. When 2% of CO is added with N_2, V_S is not significantly different from that in pure N_2 for 1 mm gap. However, an increase of V_s in 2% CO compared to N_2 is apparent when the gap size is smaller. The presence of CO apparently makes the mixture more sensitive to the more uneven electrical field at the smaller gap size. Using the same reasoning as discussed

** The heating equipment used here is a constant temperature bath which only can increase the temperature of the combustion chamber up to around 95 °C.

before at low pressure, when the gap size is smaller, the electrons have relatively less chance to encounter the collisions during the acceleration to the anode and will gain more energy, increasing the probability of the effective collisions which produce more free electrons and ions to help breakdown. Also, the UV radiation emitted by the excited molecules or ions can reach the cathode more directly and easily because of the small gap size, to liberate with high efficiency photoelectrons at its surface. As well, the heavier positive ions arrive at the cathode faster and easier, contributing to the breakdown. Hence, the breakdown can more easily be achieved with the small gap size. In addition, from Fig. 5-6 & Fig. 5-7, it can be seen that the breakdown voltage V_S under the smaller gap size appears to be less pressure sensitive, partially due to the strong absorption of UV radiation at the cathode, which releases electrons from the surface to promote the breakdown phase.

5.1.3 Tests in Three - Component Mixtures

As shown above, the binary mixture compositions tested have different effects on the breakdown voltage. Since CO_2 and CH_4 are important constituents for combustion in a real natural gas fueled SI engine, an additional set of experiments was carried out to study the effect on the breakdown voltage of the concentrations of CO_2 and CH_4, when both are present in N_2, as a foundation of the later combustible mixture tests.

Test #2 (Table 4-2) has been carried out under simulated engine conditions at 150 psig and 180 psig respectively (the reason why these two pressures were chosen is discussed in Appendix B). Figure 5-8 and Fig. 5-9 present the experimental results which

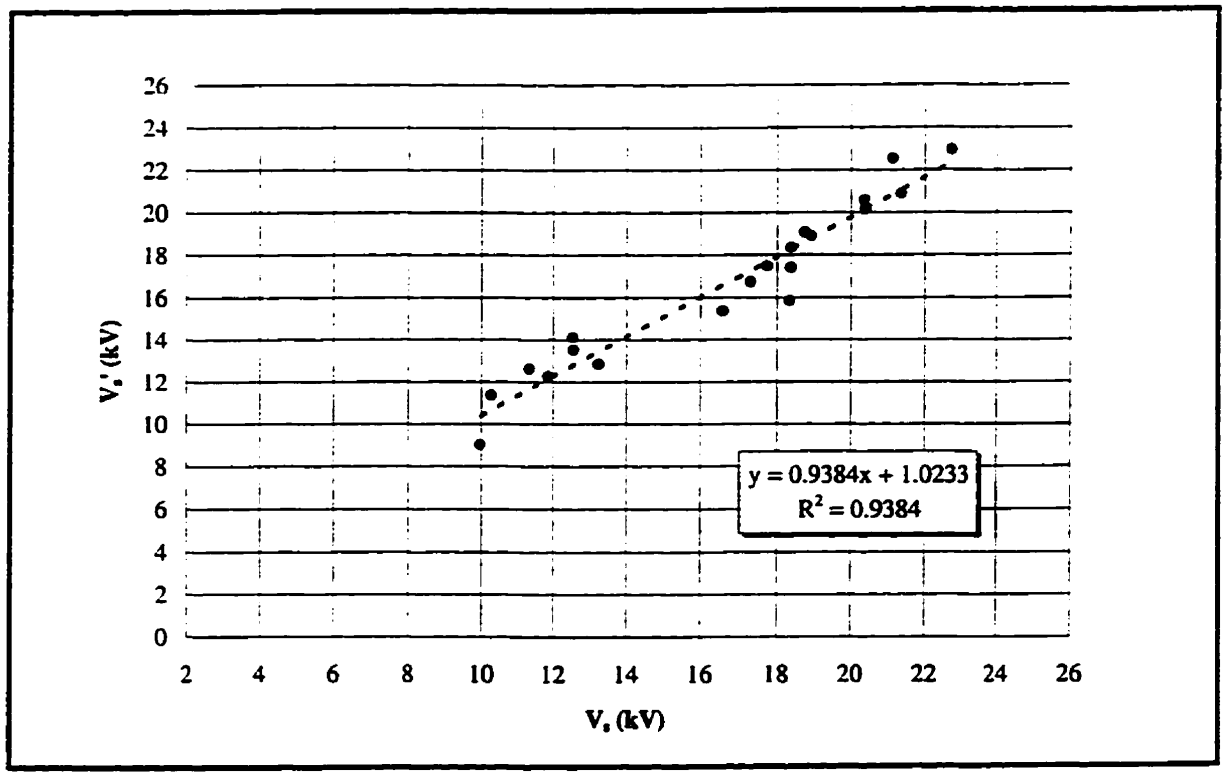

Fig. 5-10 Predicted V_s' vs. Experimental V_s at 150 psig

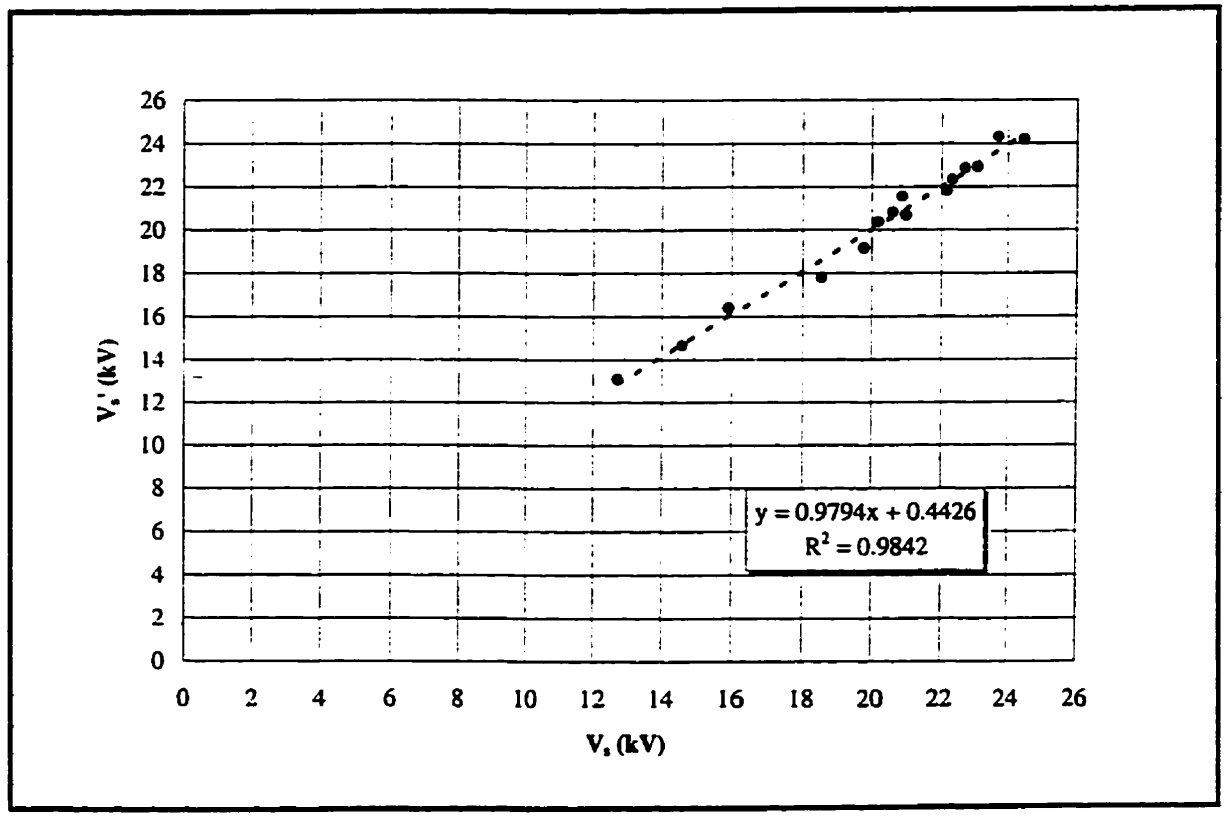

Fig. 5-11 Predicted V_s' vs. Experimental V_s at 180 psig

show the great influence of concentrations of CO_2 and CH_4 (simulating the concentrations of CO_2 from residual gas and CH_4 from fuel gas in an SI engine) on breakdown voltage. It is clear that the addition of CH_4 decreases V_s, while the addition of CO_2 to a stoichiometric combustion mixture increases V_s only within some conditional range.

The addition of CH_4 is believed to create many ions by charge transfer mechanism. The following reactions related to CH_4 show the charge transfer with chemical arrangement with very high reaction rate constant at 10^{-9} (cm^3/s) [Lawton & Weinberg, 1969].

$$CH_4^+ + CH_4 \longrightarrow CH_5^+ + CH_3$$

$$CH_3^+ + CH_4 \longrightarrow C_2H_5^+ + H_2$$

$$CH_2^+ + CH_4 \longrightarrow C_2H_3^+ + H_2 + H \text{ or } C_2H_4^+ + H_2.$$

In addition, the ionization rate would increase when CH_4 content increases, in agreement with the experimental results in Fig. 5-8 and 5-9.

Table 5-1: Electron Affinity

Species	Electron affinity (eV)	Species	Electron affinity (eV)
O	1.47	OH	1.73[††] - 2.65
F	3.5 ± 0.04	H_2O	- 0.9
Cl	3.75 ± 0.05	O_2	0.87 ± 0.13
B_r	3.55 ± 0.05	HO_2	3.04
Cl_2	≤ 1.7	O_3	2.89
B_{r2}	2.6	CO_2	- 3.8[‡‡]
I_2	2.4	CN	3.7 ± 0.2 and 3.2 ± 0.2
		NO_2	1.62

However, when CO_2 is added, since CO_2 is highly electronegtive, the CO_2 removes electrons by electron attachment. Table 5-1 shows the electron affinity for

[††] The lower value appears more reliable.
[‡‡] There is still considerable uncertainty over this.

various gases. A large electron affinity indicates that the gas is more likely to attach electrons. So, CO_2 is very affective at remaining electrons, which, as shown in Fig. 5-8 and 5-9, results in a higher V_s, even when CH_4 is present.

As pointed out before, CO_2 and H_2O are very important components in EGR and residual gas. Because of the lack of an effective mechanism for mixing vaporized H_2O with the mixture in the experimental apparatus, the effect of H_2O vapor on breakdown voltage has not been studied in these non-combustible mixtures tests. However, it has been shown that with increasing humidity, the breakdown voltage increases [Blair, Bruce and Tedford, 1963]. The effect of H_2O vapor in the residual gas on the breakdown voltage was shown in later section of combustible mixtures tests. Nevertheless, concentration related effects of EGR and residual gas fraction on breakdown voltage still need to be studied to a further extent.

The results of the test #2 show that the breakdown voltage correlates with the concentrations of CH_4 and CO_2 very strongly under simulated combustion conditions. In order to understand the relationship between them, a statistical regression analysis has been done, showing that the breakdown voltage value is a function of the concentrations of CH_4 and CO_2 (in terms of $[CH_4]$ and $[CO_2]$ in the equations) under the experimental conditions tested. The regression coefficients are presented in Table 5-2. At room temperature (298K), and pressures of 150 psig and 180 psig, the breakdown voltage in the mixtures of CH_4 and CO_2 (the balance is N_2) can be expressed by Equation 5-1 and Equation 5-2 respectively. In addition, as shown in Fig. 5-10 and Fig. 5-11, the

breakdown voltage values (V_s') calculated through the two equations agree with the measured experimental breakdown voltage values (V_s) very well.

$$V_s'_{150\,psig} = 46.3595\,[CH_4]^2 - 43.6058\,[CH_4][CO_2] - 392.306\,[CO_2]^2 - 36.8179\,[CH_4] + 106.1418\,[CO_2] + 15.8465 \qquad \textbf{Equation 5-1}$$

$$V_s'_{180psig} = 26.8943\,[CH_4]^2 + 77.8081\,[CH_4][CO_2] - 423.5044\,[CO_2]^2 - 38.1214\,[CH_4] + 103.3528\,[CO_2] + 18.2133 \qquad \textbf{Equation 5-2}$$

Table 5-2: Regression Coefficients of Statistics Analysis under Two Conditions

Variables	Regression coefficients	
	150 psig	**180 psig**
$[CH_4]^2$	56.28965	32.655
$[CH_4][CO_2]$	- 52.9462	97.47456
$[CO_2]^2$	- 476.338	- 514.219
$[CH_4]$	- 44.7043	- 46.287
$[CO_2]$	128.8774	125.4909
Interception	19.24086	22.11464

Clearly, equations 5-1 and 5-2 show good correlation between the breakdown voltage and the concentrations of CH_4 and CO_2. Since CH_4 and CO_2 are the two important components of a natural gas fueled SI engine's in-cylinder charge, there is a good potential to use the breakdown voltage to help determine the composition of the engine mixture under operating conditions. In the later combustible mixtures tests, the

breakdown voltage was also measured along with the measurements of the light emission to help understand the effect of the residual gas so as to achieve the goal of determining the gas composition in-cylinder before combustion.

5.1.4 Discussion of Agreement with Paschen's Law

The results of V_s measurements which were carried out non-combustible mixtures under various conditions give strong evidence that V_s is an efficient parameter which represents gas properties appropriately. In order to apply the experimental results to a wider range, it is of interest to study the agreement between the experimental results and some relevant theory.

It has been shown that the breakdown voltage depends on the composition and number density of the gas, the material and state of the electrodes, and the degree of pre-existing ionization [Meek and Craggs, 1978]. Townsend developed a generalized theory of breakdown by considering the overall effect of the primary ionization processes, as well as collision processes which change the state of ionization. The primary ionization process occurs when an electron, accelerated in an imposed electric field, collides with a neutral molecule to create another electron and a positive ion. Collision processes which change the state of ionization include:

(a) *secondary ionization processes* in which atoms which have received energy in a primary ionization process contribute to further ionization by the gas by positive ions or photons or by the release of an electron from the cathode due to impact of a positive ion, photon or excited atom;

(b) *electron attachment* in which an electron attaches to a neutral molecule to create a negative ion;

(c) *electron detachment* in which an electron is removed from a negative ion by collision;

(d) *ion conversion processes* in which collisions with gas molecules convert an ion from one species to another.

The latter three processes are most important at high pressures in electronegative gases.

Townsend recognized that the voltage required for electrical breakdown depends on the behavior of the electrons and ions contained in the spark gap and that the ratio E/n was the appropriate parameter to characterize this behavior, where E is the average electric field strength = $V_{applied}/d$, d is the gap size (cm) and n is the number density of molecules in the spark gap [Meek and Craggs, 1978]. Note that the sharp edge geometry of the spark plug electrodes results in locally concentrated regions of the electric field so that the real E is much more higher than suggested by this formular. The following discussion is based on that given by Lawton and Weinberg [1969].

For a simple case where a potential V is applied across two plane electrodes separated by a distance d, if the potential is large enough to cause secondary ionization, an electron emitted from the cathode will be accelerated by the electric field and will undergo ionizing collisions which create additional electrons. If α is the number of ionizing collisions per cm of path in the direction of the field, then the increase in electron current along the path length δx is given by,

$$\delta i = i \, \alpha \, \delta x$$

Integrating over the electrode separation distance gives:

$$\ln(i_a/i_c) = \alpha\, d$$

where i_c and i_a are the electron currents emitted by the cathode and collected by the anode respectively. The positive ions created by the electron collisions create a current which is collected by the cathode. This positive current is given by:

$$i_o = (e^{\alpha d} - 1)i_c$$

As noted above in the definition of secondary ionization processes, positive ions as well as excited atoms and photons which strike the cathode can cause the emission of an electron. If γ designates the probability of electron emission per ion striking the cathode, it can be shown that

$$i_a/i_c = e^{\alpha d}/\{1 - \gamma(e^{\alpha d} - 1)\}$$

Breakdown occurs when the current increases sharply to a very high value. From the equation above, this occurs when the denominator = 0 or when

$$1 = \gamma(e^{\alpha d} - 1) \qquad \textbf{Equation 5-3}$$

It can also be shown that α depends on the applied electric field as expressed (approximately) by the following equation:

$$\frac{\alpha}{n} = Ae^{\frac{-B}{E/n}}$$

where A and B are constants depending on the gas and n is the number density of molecules in the spark gap. Substituting this expression for α in the equation for breakdown, recognizing that V = Ed and solving for V gives

$$V_s = \frac{B(nd)}{C + \ln(nd)} \qquad \textbf{Equation 5-4}$$

where $C = \ln\left(\frac{A}{\ln(1+\frac{1}{\gamma})}\right)$ and the subscript s indicates the breakdown condition.

This equation shows that the breakdown voltage is a function of the product (nd) or

$$V_s = f(nd)$$

which is an empirical relation known as Paschen's Law.

In order to compare the experimental results to this empirical Paschen's Law, all the testing parameters, such as P and T, were converted to (nd) and the logarithmic terms of V_s and (nd) were calculated and plotted as ln(Vs) vs. ln(nd) as shown in Fig. 5-12. Also, a few series of data extracted from the previous studies [Cobine, 1958; Meek & Craggs, 1974] (pd was converted to nd to account for the effect of temperature at constant pressure on the mean free path) were plotted as ln(Vs) vs. ln(nd) in Fig. 5-13. In addition, the predicted values obtained from Paschen's Law[§§] (from Equation 5-4) were presented in both figures for comparison. From Fig 5-12, it can be seen that at high value of (nd), the experimental results diverge slightly from the prediction of the ideal Paschen's Law. This divergence from the ideal prediction is probably due to the different electrodes used in the experiments. In the derivation of Paschen's Law for V_s, all the assumptions were considered for parallel plane electrodes only which provides very even field strength. But the configuration of the spark plug electrodes in the present work is different from the plane electrodes. In addition, irregularities on the spark plug surfaces caused by

§§ There is not enough information of the values of γ (Nickel), A and B for different gases, here, hence γ was chosen as 0.036 in air. As well the values of A , B were chosen to be 14.6, 365 and 0.036 respectively for air too[Cobine, 1958].

accumulation of carbon or ash and by abrasions, will lead to crowding of lines of forces on protuberances, which can result in premature breakdown. Hence, the tested V_s shows a lower value than the prediction. This divergence is also shown in the other experimental results which can be seen from Fig 5-13, although these literature values are for parallel plate electrodes or some other electrodes which have less effects on the electrical field compared to the spark plug electrodes have.

Returning to the equation for the breakdown condition, it contains 3 parameters, A, B and γ, each of which will be discussed in turn.

Table 5-3: Value of γ for Different Cathodes and Different Gases

Gas / Metal	Ar	H_2	He	Air	N_2
Al	0.120	0.095	0.021	0.035	0.100
Cu	0.058	0.050	N/A	0.025	0.066
Fe	0.058	0.061	0.015	0.020	0.059
Ni	0.058	0.053	0.019	0.036	0.077
Pt	0.058	0.020	0.010	0.017	0.059

The parameter γ, the number of electrons emitted from metals per impacting positive ion, should depend on the cathode material as well as the gas which provides the ions. Table 5-3, extracted from Table 7.3 of Cobine [1958], shows both effects. In the present experiments, the electrode material has about 90% Nickel. The remaining (unknown) composition may have significant effect on work function of the surface which determins the rate of electron generation. However, a later study [Llewellyn-Jones, 1957] conducted with hydrogen showed that differences between cathode materials become unimportant at values of pd (or nd) greater than 10 mmHg-cm. At room

temperature (T = 298K), this pd value of 10 mmHg-cm can be converted to nd which equals to 3.24×10^{21} (molecules/m^2) and ln(nd) = 49.53. Lawton and Weinberg [1969] caution that, although this means that the cathode material is not important at typical combustion system pressures, surface irregularities such as carbon buildup can concentrate electrical lines of force on protrusions and lead to premature breakdown. With respect to gases, Lawton and Weinberg also point out that the denominator C + ln (nd) reduces to ln (nd) when

$$(pd) >> \left(\frac{A}{\ln(1+\frac{1}{\gamma})} \right), \text{ or } (nd) >> 3.24 \times 10^{20} \left(\frac{A}{\ln(1+\frac{1}{\gamma})} \right)$$

For typical values of γ from the table above, the denominator is on the order of 50. Values of A are < 50, so (pd) > 10, or (nd) > 3.24×10^{21} satisfies this condition. In the present experiments, $(pd)^{***} \geq 90.4 >> 10$, or $(nd) \geq 2.73 \times 10^{22} >> 3.24 \times 10^{21}$, so the breakdown criteria may be simplified to

$$V_s = B \frac{(nd)}{\ln(nd)}$$

which indicates even more clearly the functional form of Paschen's law.

In order to further understand V_s, it is necessary to get some insight into the parameters of A and B. Hence, the sensitivity of V_s to both A and B was studied. Same as before, the ln(Vs) vs. ln(nd) values were calculated and plotted in Fig. 5-14 and Fig 5-15 with different values of A and B[†††], respectively. Evidently, the change of A only changes

*** The minimum value of (pd) was calculated with the lowest value of p (20 psig) and smallest size of d (~ 0.54 mm).

††† Again, same as mentioned before, the values of γ (Nickel), A and B were chosen as 0.036, 14.6 and 365 respectively for air due to the lack of information [Cobine, 1958].

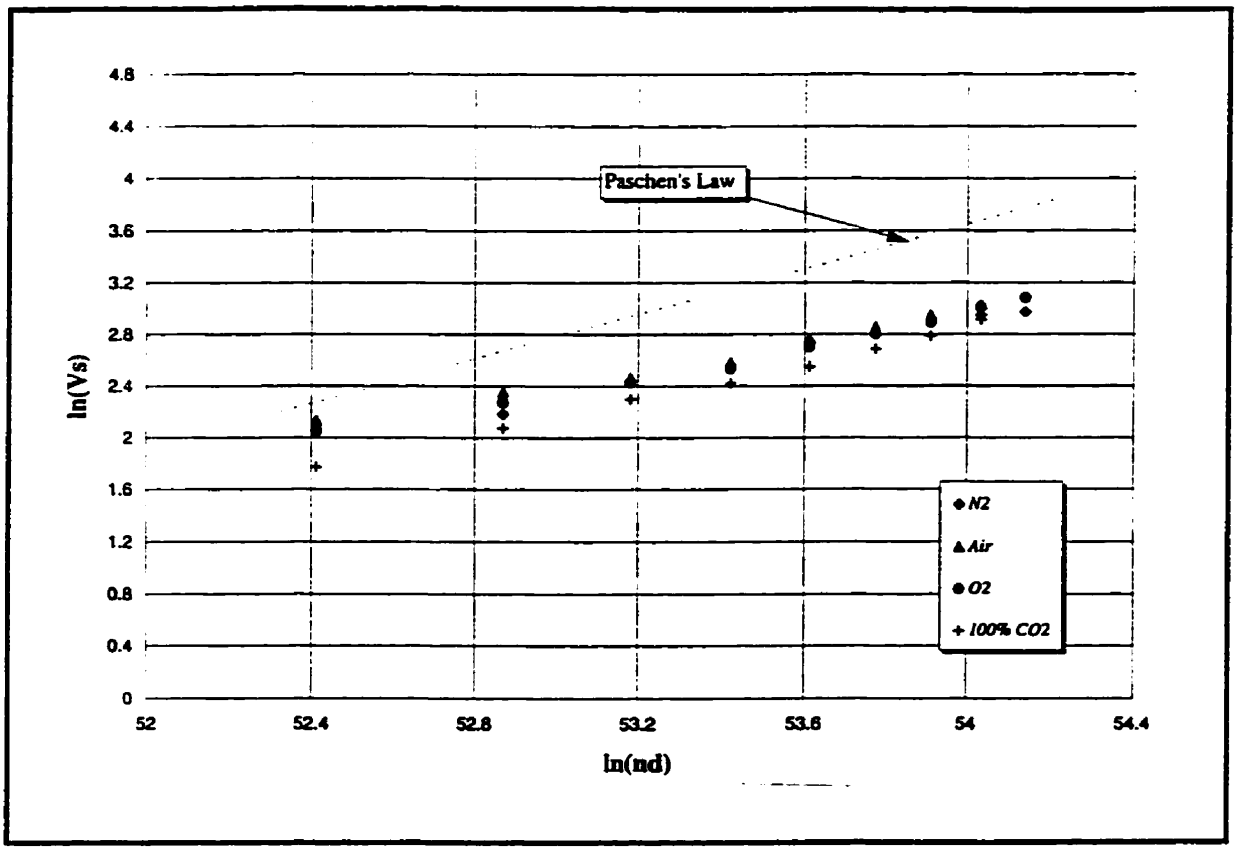

Fig. 5-12 ln(V_s) vs. ln(nd) for Experimental Results

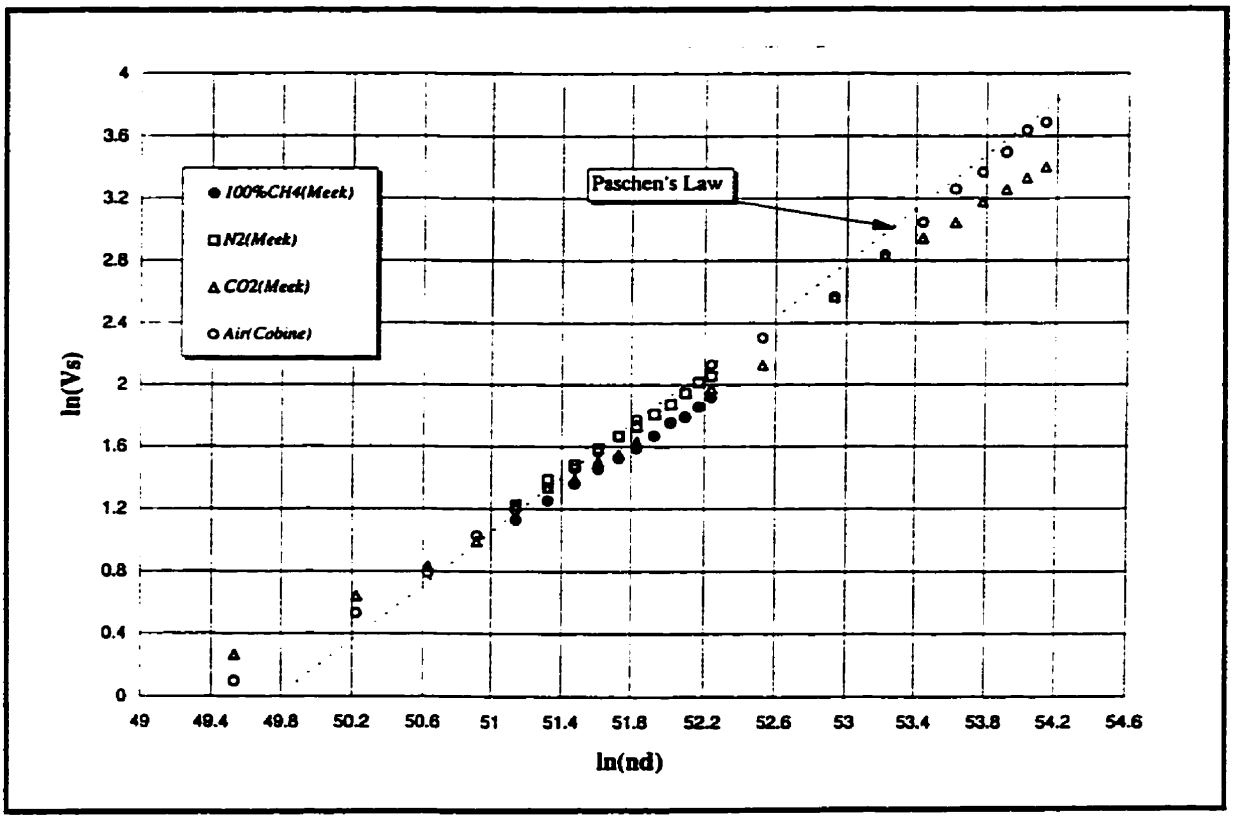

Fig. 5-13 ln(V_s) vs. ln(nd) for Previous Experimental Results

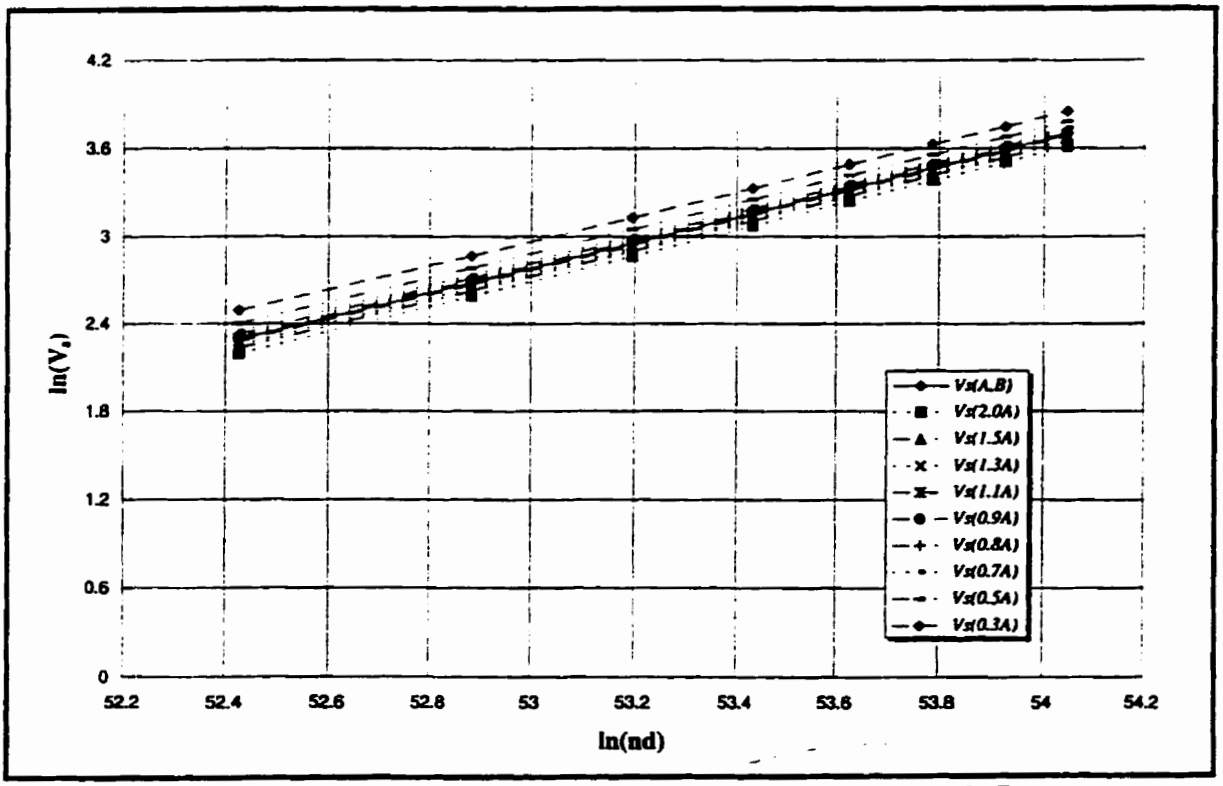

Fig. 5-14 ln(V_s) vs. ln(nd) for Different A with Constant B (Paschen's Law)

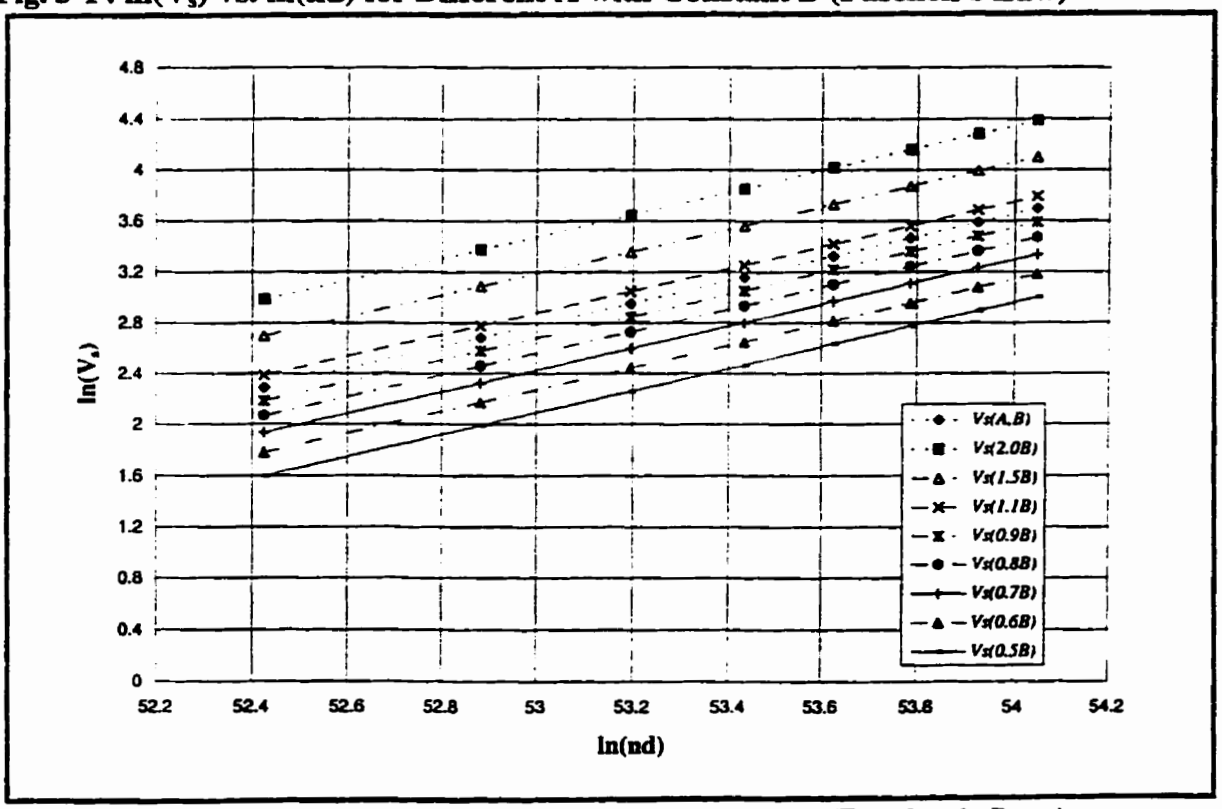

Fig. 5-15 ln(V_s) vs. ln(nd) for Different B with Constant A (Paschen's Law)

the curves of ln(Vs) vs. ln(nd) very slightly, while only a small change of B shifts the ln(Vs) vs. ln(nd) curves significantly, indicating the strong dependence of V_s on B.

Based on the assumptions made in Townsend's theory, i.e. that the electrons do not gain energy by collision, that the field is so strong that the electrons always move in the direction of the field, that the probability of ionization is zero for energies less than eV_i', and is unity for energies greater than eV_i', where V_i' is a sort of effective ionization potential for electron collisions but is not the true ionization potential of the particles. However, it can be regarded as the representative of the ionization potential in this discussion. It has been shown that, B has the value of the product of A and V_i' only. Since for different gases, A appears to be very constant, hence it is reasonable to assume that B represents an alternative value of the ionization potential of a gas. As listed in Table 5-4, different gases have significantly different ionization potentials, indicating that B can be an efficient factor which relates V_s to the gas properties appropriately. The following study gives an evidence that the gas composition has a strong effect on the breakdown voltage.

As assumed above, since B is the representative of the ionization potential of a gas, a simple equation can be made as follows,

$$\frac{B_X}{B_{N_2}} = \frac{V_{i_x}}{V_{i_{N_2}}}$$

Hence, if B_{N_2} is known, B_X can be easily determined. In order to obtain the approximate value of B_{N_2}, ln(V_s) and ln(nd) were calculated from the results of the experiments done

Table 5-4: Ionization Potentials of Some Relevant Experimental Gases [Cobine, 1958]

Species	Probable ionization process	Ionization Potential V_i (eV)	Difference of Ionization Potential (V_i-V_{IN2})	Ionization Potential Relative to N_2 (V_i/V_{IN2})
N_2	$N_2 \rightarrow N_2^+$	15.57	0	1
	$N_2 \rightarrow N^+ + N$	24.5		
O_2	$O_2 \rightarrow O_2^+$	12.5	-3.07	0.7836
	$O_2 \rightarrow O^+ + O$	20		
CO_2	$CO_2 \rightarrow CO_2^+$	14	-1.57	0.8889
	$CO_2 \rightarrow CO + O^+$	19.6		
	$CO_2 \rightarrow CO^+ + O$	20.4		
	$CO_2 \rightarrow C^+ + O + O$	28.3		
CO	$CO \rightarrow CO^+$	14.1	-1.47	0.9024
	$CO \rightarrow C^+ + O$	22		
	$CO \rightarrow C + O^+$	24		
	$CO \rightarrow CO^{++}$	44		
CH_4	$CH_4 \rightarrow CH_4^+$	12.6	-2.97	0.8092
	(uncertain)			
H_2O	$H_2O \rightarrow H_2O^+$	12.59	-2.98	0.8092
	$H_2O \rightarrow HO^+ + H$	17.3		
	$H_2O \rightarrow HO + H^+$	19.2		

in N_2 and were plotted. By extrapolating, B_{N_2} was determined as 0.7B. Taking CH_4 as an example[‡‡‡], hence, $B_{CH_4} = 0.8092 * 0.7B = 0.5664B$. As inferred by Fig 5-15, the line of the ln(Vs) vs. ln(nd) with the value of 0.5664B shifts below the line with 0.7B. To some

[‡‡‡] Other gases show good agreement with N_2 in this study.

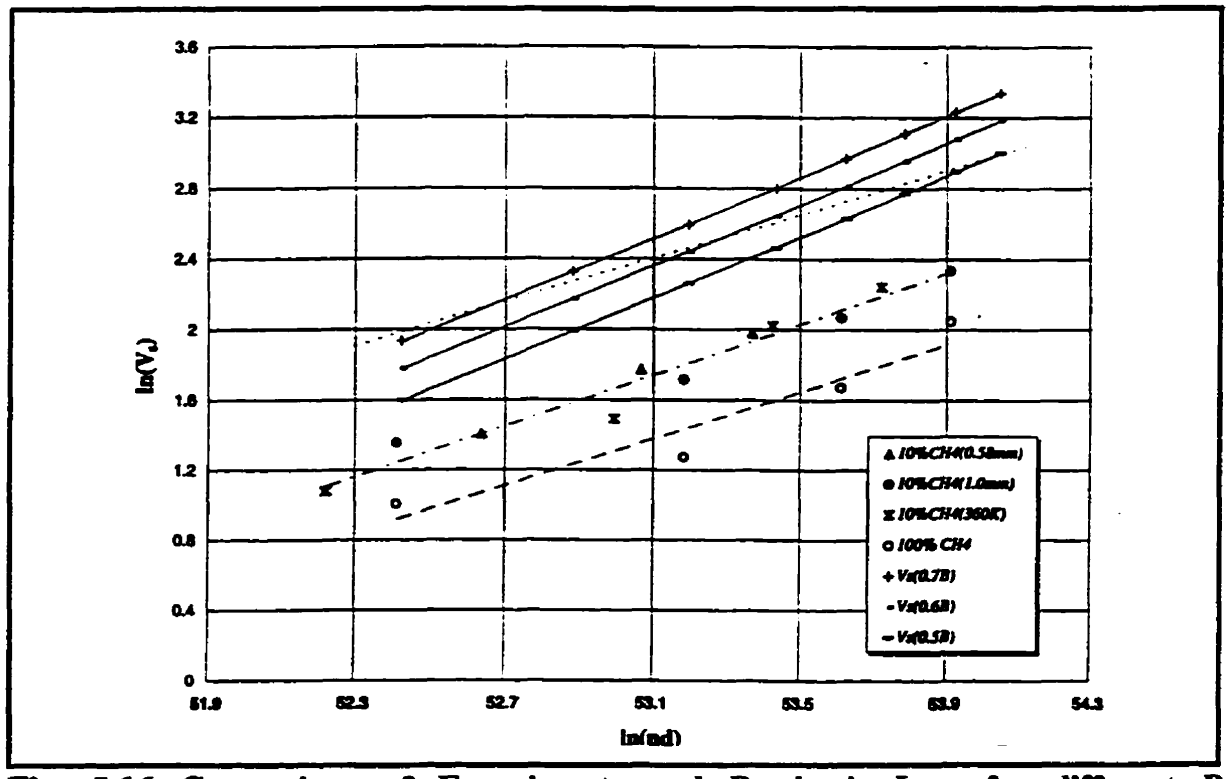

Fig. 5-16 Comparison of Experiments and Paschen's Law for different B (A=constant)

extent, the experimental results obtained with CH_4 agree with this prediction. As shown in Fig. 5-16, when the value of B changes from 0.7B to 0.5B, the three predicted ln(Vs) vs. ln(nd) lines with 0.7B, 0.6B and 0.5B were shifted downward, however, they appear to be parallel to each other. For the experimental results, the three ln(Vs) vs. ln(nd) lines of N_2, 10% CH_4 (with 90% N_2)[§§§] and 100% CH_4 show the same characteristics, even though there are large discrepancies between each other. As mentioned before, this difference is probably caused by the special configuration of the spark plug electrodes as well as the irregularities on the spark plug surfaces caused by accumulation of carbon or ash and by abrasions, leading to crowding of lines of forces on protuberances, which can

[§§§] There is not enough information about the ionization potential of this mixture. However, it can be calculated roughly according to the concentrations of the mixture components as the following, $V_{10\%CH_4} = 10\%V_{100\%CH_4} = 90\%V_{N_2} \approx 15$, hence, $B_{10\%CH_4} = 0.65B$.

result in lower value of V_s. However, Fig. 5-16 gives an evidence that the gas properties determine B, which in turn influences the breakdown voltage. All of the above discussion can be a foundation of the combustible mixtures tests.

5.2 Breakdown Voltage Measurements in Combustible Mixtures

The results of the breakdown voltage measurements in non-combustible mixtures have shown that the breakdown voltage has a strong dependence on the pressure, the temperature, the spark plug gap size and the gas composition. It has also been shown that the breakdown voltage varies with the fuel-air ratio in production engines [Ohyama, 1990; Merer, 1994]. In order to make use of the breakdown voltage measurements in determining the fuel-air ratio with residual gas under engine operating conditions, some additional experiments have been carried out in the same experimental combustion chamber as used in the non-combustible mixture tests. The advantage of using this simulated combustion chamber is the ease and accuracy of controlling the mixture composition as well as the fraction of the residual gas. To simulate the real engine combustion conditions, the temperature was maintained at ~275 °F (~135 °C) to avoid the condensation of H_2O and the pressure was maintained at 150 psi which is very similar to the pressure in-cylinder before spark ignition (with sparking time at 30° BTDC).

5.2.1 Tests without Residual Gas

In general, the flammability limits of CH_4 is 5% (by volume)**** for a lean mixture and 15% for a rich mixture. For a natural gas (100% CH_4 is used for simplicity in

**** Hereinafter all of the concentrations are shown in % is by volume.

the present work) fueled SI engine, the fuel-air equivalence ratio ranges from 0.7 (quite lean) to 1.1 (rich) generally. Hence, the combustible mixture tests were carried out within this operating range. On different days, several sets of experiments were done from lean to rich without residual gas or vice versa and the results were presented in Fig. 5-17. The small variations from day to day are probably caused by changing and cleaning the spark plugs, resulting in a change in the surface condition of the electrodes and/or possibly the gap size is not set exactly the same each time. Obviously, in these tests, when the fuel-air equivalence ratio changes from 0.7 to 1.1, the measured breakdown voltage does not change very significantly even though there appears to be a downward trend as ϕ is increased. In addition, the calculated V_s (by EQ. 5-1 for non-combustible mixtures of CH_4, CO_2 and N_2 at room temperature) were shown in the same figure for comparison. Same as the experimental results, the predicted V_s doesn't decrease very much with the increase of ϕ. Although this result is different from those of the previous study by Ohyama [1990] and Merer [1994], it is not surprising. The previous work was done in engines, one is a conventional 4-cylinder 4-cycle 1.8 L SI unit and the other one is a single-cylinder Waukesha CFR engine. For engines, when the fuel-air equivalence ratio changes, the flame temperature of the combustion varies. The flame temperature increases when the mixture changes from lean to stoichiometric and the highest flame temperature occurs when the mixture is slightly richer (ϕ = ~1.05). After the peak, the temperature decreases when the mixture becomes richer and richer until the rich flammability limit is reached [Glassman, 1987]. This is because of the change of the specific heat of the mixtures. With the residual gas left from the last cycle, the

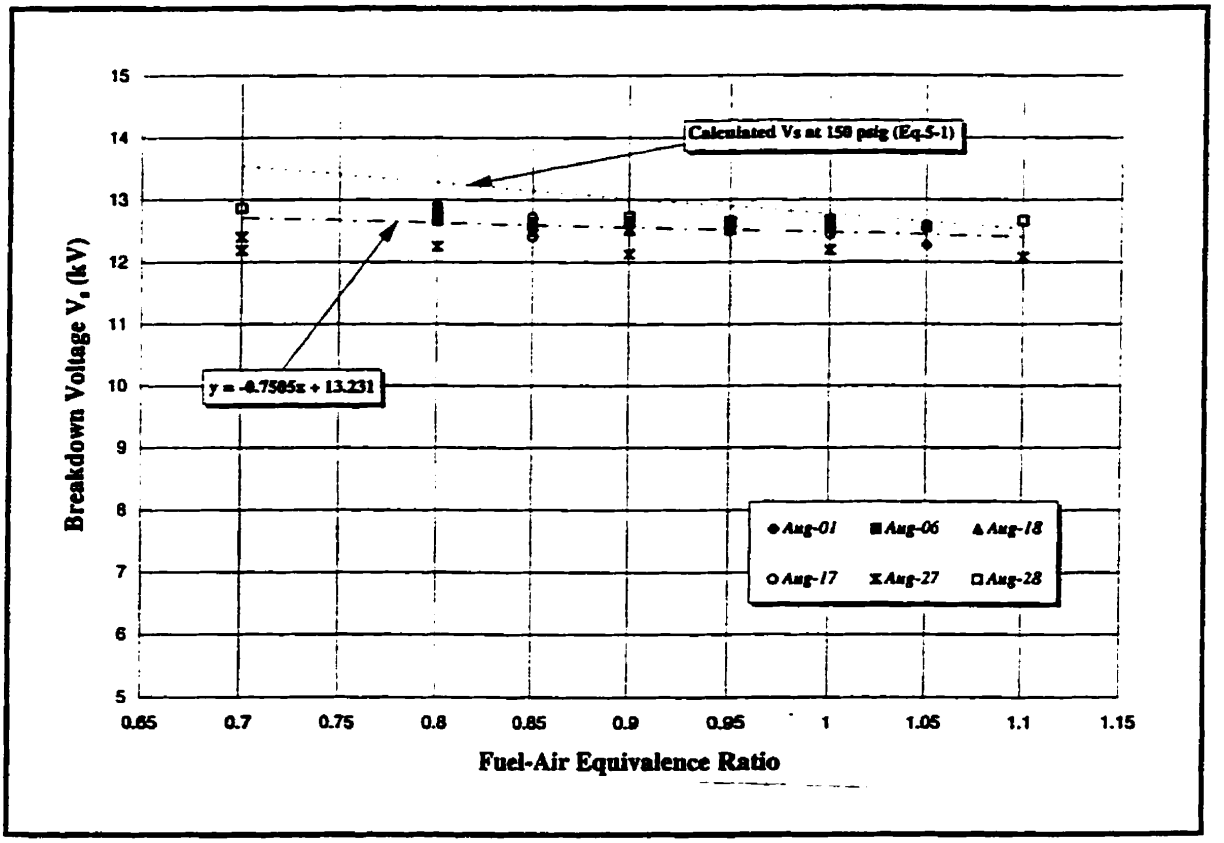

Fig. 5-17 Effect of the Fuel-Air Equivalence Ratio on the Breakdown Voltage

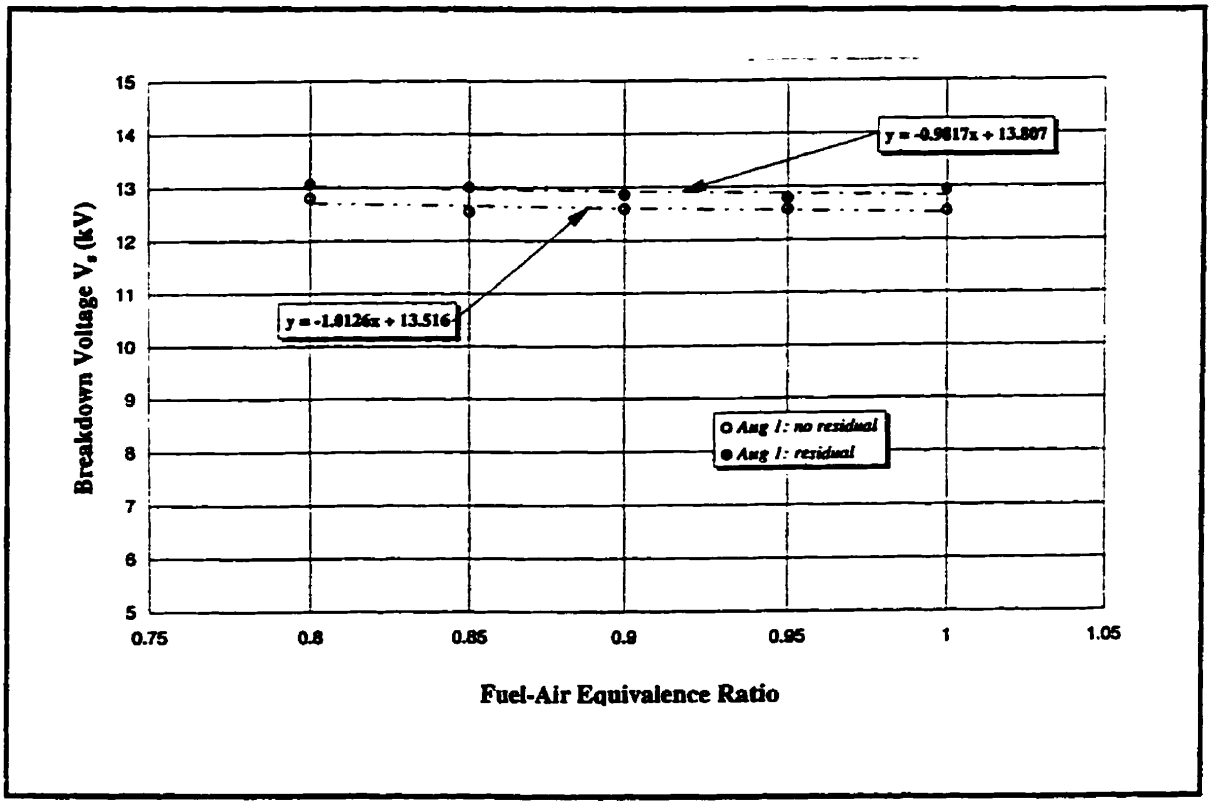

Fig. 5-18 Effect of the Residual Gas Fraction on the Breakdown Voltage (1)

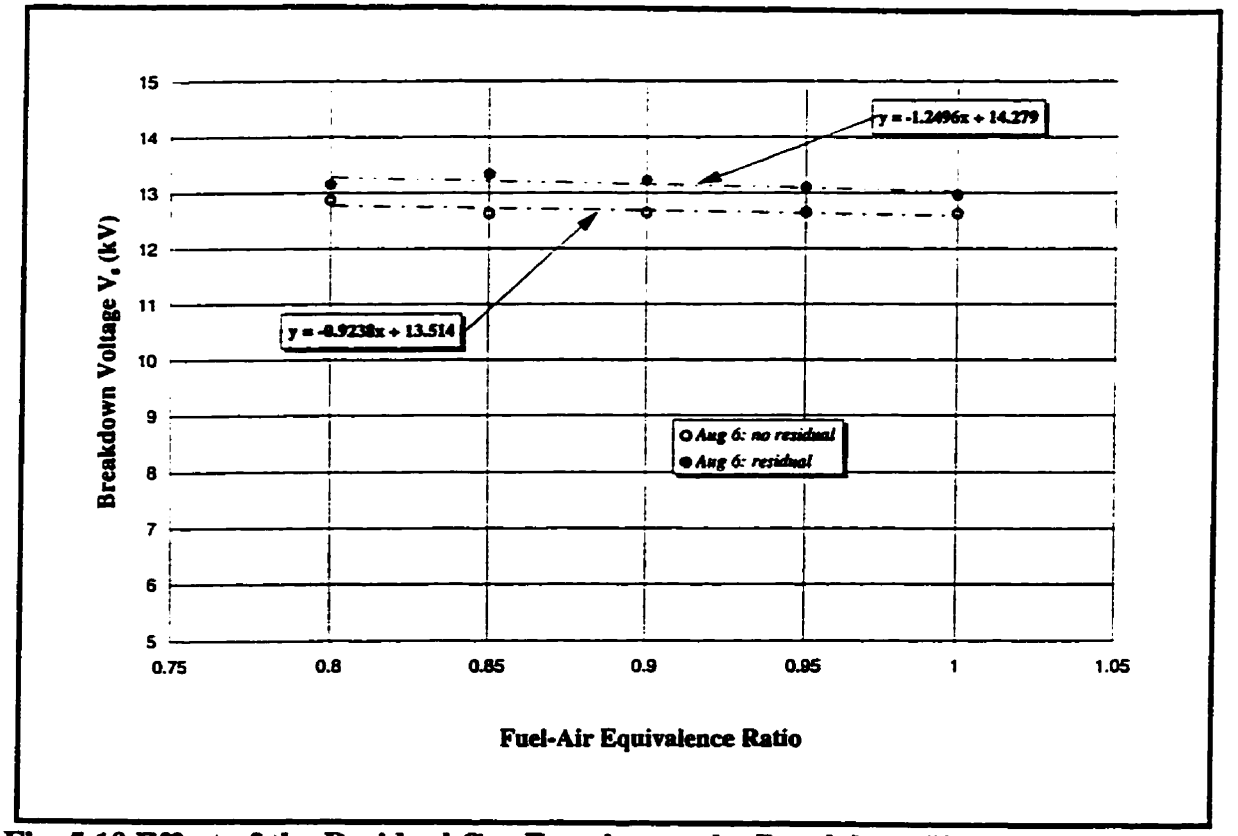

Fig. 5-19 Effect of the Residual Gas Fraction on the Breakdown Voltage (2)

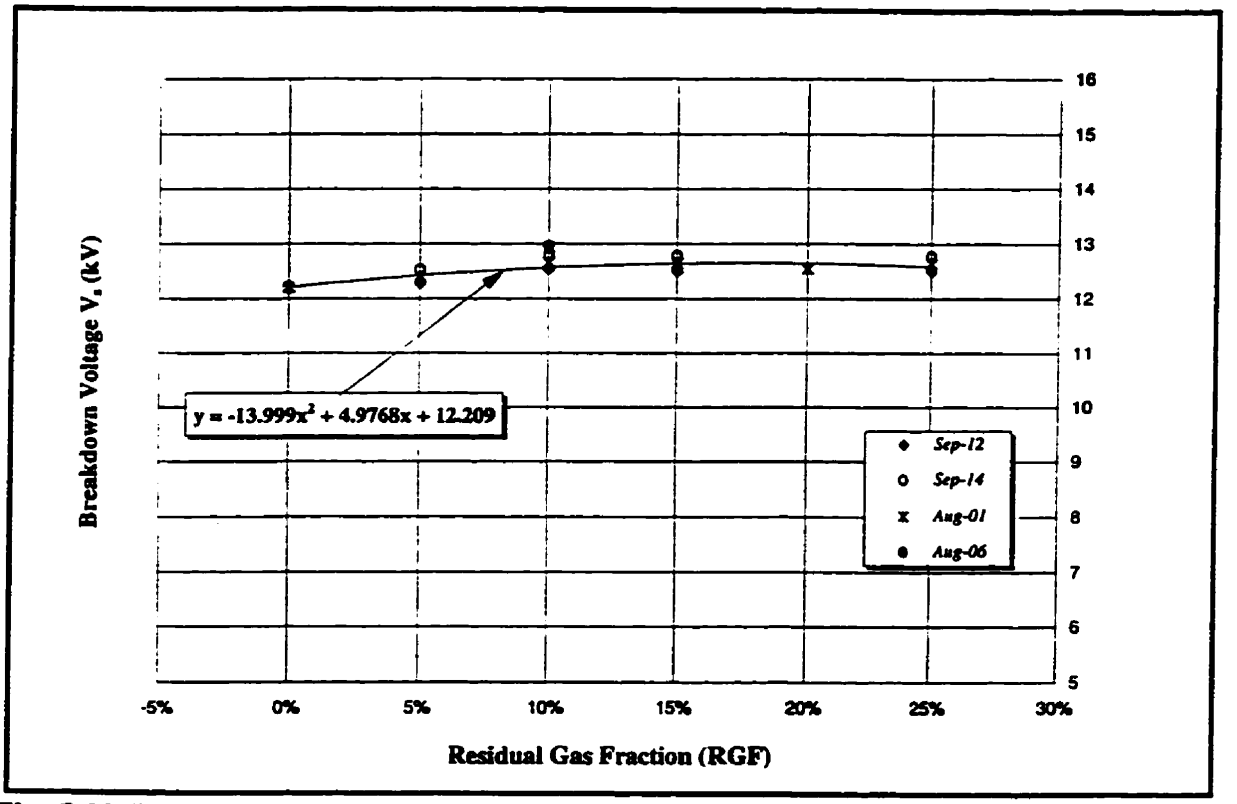

Fig. 5-20 Effect of the Residual Gas Fraction on the Breakdown Voltage (3) (ϕ=1)

temperature of the combustion chamber varies when engines run at different ϕ. Hence, the breakdown voltage measured in engines was affected by the temperature of the gas mixtures in the combustion chamber to some extent. For the simulated combustion chamber, although the operating conditions of the present experiments are quite similar to those of the engines, since the temperature inside the chamber was maintained (heated by a steam generator with a thermostat) at ~275 °F and the pressure was maintained by a pressure transducer at 150 psia (final filling pressure of air) as well, the variations of the temperature and the pressure which happen in real engines as a result of cyclic variations or variations of the operating conditions can be neglected in the present experiments. Also, the composition of residual gas changes. Therefore, the variations of the measured V_s in those tests can be regarded as the results of the change of the fuel-air equivalence ratio in the tests only. As shown in Table 4-4, while ϕ increases from 0.7 (CH_4: 6.83%) to 1.1 (CH_4: 10.33%), the change of the CH_4 concentration in the mixture is only about ~3.5% which does not affect the breakdown voltage significantly. Hence, V_s changes very slowly with the change of ϕ within the range tested.

5.2.2 Tests with Residual Gas

However, when the measurements were carried out under the same operating conditions with different fractions of residual gas added, V_s shows a significant increase comparing to those tests done without RG. Figure 5-18 and Fig. 5-19 show the results of the breakdown voltage measurements carried out on two days (without changing the spark plug) with 10% residual gas. Even with 10% residual gas present, V_s does not

change very much with the increase of the fuel-air equivalence ratio, but it does increase comparing to that without residual gas at the same ϕ. In order to understand the effect on the breakdown voltage of the residual gas fractions, additional sets of experiments were carried out in a stoichiometric mixture (ϕ=1) with the increase of the residual gas fractions from 5% to 25% in 5% increments and the result is presented in Fig. 5-20. When the fraction of the residual gas was increased from 0% to 10%, the breakdown voltage increases significantly. But when the RGF was increased to higher than 10%, V_s does not continue to increase with the increase of the RGF.[††††] The deviation between the two sets of data is probably caused by changing the spark plugs, causing the change of the electrode surface conditions (which has a strong effect on V_s). As well, the results of the tests done with 10% RGF at ϕ = 1 (from Fig. 5-18 and Fig 5-19) were shown in Fig 5-20. For simplicity, the correlation between V_s and RGF can be expressed by a function as follows,

$$V_s = x\,(RGF)^2 + y\,(RGF) + z$$

where x = -13.999, y = 4.9768 and z = 12.209 in this case.

For simplicity, the components of the residual gas in the case of a stoichiometric mixture can be regarded as the mixture of CO_2, H_2O vapor and N_2. As shown in Table 4-6, when the RGF increases, the concentrations of CO_2 and H_2O in the mixture increase too, resulting in the decrease of the concentration of CH_4 in the mixture. It has been shown that both CO_2 and H_2O vapor, especially H_2O vapor, have positive effects on the breakdown voltage, while CH_4 has a negative effect on the breakdown voltage. Therefore,

[††††] Misfires happens sometimes when the RGF was increased up to 25%.

the breakdown voltage increases with the increase of the residual gas fractions.[‡‡‡‡] However, in spite of the change of the RGF, the concentration of N_2 accounts for up to 71.55% (constant) in the stoichiometric mixture, it contributes greatly to the effect on the breakdown voltage of the mixture compared to all the other constituents. Thus, when with low RGF in a stoichiometric mixture, V_s does increase. However, when the RGF is increased to a relatively higher level, the effect of the N_2 on the breakdown voltage becomes more dominant, and the increase of the concentrations of H_2O vapor and CO_2 will not continue to increase V_s.

In summary of the above discussions, under experimental operating conditions (constant T and P before ignition), V_s doesn't depend on ϕ very much. With the increase of ϕ from 0.7 to 1.1, V_s only shows a slight downward trend even when there is 10% RG present in the mixture. This is probably because the increase of ϕ from 0.7 to 1.1 doesn't change the mixture composition very much, in turn doesn't affect V_s. Hence, in this case, the fuel-air ratio cannot be determined by V_s only. However, V_s tested with 10% RG has a higher value than that tested without RG at the same ϕ, indicating that V_s is quite sensitive to RG to some extent. In addition, the results of the experiments conducted in stoichiometric mixtures with different RGF show that, V_s increases with the increase of the RGF (up to 10% of RGF) and after, V_s appears to be constant until RGF reaches 25% (the flammability of the experimental condition). This correlation between V_s and RGF gives a good potential in the determination of RGF in a stoichiometric mixture by the

[‡‡‡‡] Again, different from the conditions of engines, under the experimental operating conditions, the temperature and the pressure will not change with the added residual gas which usually has a higher temperature than the fresh charged fuel and air and will affect the temperature of the mixture in engines.

equation in the form of $V_s = x\,(RGF)^2 + y\,(RGF) + z$. In a further way, it can be applied to engines under different combustion conditions after considering the effect that residual gas has on the temperature in the cylinder at the time of ignition.

CHAPTER 6 RESULTS AND DISCUSSION OF SPARK LIGHT EMISSION MEASUREMENTS

It has been shown that, at the beginning of the spark discharge, the spectrum of the spark emissions is mostly from atomic and ionic emissions since the molecular and recombination spectra are relatively weak; after 5 μs, the nitrogen containing molecules CN, NO and NH are spectroscopically dominant as energetic N is the dominant component of the plasma [Maly, 1984]. Although theoretically it is possible to study the atomic emissions to determine the composition of the combustion mixture, it is difficult to resolve it since the detection of the atomic emission is precluded by the strong molecular emissions, especially from CN (385 nm - 389 nm), which occurs a few μs after the spark discharge [Borghese et al., 1985]. In Merer's work [1994], the spark spectroscopy method has been studied to correlate the spectral light emission of CN to the fuel-air ratio in a CFR engine. Also, the effect of EGR on the spectral light emission was studied.

In order to evaluate the spark spectroscopy method as an efficient diagnostic technique in an SI engine to a further extent, additional work has been carried out in a simulated combustion chamber in which the concentrations of the combustible mixture as well as the fraction of the residual gas can be controlled more accurately.

In general, the spark occurs between the center and ground electrodes of the spark plug. However, the orientation of the spark varies cyclically. Since the spark light

emission was detected by the optical probes (with a limited field of view)[†], the variations of the spark positions will affect the detection of the spark emissions. In order to reduce the effect of the variation of the initiation of the spark, two channels of the spark light emission were measured simultaneously after a 50R/50T beamsplitter. One channel is for the measurement of the broadband intensity of the spark emission — the shot intensity. The other channel is for the spectral intensity measurement which was regarded as the light emission from CN[‡]. The shot intensity was used to normalize the spectral intensity[•] so as to reduce the effect on the spectral intensity of the variations of the spark initiation. In order to keep the light intensity of the two channels comparable, both of them were maintained within the linear response range of the optical detectors (PMTs) by the use of neutral density filter as well as black shields (with a tiny hole in the center). The feasibility of using the relative intensity (spectral intensity normalized by shot intensity) for analysis in the present work was discussed in Appendix I.

6.1 Verification Tests of the Spectral Light Intensity (at 385 nm)

From the band spectra which are shown in Table 6-1 [Gaydon, 1974], it can be seen that among the molecular emissions of the combustible mixtures in the experiments, the strong intensities of CH and CN at some wavelengths are overlapped within the

---

[†] Two optical probes were used in the experiments. At the beginning, a modified offset FFID optical spark plug (described in Appendix G) was used. After, it was replaced by an SImple optical probe which was inserted inside the steel plate with the polished end facing the spark plug gap perpendicularly (see FIg. 3-3).

[‡] At the beginning, a narrow bandpass filter was used to separate the light emission of CN from the total spark light emission. Later on, it was replaced by a monochromator.

[•] For all the spark light emission measurements, the peak value of each signal is used to determined the intensity of the shot and spectral emissions.

resolution of either the narrow bandpass filter (10 nm bandwidth) or the monochromator (5 nm bandwidth).

Table 6-1: Some Important Band Spectra of CN and CH

λ (nm)	CN	CH
~ 360	strong	very weak
385.5	strong	N/A
386.2	strong	N/A
387.1	very strong	very strong
~ 388.3	very strong	strong
431.4	very weak	very strong

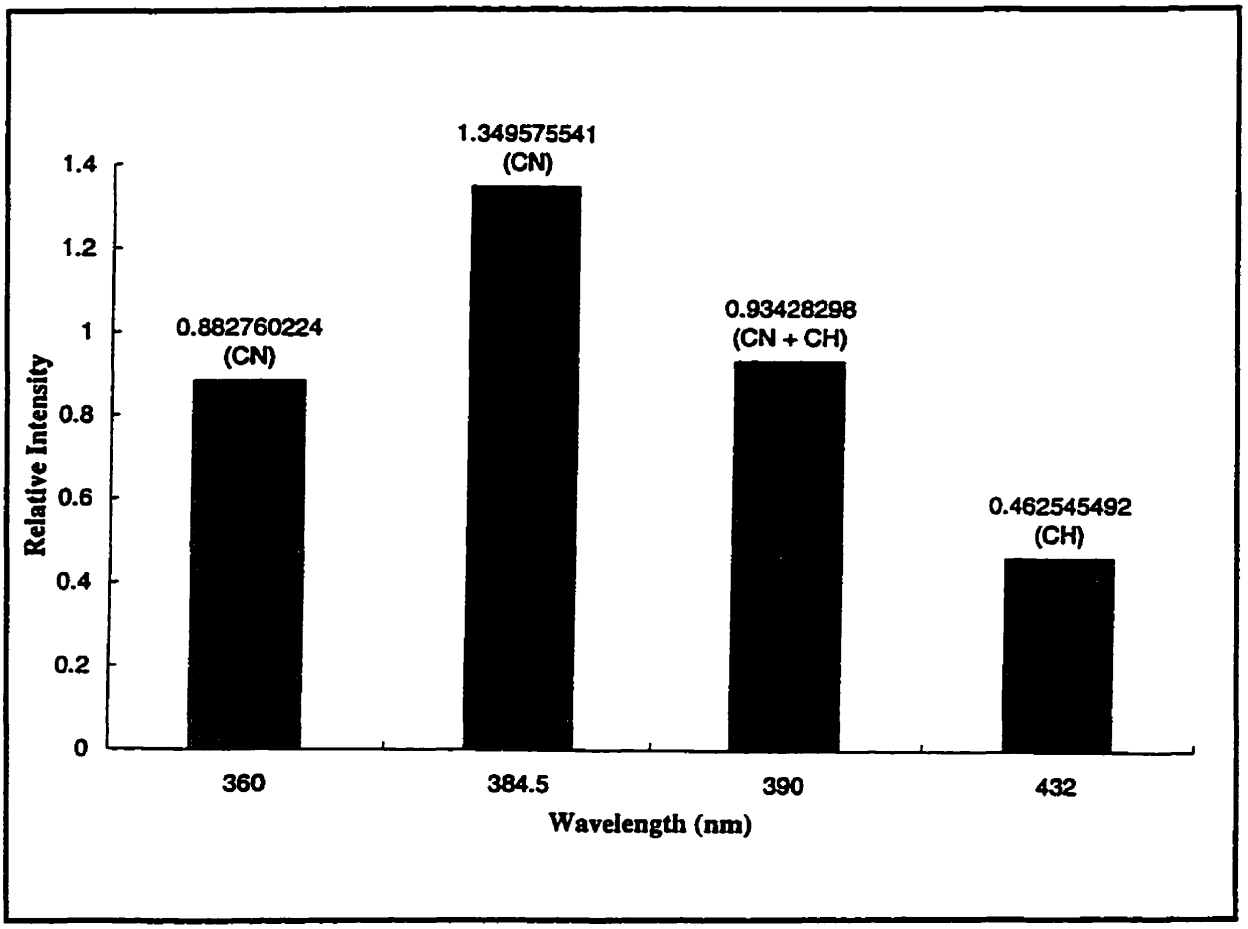

Fig. 6-1 Verification Test of Spectral Intensity of CN at 385 nm

Although the CN emission (at 385 nm) has been tested to have the strongest intensity among the molecular emissions 5 μs after the spark discharge, it has been suspected that the spectral intensity measured through either the filter or the monochromator (center wavelength was set at 384.5 nm) may have some contribution from the emission of the CH at a near wavelength (around 387 nm).

In order to verify that the measured spectral light intensity (first through the filter and then through the monochramator) in the present work is mainly from the CN, a set of preliminary experiments was conducted (using the monochromator) in stoichiometric mixtures and with the same in-cylinder pressure and temperature as those of other tests (150 psia and 275 °F) to study the relative intensities at some interesting wavelengths. The result presented in Fig. 6-1 shows that the relative spectral intensity at 384.5 nm (shifted a little from 385.5 nm in order to avoid the CH band spectra around 387 nm) is the strongest among all the band spectra in the tests. The intensity of the expected strongest band spectrum of CH at 431.5 nm does not have high intensity as shown in Fig. 6-1. In addition, the relative intensity at 390 nm which is supposed to include the emissions of CN and CH is not as strong as that tested at 384.5 nm, and it has almost the same magnitude as that tested at 360 nm which includes only the emission of CN. All these results show that the emission of CH is not as dominant as that of CN within the interesting time duration (5 μs to 10 μs after spark discharge) in the project. Hence, the spectral intensity tested in the experiments at 384.5 nm through a monochromator (the digital wavelength dial of the monochromator was set at 384.5 nm) can be regarded as the

intensity of CN emission only. So does the relative intensity tested through the filter[5]. This conclusion can be applied to all the combustible mixtures tests under the same testing condition in this project.

6.2 Effect of the Fuel-Air Equivalence Ratio on the Relative Intensity of CN

As observed by Borghese et al. [1985], with 10% CH_4 in N_2, no emissions other than CN are significant in the emissions of the spark after 5 μs. In engine studies, a correlation was found between the ratio of the spectral intensity (at 385 nm) to the shot intensity, to the fuel-air equivalence ratio ϕ for well-scavenged (skip-fired) cycles. The presence of burned gas, including residual gas and EGR reduces the spectral intensity at 385 nm. This in turn weakens the correlation between the 385 nm spectral intensity and ϕ [Merer, 1994]. In order to further study this correlation, especially to understand the effect of the residual gas on the spectral intensity, several sets of experiments have been carried out with the fuel-air equivalence ratio ϕ varied from 0.7 to 1.1 at an increment of 0.1.

Different from the engine operating conditions, the cyclic variations of the mixture composition in the simulated combustion chamber were controlled and can be neglected during the experiments. Therefore, with all the other parameters (e.g. the temperature and the pressure) constant, the variations tested in those experiments with the

[5]Although the relative intensity tested through the filter (with 10 nm bandwidth) has more probability of encountering variations due to the influence of the CH emission, there is not much difference between the results tested through the filter and that tested through the monochromator (discussed in a later section).

change of the fuel-air equivalence ratio and the residual gas fraction (RGF) can be considered as the result of only the change of the gas composition.

As discussed before, for the combustion without residual gas (the combustion chamber was evacuated before filling with fresh fuel and air at each cycle), the change of the concentration of CH_4 was quite small (there is only a 3.5% increase when ϕ is increased from 0.7 to 1.1). In this case, the breakdown voltage measurements didn't show very significant change when the mixture was changed from lean to rich. However, the results from the spark light emission measurements did give some information on the gas composition.

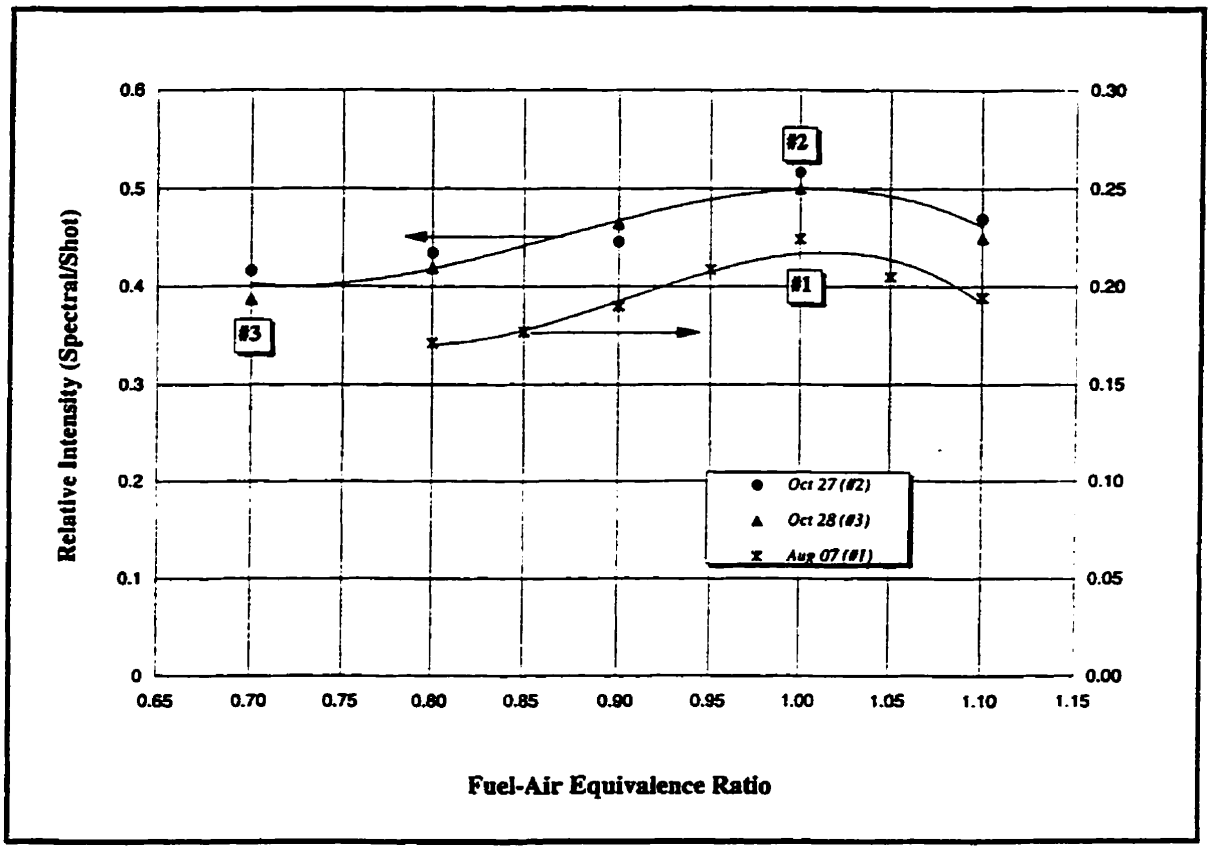

Fig. 6-2 Effect of Fuel-Air Equivalence Ratio on the Relative Intensity of CN (Without Residual Gas, T = ~ 275 °F, P = 150 psia)

Figure 6-2 presents the results of the spark light emission measurements (without residual gas) carried out on three different days and in two different ways. The first set of data (#1) was tested by using the optical probe which was discussed in Appendix G (the second design with an FFID spark plug) and a narrow band filter (described in Appendix H), while the other two sets of data (#2 & #3) were taken on two later sequential days by using the optical probe which was described in section 3.3.1 and the monochromator. Since the second orientation of the optical probe provides a wider view of the spark than the first one, an additional black shield (with a tiny hole in the center) was assembled in front of the PMT tube such as to limit the shot intensity.** Note that, since the filter has large bandwidth 10 nm, the relative intensity of CN tested by the filter could be affected more by the relative intensity of other radicals at the close wavelength compared to that tested by the monochromator.

Clearly, regardless of the difference of the absolute values of the three sets of data, their trendlines conform to each other very well within the experimental operating conditions. This comparison gives a strong evidence that the experimental results were not affected by either the location of the optical probes or the orientation of the spark initiation, indicating that there is a strong correlation between the relative intensity of CN and the fuel-air equivalence ratio. In order to clarify this correlation, the relative intensity at $\phi = 1$ was used to normalize those relative intensities at other fuel-air equivalence ratios such as to reduce the influence caused by the spark view variations (which probably

** It has been studied that when the magnitudes of the spectral intensity and the shot intensity are close to each other, the repeatability is better because the reduction of the shot intensity will keep the light intensity within the linear response range of the PMT, improving the comparability of the spectral and shot intensity [Merer, 1994].

affects the magnitudes of the testing results). Figure 6-3 presents the results of the normalized relative intensities of several days' experiments. It shows clearly that, when there is no residual gas present, the normalized relative intensity of CN increases until the mixture reaches stoichiometric. After stoichiometric, it decreases when the mixture becomes richer.

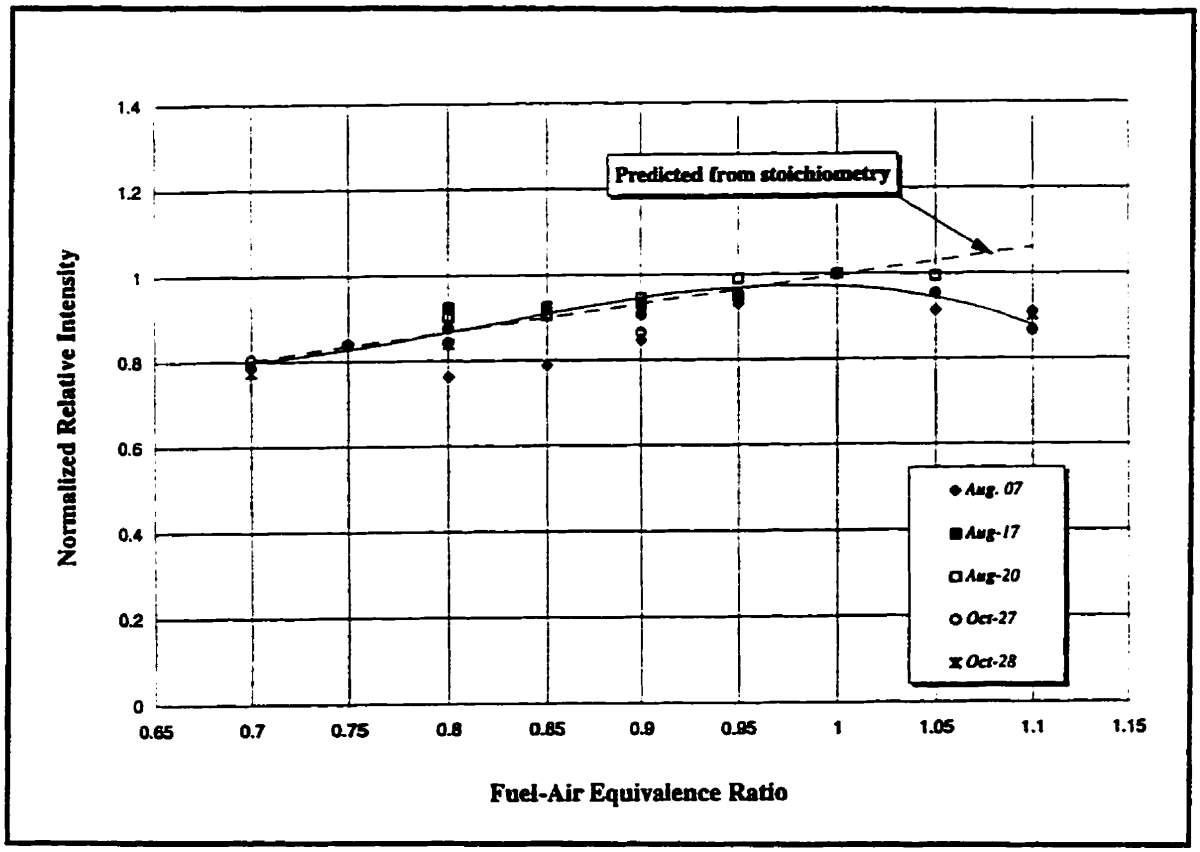

Fig. 6-3 Effect of Fuel-Air Equivalence Ratio on the Normalized Relative Intensity (Without Residual Gas, T = ~ 275 °F, P = 150 psia)

During the breakdown phase, all the heavy particles N, O, H, C are present as highly excited atoms and ions. If it is assumed that all of the molecules present in the mixture are dissociated into their constituent atoms during the breakdown phase, the mole fractions of each atom present in the mixture can be calculated from the stoichiometry. Figure 6-4 shows how the composition changes with ϕ. In addition, for simplicity, the

product of any two mole fractions of two different atoms were assumed as the relative rate at which mole fraction of the radical probably formed after the breakdown. Although chemical kinetic data for recombination reactions is available only for low temperatures [NIST database], the activation energy should be very low, so these reactions should all be fast. Thus the products of the atomic mole fractions, presented in Fig. 6-5 are likely a reasonable representation of how the relative formation rates of the different radicals vary with ϕ. Since the concentration of N is greatly in excess over the other species, the relative proportions of NO, CN and NH formed depend on the relative proportions of O, C, H in the mixture. The proportions of C to H are fixed by the fuel choice (CH_4), while the proportions of O to H and O to C depend on ϕ. This is shown in Fig. 6-5. Both Fig. 6-4 and Fig. 6-5 will be referred to extensively through out the remainder of this chapter to help elucidate the experimental results clearer.

In order to verify that it is feasible to use these predictions to help explain the experimental results, the relative rate of formation of CN at different ϕ was normalized by the value at $\phi = 1$ and the results were presented in Fig 6-3 as a predicted result for comparison with the experimental results. Clearly, when $\phi \leq 1$, the experiments behave as predicted by the stoichiometry, while when $\phi > 1$, there appears to be some difference.

Compare to the work done by Merer [1994] with skip-fired cycles (no RG) in a CFR engine, there appears some discrepancies in rich side. This is probably due to the different configuration of the spark plug electrodes used in his work. Instead of a standard spark plug, a modified optical spark plug was used with an optical fiber inserted through the central electrode and a secondary ground electrode (was made of Pt) to control the

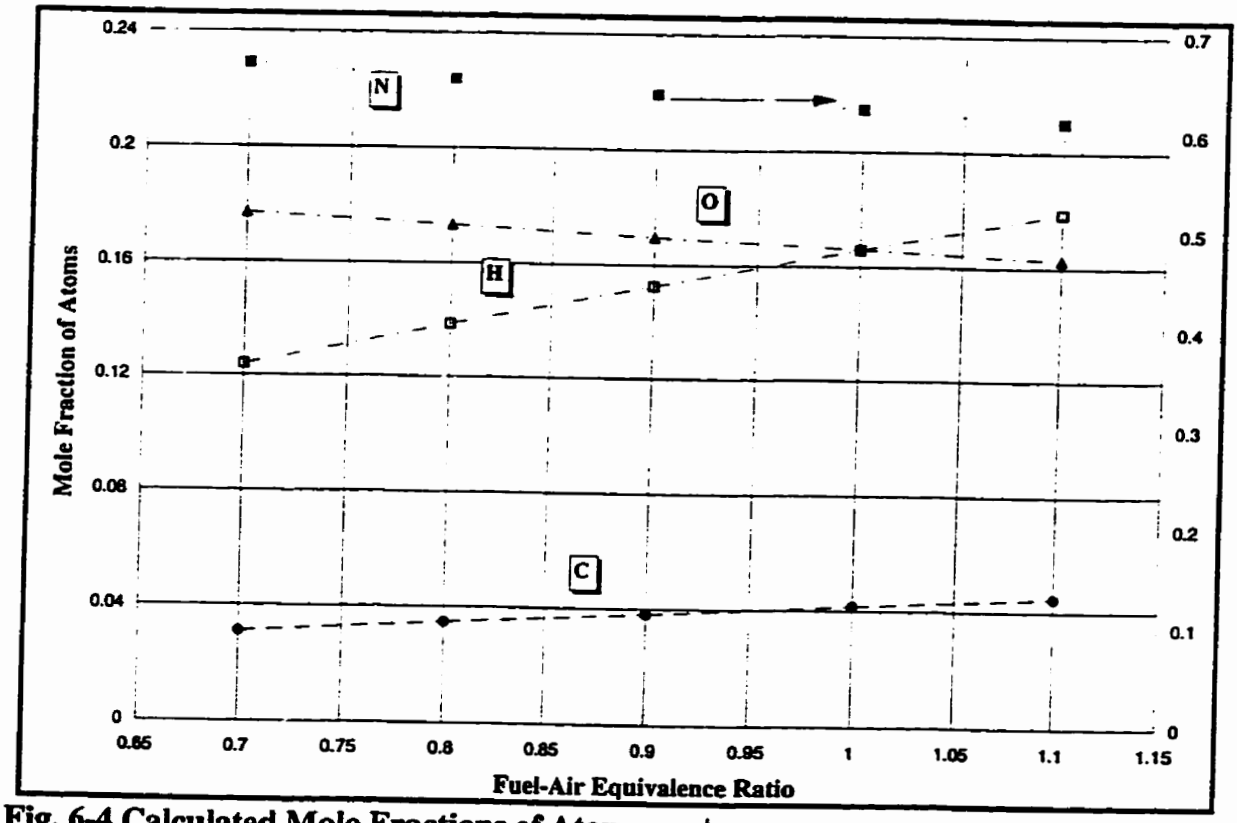

Fig. 6-4 Calculated Mole Fractions of Atoms vs. ϕ

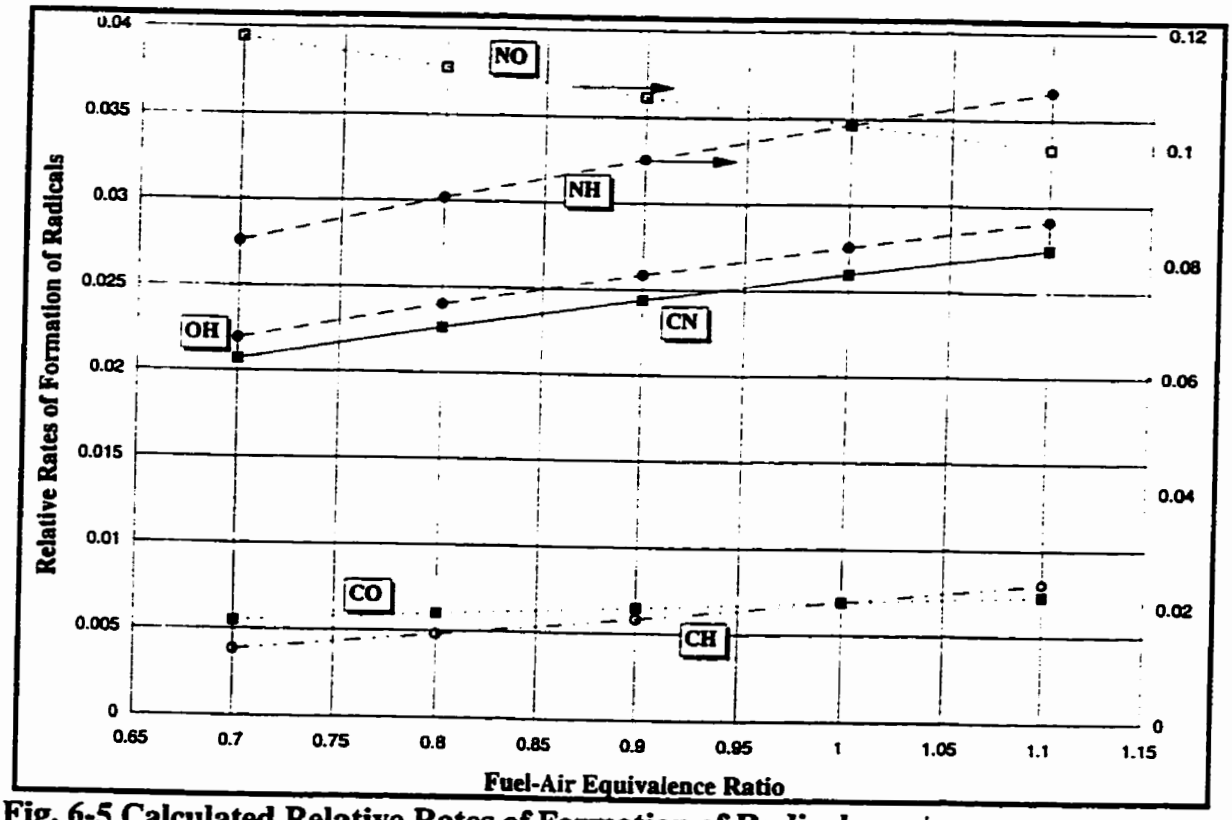

Fig. 6-5 Calculated Relative Rates of Formation of Radicals vs. ϕ

spark orientation. Under the combustion conditions with high pressure, this configuration of spark plug electrodes probably causes the accumulation of carbon easily, especially when the mixture is richer. Hence, V_s decreases very much due to the premature breakdown, decreasing the shot intensity, resulting a higher value of the relative intensity of CN.

Combining the above discussions, at the beginning of the breakdown, since the kernel temperatures are too high to allow stable molecules to exist, the chemical reactions (e.g. formation of CN) can only take place at the low temperature end of the plasma surface. Due to the high nitrogen content of combustible mixtures with air, reactions with the very energetic N radical are dominating during the inflammation phase where the temperature level is still appreciably higher than in ordinary premixed flames. Molecules such as CN, NO, and NH are readily formed. As shown in Fig. 6-4, when the mixture is relatively lean, the concentration of O is high such that the active oxygen radicals may pull away the reactive nitrogen radicals to form NO[††] instead of CN, as shown in Fig 6-5 due to the relatively low concentration of CH_4 in a lean mixture. As well, when the mixture is lean, the breakdown voltage tested is relatively high resulting in a smaller increase of the shot intensity[‡‡]. Therefore, the relative spectral intensity is low when the mixture is lean. On the other hand, when ϕ increases, the concentration of CH_4 increases while the concentration of O_2 decreases. Hence the probability of atomic recombination to form CN and NH is higher than that of NO formation (the relative rate of formation of

[††] Since NO emissions are all below 280 nm [Gaydon, 1974], the apparatus used in the present work is incapable of measuring so short a wavelength. Hence, the tests of the spectral intensity of NO was not done.
[‡‡] It has been studied that the breakdown voltage represents the energy transferred to the gas molecules during the breakdown phase in turn determines the spark light emission. [Merer, 1994]

NO decreases very fast when ϕ increases, as shown in Fig 6-5), increasing the spectral intensity of CN.

From the above discussion, it can be seen that, by measuring the relative intensity of CN, the effects on the experimental results of changing optical probes or the orientation variations of the spark initiation can be controlled. The relative intensity of CN only vary with ϕ. Based on the agreement of the predicted and the experimental results within the range of lean to stoichiometric which was shown in Fig 6-3, the fuel-air equivalence ratio ϕ can be determined by measuring the relative intensity of CN when there is no RG present. The correlation between them can be expressed by the following equation,

$$V_{CN}' = x \cdot \phi + y$$

where V_{CN}' is the normalized relative intensity of CN, while x = 0.65a, y = 0.35a in this case with $\phi \leq 1$.

6.3 Effect of the Residual Gas on the Relative Intensity

As pointed out before, the presence of burned gas, including residual gas and EGR reduces the spectral intensity centered at 385 nm, in turn weakening the correlation between the 385 nm spectral intensity and ϕ. In order to further understand the effect of the residual gas on the spectral intensity, sets of experiments were carried out in the same simulated combustion chamber and under the same operating conditions (T = ~ 275 °F, P = 150 psia).

6.3.1 Tests with 10% Residual Gas

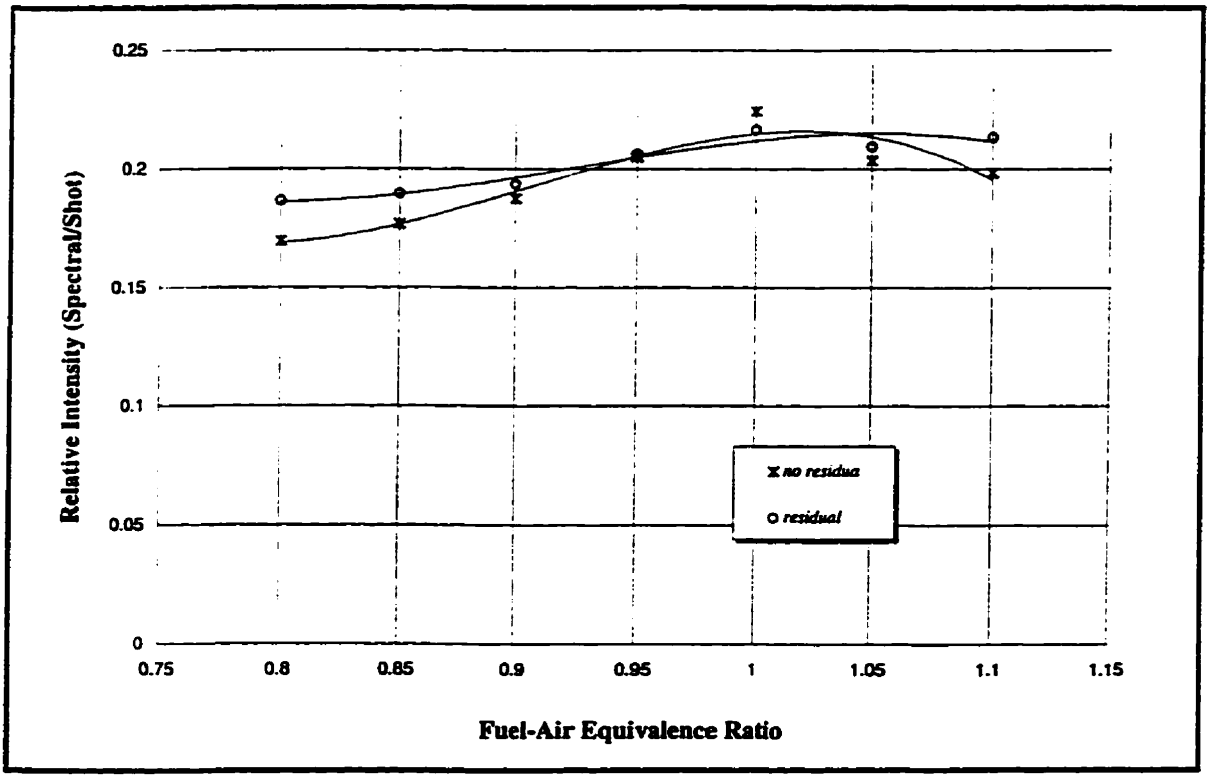

Fig. 6-6 Effect of 10% Residual Gas on the Relative Intensity (T = ~ 275 °F, P = 150 psia)

Figure 6-6 presents the results of the tests carried out in the mixtures without and with 10% residual gas with ϕ changed from 0.7 to 1.1 in 0.1 increments. From Fig. 6-6, it can be seen that the relative intensity tested in the mixtures with 10% residual gas present increases all the way when the mixture is changed from lean to rich while the relative intensity tested without residual gas increases first and then starts to decrease after the mixture becomes rich. The reason why the relative intensity tested in the mixture without residual gas changes in this way was discussed in the previous section. For the experiments with RGF, since nothing else is changed but the addition of the 10% residual gas, hence, the only reason why the relative intensity changed is caused by the added residual gas. When there is 10% RG present in the mixture, the gas molecular

composition is changed. As shown in chapter 5, this increases the breakdown voltage. However, for a given ϕ, the relative proportions of atoms O, H, N, C are unchanged by the presence of residual gas, so the information in Figures 6-4 and 6-5 suggests that there should be no effect on light emissions other than that caused by the change in breakdown voltage. As shown in Fig. 5-17, with RGF, the breakdown voltage in the mixture increases, thus, the shot intensity increases too. The increase of the shot intensity compensates the increase of the spectral intensity of CN with ϕ in the calculation of the relative intensity. As a result, the relative intensity tested with 10% residual gas does not increase very much when ϕ increases from 0.7 to 1.1. As shown in Fig 6-6, the fitting curve is quite flat.

6.3.2 Tests with Different Diluents — Real Combustion Products and 9% CO_2 [§§] (the Balance is N_2)

6.3.2.1 Relative Intensity of CN

In order to study the effect of the residual gas fraction on the relative intensity of CN, two sets of tests were carried out with two different diluents, one is the real combustion product[***] and the other one is the 9% CO_2 (the balance is N_2)[†††] [‡‡‡]. The comparison of the results displays the strong dependence on the gas compositions of the relative intensity.

[§§] All the concentrations used in the present work is by volume.

[***] Hereinafter, the real combustion product is called residual gas when it is used as the diluent.

[†††] Hereinafter, the 9% CO_2 (the balance is N_2) is called 9% CO_2 for simplicity.

[‡‡‡] The reason to choose 9% CO_2 (the balance is N_2) as the substitution of the residual gas is the similar fraction of CO_2. For stoichiometric mixture, the complete combustion product is: $CO_2 + 2\ H_2O + 7.546\ N_2$. Hence, the fraction of CO_2 in the residual gas is 9.482% which is close to 9%.

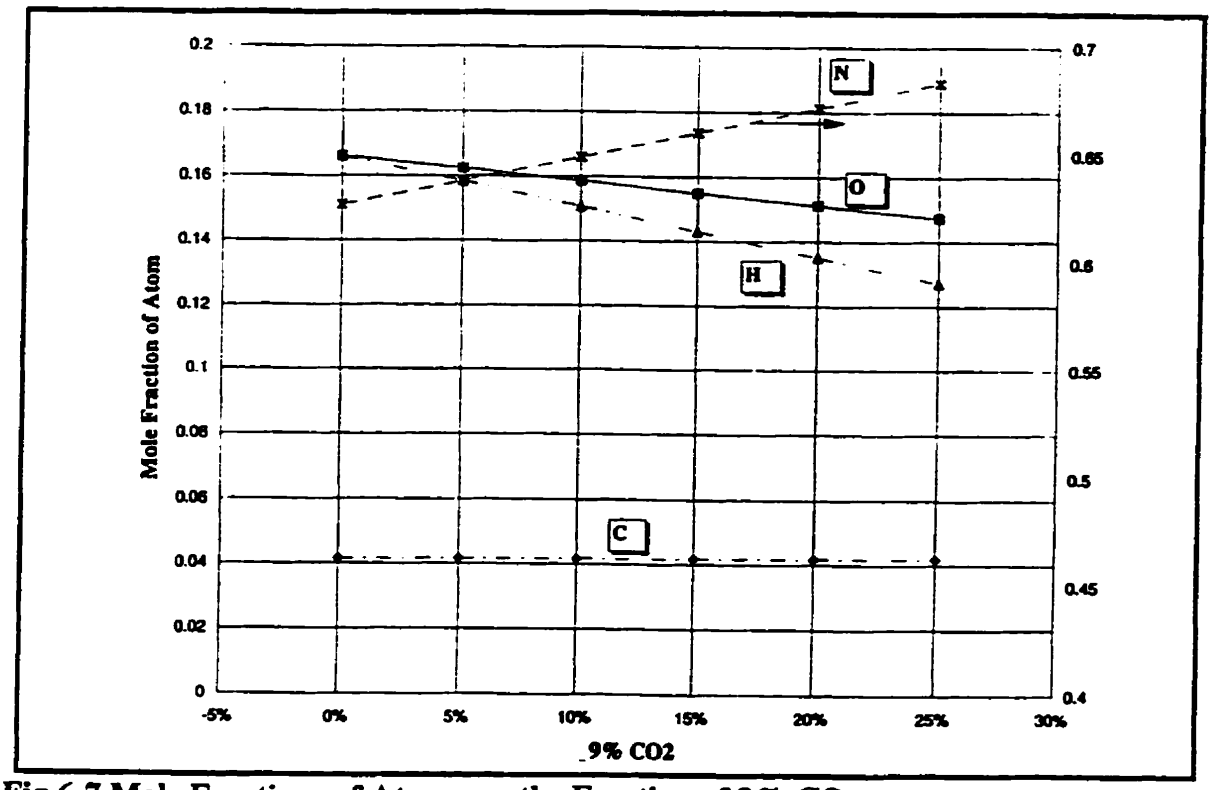

Fig 6-7 Mole Fractions of Atoms vs. the Fraction of 9% CO_2

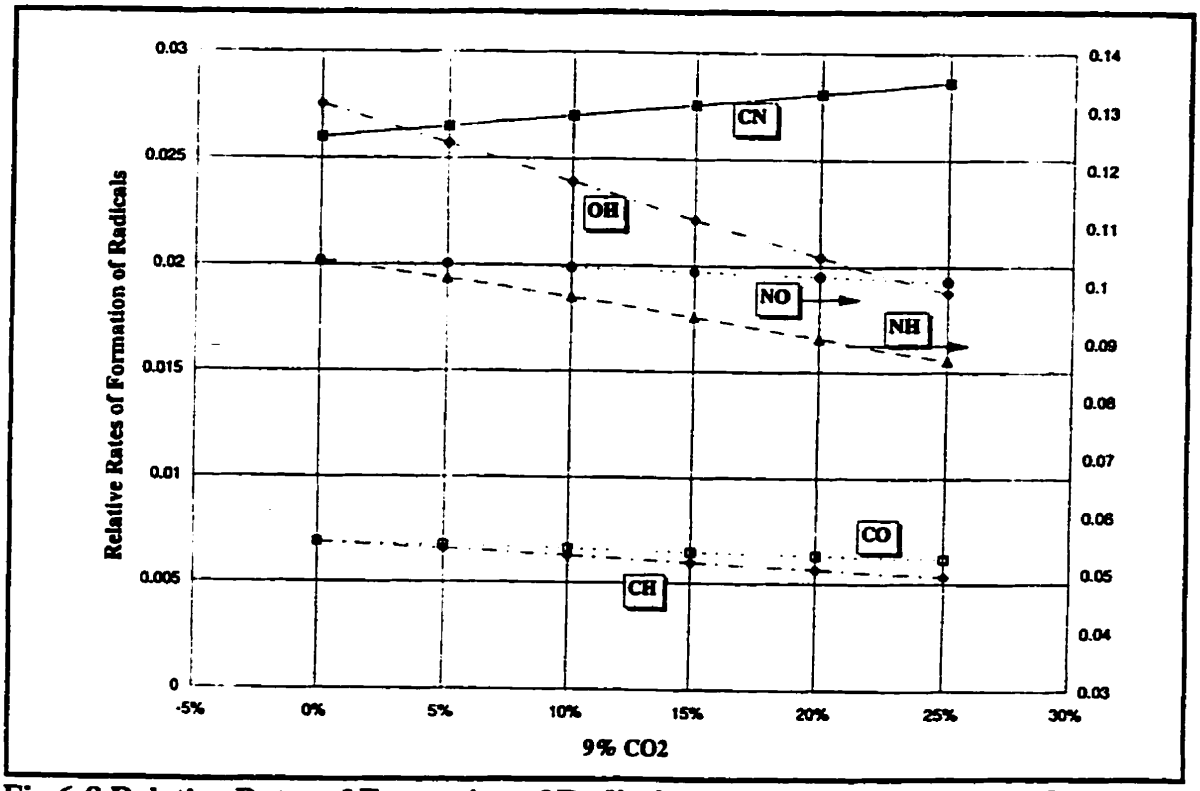

Fig 6-8 Relative Rates of Formation of Radicals vs. the Fraction of 9% CO_2

Same as discussed in Section 6.2, the mole fraction of each atom present in the mixture as well as the relative reaction rates for formation of molecular species probably formed after the breakdown were calculated from the stoichiometry in stoichiometric mixtures with 9% CO_2 present in N_2 and the results were presented in Fig 6-7 and Fig. 6-8 respectively, as an aid of the explanation in the discussion. When residul gas is used as a diluent, the relative atomic proportions do not change with the percentage of RG added and so are constant at the values shown of 0% CO_2 in Figs. 6-7 and 6-8.

Figure 6-9 presents the results of the experiments carried out in stoichiometric mixtures with the fraction of residual gas[§§§] changing from 0% to 25% in 5% increments. As well, Fig. 6-9 shows the results of the tests done in the stoichiometric mixtures with the fraction of 9% CO_2 increasing from 0% to 25% in 5% increments. The second set of the experiments was done for comparison such as to study the influence of the change of gas composition on the relative intensity. Obviously, with RG added to the freshly charged fuel and air, the tested relative intensity changes differently from that tested in the mixtures without RG (0% RGF). As shown in Fig. 6-9, first, the relative intensity decreases when the RGF is increased from 0% to around 10% and the relative intensity starts to increase slightly when the RGF continues to increase up to 20% (approximate). But when the RGF is very high (say above 20%), the relative intensity starts to decrease again.

When the residual gas was replaced by 9% CO_2, the change of the relative intensity displays in a different way. In general, the magnitude of the relative intensity

[§§§] The residual gas used here is the real combustion product from the previous combustion cycle. The fraction of the residual gas was controlled by the pressure transducer which was described in Section 3.2.1.

with 9% CO_2 is higher than that with real residual gas at the same fraction. Same as that observed with RG, the relative intensity decreases when the fraction of the 9% CO_2 is increased from 0% to a low percentage (below 10%). But after that, the relative intensity with 9% CO_2 increases faster and greater and it doesn't drop even when the fraction of 9% CO_2 is as high as 25%[****].

In order to isolate the effect of the breakdown voltage on the relative intensity, all the relative intensities either with RGF or 9% CO_2 were normalized by the simultaneously tested breakdown voltage and the results were shown in Fig. 6-10. In addition, the predicted values for both RGF and 9% CO_2 calculated from Fig 6-8 were shown as well. It can be seen that, with RG, the normalized relative intensity of CN does not change much with the change of RGF, probably due to the unchanged concentration of each atom. This can be seen from the predicted values which is a horizontal line. However, when the diluent is 9% CO_2, the experimental and prediction all show that the normalized relative intensity of CN increase with the increase of the fractions of 9% CO_2, indicating that the spectral light emission has strong dependence on the compositions of the mixture and the spectral light emission can be measured for the determination of the mixture compositions.

When there is a diluent, either residual gas or 9% CO_2, added to a mixture, the mixture composition changes with the change of the fractions of the residual gas or the 9% CO_2. However, in the stoichiometric mixtures, when the diluent used is the residual

[****] Misfire happens during the experiments which were carried out in the mixtures with either the 9% CO_2 or the real residual gas when the fraction of the 9% CO_2 or residual gas is was 25 %, the highest ratio tested.

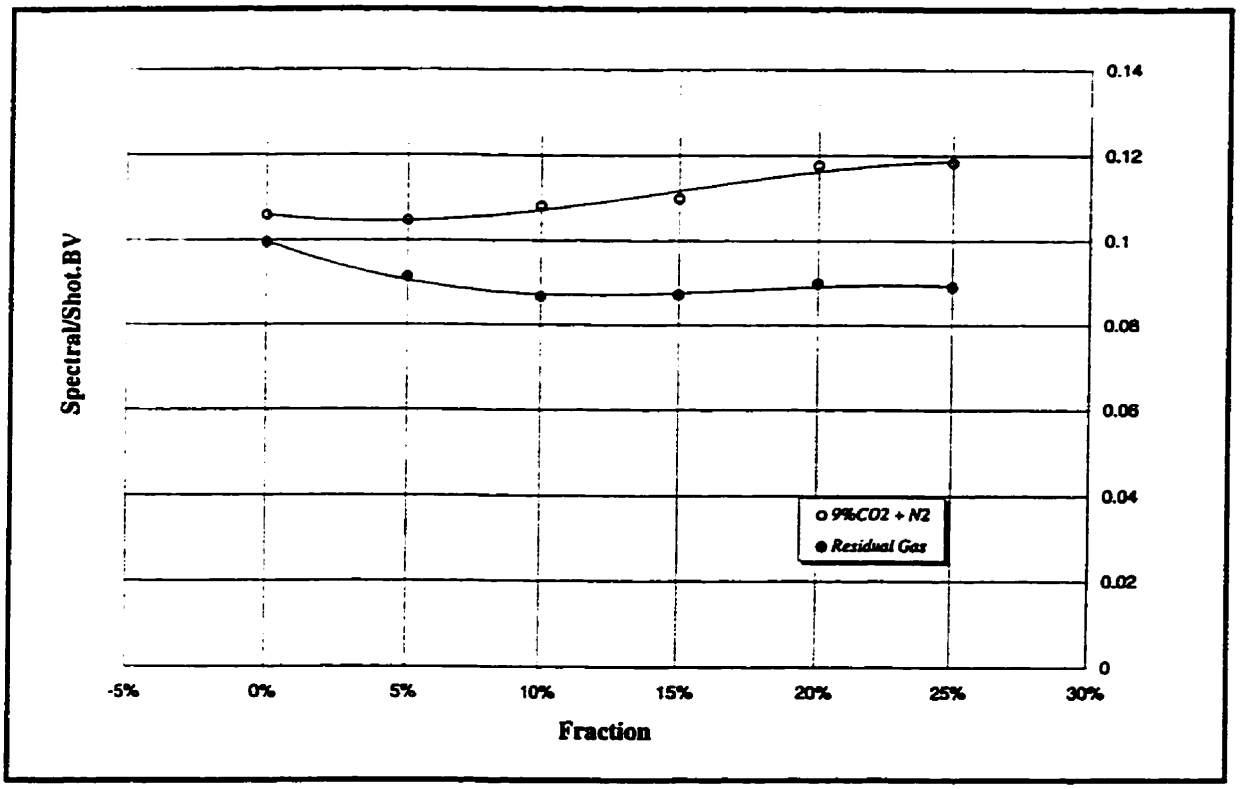

Fig. 6-9 Comparison of the Relative Intensity of CN with either Residual Gas or 9% CO_2 (P = 150 psia, T = 275 °F, d = 1.0 mm)

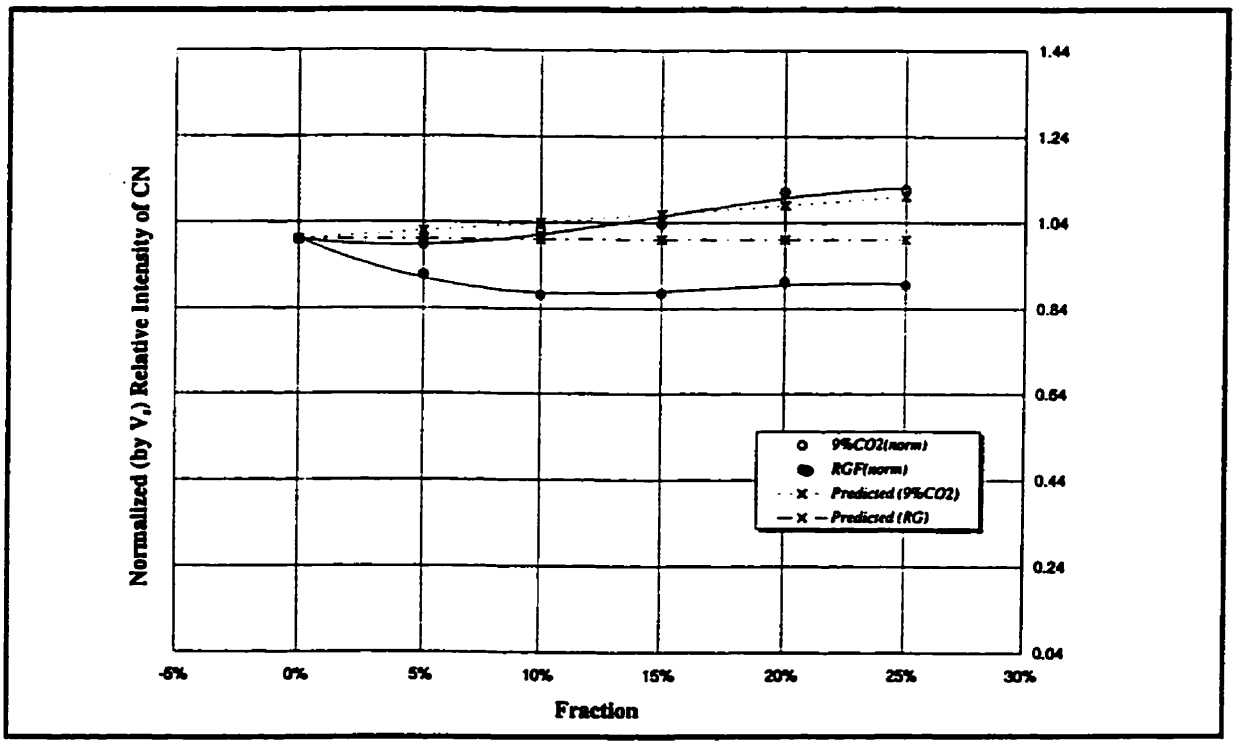

Fig. 6-10 Predicted and Experimental Relative intensity of CN Normalized by V_s with either Residual Gas or 9% CO_2 (P = 150 psia, T = 275 °F, d = 1.0 mm)

gas (CO_2 + 2 H_2O + 7.546 N_2), the concentrations of the atoms N, O, H, C will not be affected by the change of the RGF. Hence, in general, adding the residual gas in the stoichiometric mixture and changing the fractions will not influence the CN spectral intensity. As discussed in Section 5.2.2, the breakdown voltage (simultaneously measured with the measurements of the spark emissions) increases with the increase of the RGF in stoichiometric mixtures, indicating that the shot intensity increases as well when the RGF is increased. Therefore, on the contrary to the change of the breakdown voltage (as shown in Fig. 5-18), the relative intensity decreases first from low RGF to around 10% and then increases again until the RGF is around 20%, as shown in Fig 6-9. However, after the relative intensity was normalized by V_s, the lines become flat, indicating that only dependence on the gas compositions of the spectral intensity.

On the other hand, when 9% CO_2 was used as the diluent instead of the real residual gas, the situation is different from the above because of the change of the atom concentrations. Obviously, when the diluent is 9% CO_2, there is no H_2O vapor present in the mixture. Hence, when increasing the fraction of the diluent, the concentration of the atoms H and O decreases while the concentration of N increases, as shown in Fig. 6-7. Thus, the recombination of C and N to form CN has a higher probability of occurrence than the formation of the other radicals, such as NH[††††] and NO. It can be seen from Fig. 6-8 that the relative formation rates of NO and NH decrease with the increase of 9% CO_2 fraction while the relative formation rate of CN increases.

6.3.2.2 Relative Intensity of NH (336 nm)

[††††] The strongest emission from NH is at the wavelength of 336 nm [Gaydon, 1974]

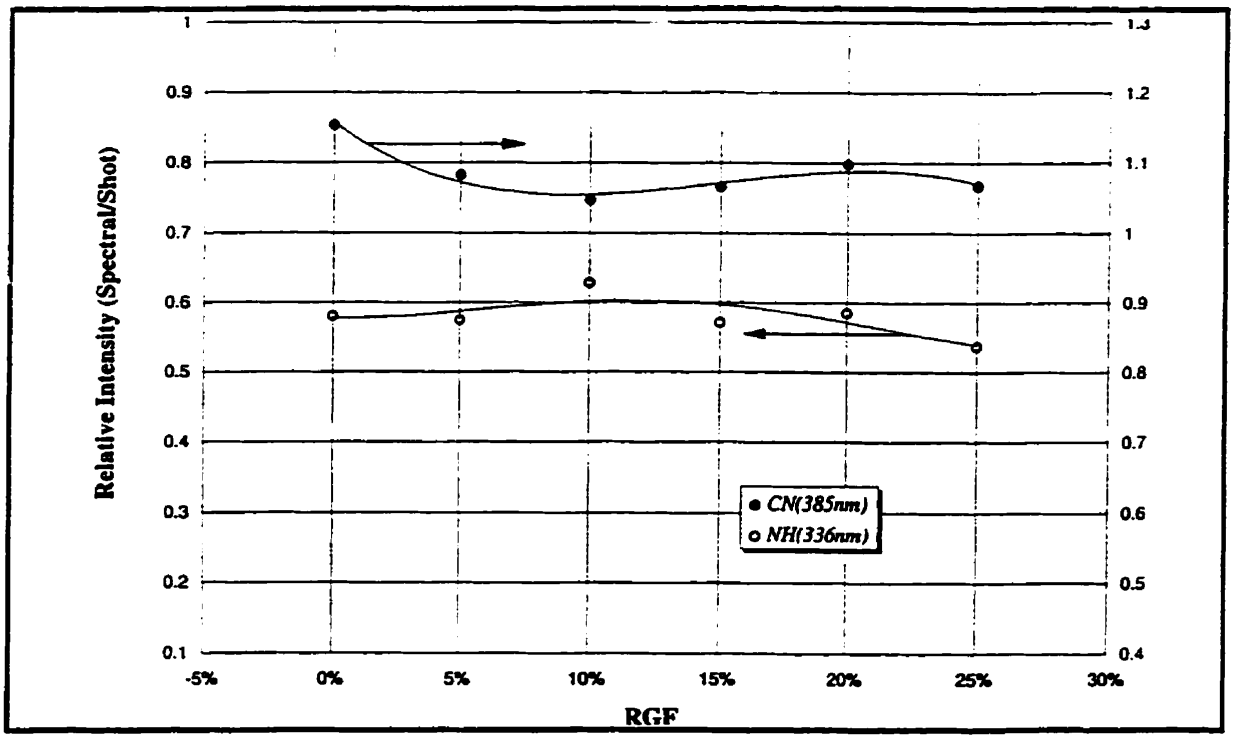

Fig. 6-11 Comparison of the Relative Intensity of CN & NH with Residual Gas (P = 150 Asia, T = 275 °F, d = 1.0 mm)

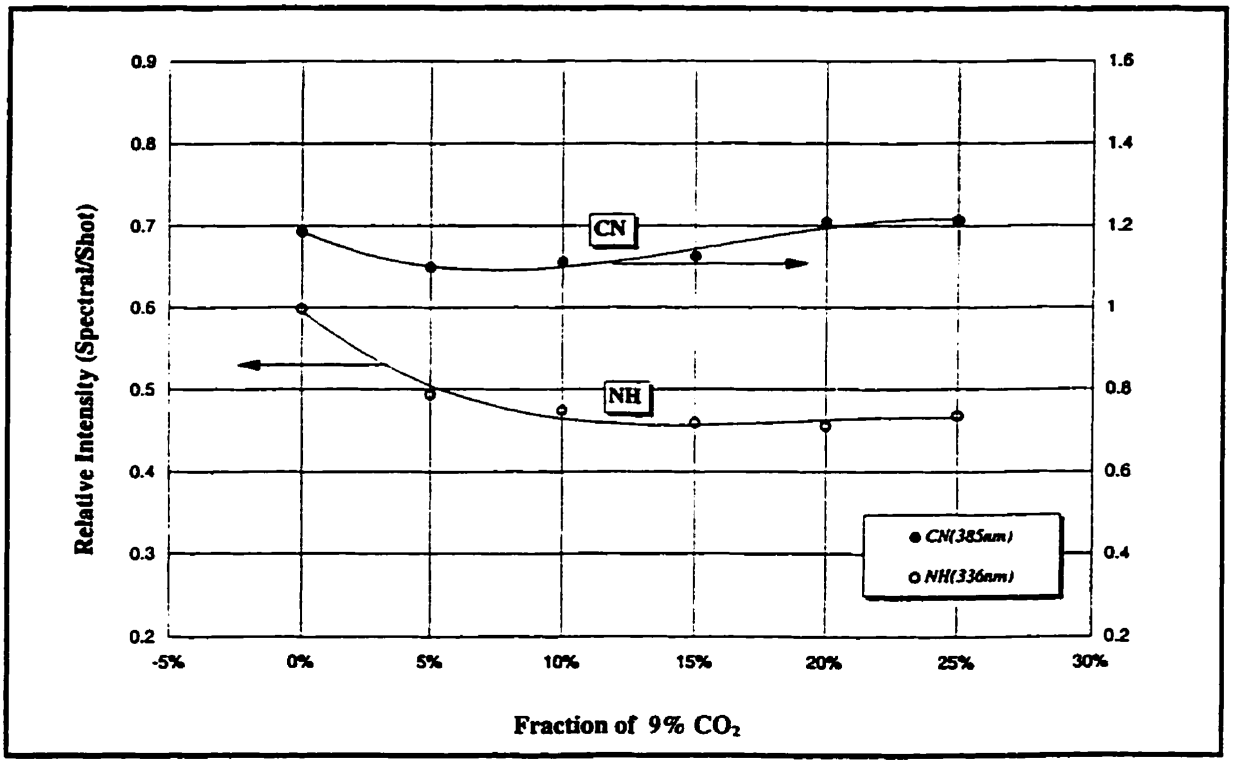

Fig. 6-12 Comparison of the Relative Intensity of CN & NH with 9% CO_2 (P = 150 psia, T = 275 °F, d = 1.0 mm)

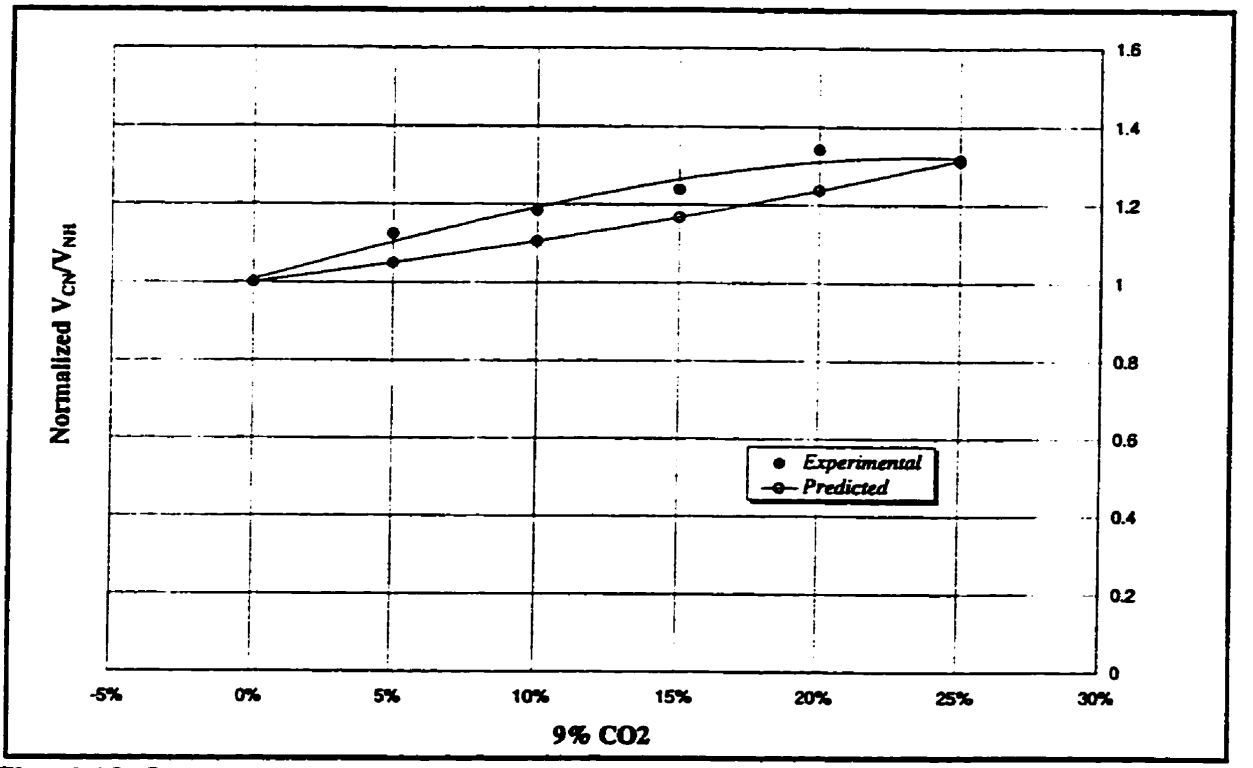

Fig. 6-13 Comparison of the Predicted and Experimental Rates Formation of CN and NH with 9% CO_2 as Diluent

In addition, in order to further understand the correlation between the relative intensity of CN and the RGF, the effect of the intensity of NH emission (centered at 336 nm) on the correlation was studied by carrying out the experiments in stoichiometric mixtures with either residual gas or 9% CO_2 as diluents. The results are presented in Fig. 6-11 and Fig. 6-12 respectively and the relative intensities of CN were also shown for comparison. It is clear that, whichever is used as the diluent, the relative intensity of NH is much weaker than that of CN. As shown in Fig. 6-11, when the diluent used is the real residual gas, the relative intensity of NH (336 nm) increases first with the increase of the RGF and reaches the highest value at the point of 10% RGF while the relative intensity of CN reaches the lowest value at the same point. This result explains the change of the relative intensity with RGF experimentally that the increase of the relative intensity of

NH contributes to the decrease of the relative intensity of CN while the decrease of the relative intensity of NH contributes to the increase of that of CN. The reason why this happened is not very clear and need to be investigated in the future. Since the recombination process is a very complicated phenomenon, it was not studied in detail here. Different from that observed as above, when tested with 9% CO_2, as shown in Fig 6-12, the relative intensity of NH keeps decreasing when the increase of the fraction of 9% CO_2. This is because of the lack of H atoms (as shown in Fig. 6-7), supporting the formation of CN instead of NH (as shown in Fig. 6-8). In order to show this, the ratio of the rates of formation of CN and NH at different fractions of 9% CO_2 was normalized by the ratio at 0% CO_2 and was presented in Fig. 6-13 for comparison to the experimental results which are the ratios of the relative intensities of CN and NH normalized by the value at 0% CO_2. Clearly, both the predicted and experimental results indicate that the rate of CN formation increases faster than that of NH with the increase of the fractions of 9% CO_2, resulting in the increase of the relative intensity of CN.

6.4 Summary

In summary of the above discussions, 5 μs after the spark discharge, the molecular emissions have dominant contributions to the spark light emission, among which, the emission of CN at 385 nm has the strongest intensity. The results of the experiments shows that neither the location of the optical probes nor the orientation of the spark initiation affect the relative intensity (normalized by the shot intensity) under the simulated engine operating conditions. The relative intensity of CN shows strong

correlation with the fuel-air equivalence ratio as well as the residual gas fraction in stoichiometric mixtures. For the combustion without RG present, based on the agreement between the predicted and experimental results within the range of lean to stoichiometric, ϕ can determined by the measurement of the relative intensity of CN through the equation in the form of $V_{CN}' = x \cdot \phi + y$ for $\phi \leq 1$. In addition, in stoichiometric mixtures, first, the relative intensity of CN decreases with the increase of RGF from 0% to 10%. After, the relative intensity of CN increases until the RGF reaches 20%. However, after being normalized by V_s, the relative intensity of CN doesn't change much with the change of the RGF, indicating that the spectral light emission only has strong dependence on the gas compositions. When tested with 9% CO_2, since the gas compositions changes with the change of the fractions of 9% CO_2, the normalized relative intensity of CN increases faster and greater than that tested with RG. Also, the relative intensity of NH was tested to be lower than that of CN under the same operating conditions with either RGF or 9% CO_2. The experimental and predicted results with 9% CO_2 all show that the relative rates of CN formation increases much faster than that of NH, resulting the increase of the spectral intensity of CN in the tests with 9% CO_2..

In summary, based on the non-intrusive spark emission test technique, the relative intensities of CN and NH was found to have strong correlation with the fuel-air equivalence ratio as well as the residual gas fraction under the simulated engine operating conditions. Combined with the simultaneous breakdown voltage measurements, the fuel-air ratio can be determined within some conditions by measuring the relative intensity of CN as well as that of NH.

CHAPTER 7 CONCLUSIONS & RECOMMENDATIONS

7.1 Conclusions

The objective of this research was to study the feasibility of using the spark plug based diagnostics to determine the fuel-air ratio for the study of cyclic variations in an SI engine. All the experiments were carried out in a simulated engine combustion chamber in order to control the mixture composition more accurately and easily. From the experiments, the following conclusions can be made:

1. In the present work, over the range of the testing pressure, for most of the gases (such as N_2, O_2, CO_2), V_s appears to be a function of (nd). At low pressure, the experimental results agree with Paschen's Law very well, while at high pressure, some discrepancies appear. The same phenomenon was observed in the previous studies as well. However, V_s still appears to be a function of (nd) which can be expressed as the form of the simplified Paschen's Law $V_s = f(nd)_s$.

2. When some special gas, such as CH_4, mixed with the main diluent gas N_2, V_s show a strong dependence not only on (nd), but also on the special gas property, e.g. the ionization potential of the special gas. The values of V_s in 10% CH_4 and 100% CH_4 are lower than that in N_2, mainly due to the lower effective ionization potential V_i CH_4. This result also agrees with the simplified Paschen's Law.

3. At high pressure, electron attachment has a strong influence on V_s in electronegative gases. This was observed in the tests done in O_2 and air. Also, it has been shown that H_2O has a very high value of electron attachment coefficient as well as a high

value of elastic scattering collision cross section, indicating that adding H_2O into a gas mixture will change V_s significantly. In general, V_s increases with the increase of the percentage of H_2O.

4.At the pressures that are encountered in combustion, the effect of the electrodes materials on V_s can be neglected. Nevertheless, the configuration of the spark plug electrodes, as well as the irregularities on the electrodes surfaces caused by accumulation of carbon or ash or by abrasions probably lead to crowding of lines of force on protuberances, resulting in premature breakdown. Hence, in general, at high pressure, V_s has a relative lower value than the prediction of Paschen's law, indicating that under combustion conditions, V_s not only depends on the (nd) and gas properties, but also is affected by the different combustion conditions.

5. From the combustible mixtures tests, it was observed that V_s exhibits only a slight downward trend with the increase of ϕ . However, the sensitivity of V_s to 10% RG shows the possibility of using V_s to determine RGF.

6. In stoichiometric combustible mixtures tests, V_s was found to have a strong dependence on RGF. Hence, RGF can be determined by V_s through an equation in the form of $V_s = x\,(RGF)^2 + y\,(RGF) + z$, with the coefficients x, y and z obtained from the statistical analysis of the experimental results.

7. In the combustible mixtures, the spectral intensity of CN (centered at 385 nm), 5 μs after spark ignition was observed to have the strongest intensity compared to the relative intensities of the other radicals, such as CH and NH. The spark light intensity as well as the spectral intensity depends on the mixture composition and other combustion parameters.

The configuration of the optical probes will not affect the characteristics of the spark light emission.

8. Without RG present, the spectral intensity of CN has a strong dependence on ϕ. Within the range of $\phi \leq 1$, ϕ can be determined by the experimental relative intensity of CN through the linear equation in the form of $V_{CN}^{\cdot} = x \cdot \phi + y$, while x and y were obtained from the statistical analysis of the experimental result. This result agrees with the work done by Merer [1994] with skip-fired cycles in a CFR engine. However, when $\phi>1$, some discrepancies appear, probably due to the difference between the configurations of the two different spark plug electrodes.

9. In the stoichiometric mixtures with RG, the relative intensities of CN and NH didn't show strong dependencies on the fractions of RG, while they did exhibit good dependence on the fraction of 9% CO_2. This difference between the tests with RG and 9% CO_2 gives evidence that the spectral light emission of certain radicals depends mostly on the mole fractions of relevant atoms, indicating a strong correlation between the spectral intensity and the gas composition only.

7.2 Recommendations

The repeatability is the most important thing in this project. In order to improve the efficiency of this spark plug based diagnostics for fuel-air ratio determination, it is desirable to avoid any discrepancy of the apparatus that probably causes the variations of the spark discharge which will affect the repeatability of the experiments. It has been observed in the non-combustible mixtures tests that, there were multiple breakdown phases

happened sometimes. Since this unexpected multiple breakdown phase probably causes variations in the energy transferred to the gas molecules during the breakdown which in turn affects the breakdown voltage measurement, this phenomenon needs to be avoided in the further research. An improved discharging system will be very helpful to reduce the variations caused by this unexpected phenomenon, improving the repeatability of the experiments.

Although the experimental results show that the location of the optical probe doesn't affect the relative intensity, a closer view of the spark emission will optimize the repeatability of the spark light detection. The central electrode modified optical spark plugs have been shown to have some benefits in the previous studies. However, since the conditions of the spark plug electrodes will affect the consistency of the breakdown phase and in turn will affect the spark light emission, a spark plug with less modification of the electrodes is required to reduce the variations (resulted from the change of the electrode surface conditions) of the experimental results. A modified off-set spark plug with a side-view of the spark emission has been designed and the feasibility has been studied to some extent. It is worth while to put this design into use for the further research (refer to Appendix G).

Use of a monochromator provides high resolution equipment in the study of the spectral light intensity. However, sets of suitable narrow bandpass filters with high resolution will have the advantages of simplicity, portability and accuracy when applying this diagnostic technique to a production SI engine.

Temperature of the combustion chamber is a very critical criterion for a real engine. In order to apply this method to a real engine, the variations of the temperature of the combustion chamber wall caused by either RG or EGR should be considered in the further research.

For any experiments, the noise/signal ratio can't be avoided completely, but it should be controlled as small as possible. In this project, it is more important to reduce the noise/signal ratio because the detectable signals of the spectral light intensity of the spark emission is very weak. Otherwise, the detection will be distorted. Presently, the electronic noise was controlled by aluminum shielding only. In order to improve the quality of the signal, it is also worth to study other optional solutions of noise control, such as an opto-isolator. In addition, an improved amplifier with high temporal resolution will be very useful in conjunction with the high temporal resolution detectors to reduce the noise.

In addition to the improvements of the equipment mentioned above, the simultaneous measurements of the spectral intensities of different radicals will be very helpful because the spectral light intensities of other radicals (formed at the same time with CN, such as NO, centered at 280 nm, and NH, etc.) also have dependencies on ϕ and RGF or EGR. The combined measurements of those different detectable radicals will provide more accurate information of the characteristics of the gas composition. Therefore, it will be very useful in the determination of fuel-air ratio.

The spark plug based diagnostics has been shown to be a promising method in the determination of fuel-air ratio and it is worth further study in the future.

References

Albrecht, H., W.H. Bloss, W. Herden, R. Maly, B. Saggau, and E. Wagner [1977], "New Aspects on Spark Ignition," SAE 770853.

Blair, D.T.A., F.M. Bruce, and D.J. Tedford [1963], Proc. 6th Int. Conf. on Phenomena in Ionized Gases, Paris, Vol. 1, p 321, etc.

Borghese, A., A. D'Alessio and C. Venitozzi [1985], " Time-Resolved Electrical and Spectroscopic Study of Very Short Spark Discharge", Proceeding of the Int. Symposium on Diagnostics and Modelling of Combustion in Reciprocating Engines,Tokyo. (N/A)

Clark, G.L., A.L. Henne [1927], "Ultra-violet Spectroscopy of Engine Flames," SAE Journal v.XX, no.2, February 1927.

Cobine, J.D. [1958], "Gaseous Conductors," Dover, New York.

Crawford, J.G. and J.S. Wallace [1996], "Validation Tests for a Fast Response Flame Ionization Detector for In-Cylinder Sampling Near the Spark Plug," SAE 961201.

Dutton, J. [1978], "Spark breakdown in uniform fields," in "Electrical breakdown of gases", J.M. Meek and J.D. Craggs, Eds., John Wiley, New York.

Dyer, M. [1979], "Rayleigh Scattering Measurement of Time-Resolved Concentration in a Turbulent Propane Jet," AIAA, Vol.17, No.8.

Galliot, F., W.K. Cheng, C. Cheng, M. Sztenderowicz, J.B. Heywood and N. Collings [1990], "In-cylinder Measurements of Residual Gas Concentration in a Spark Ignition Engine," SAE 900485.

Gatowski, J.A. [1984], J.B. Heywood, C. Deleplace, "Flame Photographs in a Spark-Ignition Engine", Combustion and Flame, vol. 56, pp.71-81, 1984.

Gaydon, A.G. [1974], "The Spectroscopy of Flames".

Hancock, M.S., M.R. Belmont and D.J. Buckingham [1988], "The Correlation Between Early Light Emission and Peak Pressure in a Spark-Ignition Engine," IMechE Proceedings, Combustion in Engines - Technology and Application, C56/88, p. 1.

Heywood, J.B. [1988], "Internal Combustion Engine Fundamentals," McGraw-Hill Book CO., Inc., U.S.A..

Howatson, A.M. [19??], "An Introduction to Gas Discharges".

Johnston, S.C. [1980], "Raman Spectroscopy and Flow Visualization Study of Stratified Charge Engine Combustion", SAE 800136.

Klimstra, J. and F. Overmare [1991], "monitoring the spark - Plug Gap of Natural-Gas-Fuelled Stationary Engines," SAE 912361.

Koenig, M. and M.J. Hall [1997], "Measurements of Local In-Cylinder Fuel Concentration Fluctuations in A Firing SI Engine," SAE 971644.

Kollmeier, H.-P. [1986], "Detection of Flame Propagation During Knocking Combustion by Optical Fiber Diagnostics," SAE 861532.

Kuffel, E. [1959], Proc. 4th Int. Conf. on Phenomena in Ionized Gases Uppsala, Vol. 1, p.418, 1959

Lawton, J. and F.J. Weinberg [1969], "Electrical aspects of combustion", Clarendon Press, Oxford.

Lee, K-H. and D.E. Foster [1995], "Cycle-by-Cycle Variations in Combustion and Mixture Concentration in the Vicinity of Spark Plug Gap," SAE 950814.

LLlewellyn-Jones, F. [1957], "Ionization and breakdown in gases," p. 65, Methane, as quoted by Lawton and Weinberg [1969], p. 139.

Maly, R. [1976], "Ignition and Propagation of Flame Fronts in Lean CH4-Air mixtures by the Three Modes of the Ignition Spark," Proceedings of Seventeenth International Symposium on Combustion, pp. 821-831, The Combustion Institute.

Maly, R. [1984], "Spark Ignition: Its Physics and Effect on the Internal Combustion Process," in J.C. hilliard & G.S. Springer (eds.), Fuel Economy in Road Vehicles Powered by Spark Ignition Engines, chap.3, plenum Press, New York.

The Matheson Unabridged Gas Data Book [1974].

Meek J. M. & J. D. Craggs [1978], "Electrical Breakdown of Gases," A Wiley-Interscience Publication, 1978.

Merer, R.M. [1994, "Spark Spectroscopy for Spark Ignition Engine Diagnostics," M.A.Sc Thesis.

Merer, R.M. and J.S. Wallace [1995], University of Toronto, "Spark Spectroscopy for Spark Ignition Engine Diagnostics," SAE 950164.

Moeser, P. and W. Hentschel [1996], "Development of a Time Resolved Spectroscopic Detection System and its Application to Automobile Engines," SAE 961199.

Moruzzi, J. L., and J. Lucas [1974], Proc. 3rd Int. Conf. on Gas Discharges, IEE Conf. Publ. No.118, p114, 1974

Nagase, K., K. Funatsu, Y. Muramatsu and M. Kawakami [1985], "An Investigation of Combustion in Internal Combustion Engines by Means of Optical Fibers", SAE 851560.

Nelson, G.O. [1992], Gas Mixtures

Nishimura, Y. [1987], "Engine Control System For Lean Combustion," SAE 871171.

Ohyama, Y., M. Ohsuga and H. Kuroiwa [1990], "Study on Mixture Formation and Ignition Process in Spark Ignition Engine Using Optical Combustion Sensor," SAE 901712.

Peckham, M. and N. Collings [1992], "Study of Engine Wall Layer Hydrocarbons with a Fast-FID," SAE 922237.

Pendlebury, M.A., C.O. Nwagboso [1996], "An optical Sensor for Determination of Combustion Parameters in a Natural Gas Fueled Spark Ignition Engine," SAE 960856.

Pinnock, R.A., P. Extance and C.P. Cockshott [1987], "Combustion Sensing Using Optical Fibbers," Paper presented at Sixth International Conference on Automotive Electronics, IEE, London, 1987.

Rassweiler, G.M., L. Withrow [1932], "Emission Spectra of Engine Flames," Industrial and Engineering Chemistry v.24, no.5, May 1932.

Rather, H. [1964], "Electron avalanches and breakdown in gases," Butterworths, London.

Remboski, D.J., S.L. Plee, K. Jay and J.K. Martin [1989], "An Optical Sensor for Spark-Ignition Engine Combustion Analysis and Control", SAE 890159.

Shimasaki, Y., M. Kanehiro, S. Baba., S. Maruyama, T. Hisaki, and S. Miyata [1993], "Spark Plug Voltage Analysis for Monitoring Combustion in an Internal Combustion Engine", SAE 930461.

Shoji, H., T.Shimizu, K. Yoshida, and A. Saima [1995], "Spectroscopic Measurement of Radical Behavoir Under Knocking Operation," SAE 952407

Sleighthholme, G. [1990], "In-Cylinder Measurements of Charge Inhomogeneity in a Spark Ignition Engine," SAE 900484.

Soltau, J.P. [1960], " Cylinder Pressure Cariations in Petrol Engines," pp. 99-116, July 1960. (Instn Mech. Engrs Conf. Proc.)

Sphma, K., T. Yukitake, S. Azuhata, and Y. Takaku [1991], "Application of Rapid Optical Measurement to Detect the Fluctuations of the Air-fuel Ratio and Temperature of a Spark Ignition Engine," SAE 910499.

Spicher, U. and G. Schmitz, H.-P. Kollmeier [1988], " Application of a New Optical Fiber Technique for Flame Propagation Diagnostics in IC engines," SAE 881637.

Summers, T. and N. Collings [1995], "Modelling the Transit Time of a Fast Response Flame Ionization Detector During In-Cylinder Sampling," SAE 950160.

Verhoeven, D. [1995], " Spark Heat Transfer Measurements in Flowing Gases", SAE 952450.

Witze, P.O., M.J. Hall and J.S. Wallace [1988], "Fiber Optic Instrumented Spark Plug for Measuring Early Flame Development in Spark Ignition Engines," SAE 881638.

Witze, P.O., M.J. Hall, and M.J. Bennett [1990], "Cycle-Resolved measurements of Flame Kernel Growth and Motion Correlated with Combustion Duration, " SAE 900023.

Young, M.B. [1981], "Cyclic Dispersion in the Homogeneous - Charge Spark-Ignition Engine - A literature Survey," SAE Paper 810020.

Appendix A Time Setting for the Time-Control-Switch of the Discharging System

Based on the previous experimental results which show that at constant temperature, with the same electrodes gap size, the breakdown voltage will increase while the pressure increases in a gas [Meek & Craggs, 1978], a series of preliminary experiments have been done in N_2 as to set the proper charging time of the ignition coil. The experimental temperature was set at room temperature (T = 25 °C) and the pressure

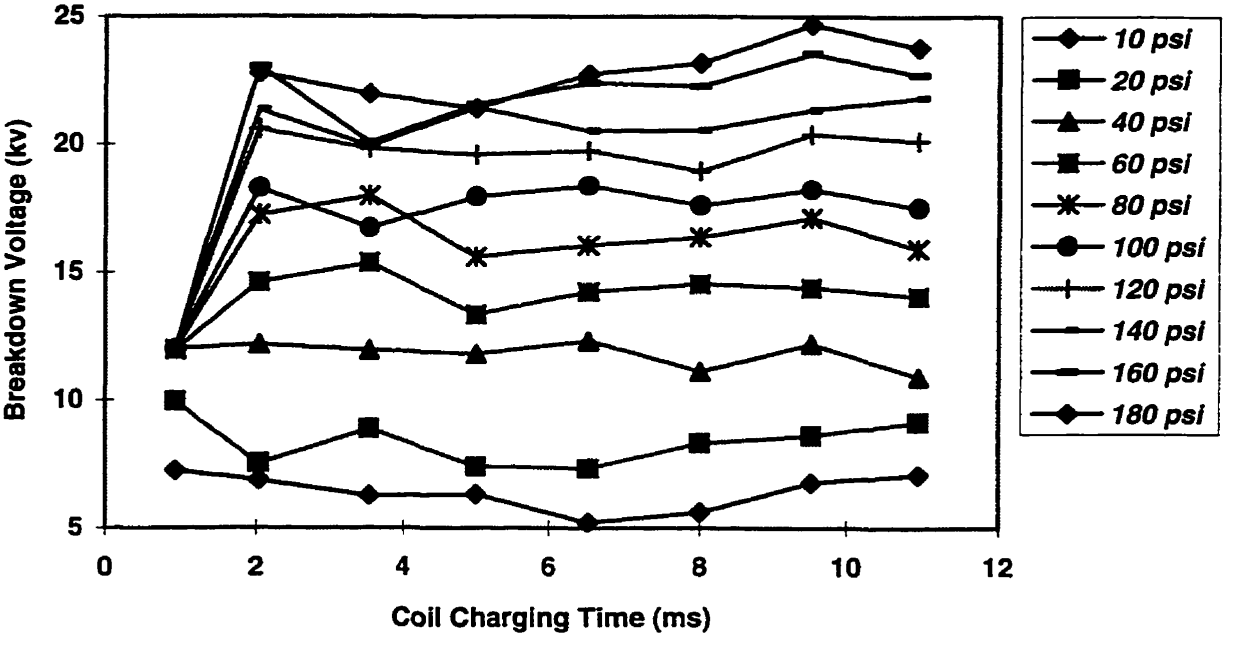

Fig. A-1 Breakdown Voltage vs. Coil Charging Time at Different Pressure (in Pure N_2, T=25 °C, Spark Plug Gap Size d=1.0 mm)

of the combustion chamber was monitored from 20 psig to 180 psig by a pressure gauge.

By adjusting the coil charging time period from 1 ms to 11 ms, eight sets of data have been recorded. Figure A-1 presents the results which showed that the measured breakdown voltage of N_2 varied with the change of the coil charging time and incresed when the pressure increases. From this plot, it is clear that when the switch "on" period is longer than 8 ms (coil charging time is longer than 8 ms), the change of the breakdown voltage only affected by the pressure change, agreeing with the previous studies. Therefore, a period of 8.5 ms was chosen for the coil charging time. In addition, this 8.5 ms long coil charging time is reasonable even for a production engine. For example, when a 4-stroke engine runs at 2000 rpm, each cycle lasts as long as 0.06 s (60 ms). For a 4-cylinder engine, only 2 cylinders fire every cycle. Hence, each cycle for each cylinder lasts 30 ms and each stroke lasts 15 ms. Clearly, an 8.5 ms long coil charging time was suitable.

Appendix B Pressure Setting for Testing the Effects of CO_2 and CH_4 on the Breakdown Voltage

In order to well simulate the engine operating conditions, a real engine cylinder head has been used as the important part of the experimental combustion chamber. The cylinder head is from a Chev-V8 5.0 liter engine (GM 1977-1993) which has the following engine specifications while the geometry of the cylinder, the piston, the connecting rod and the crankshaft was shown clearly in Fig. B-1.

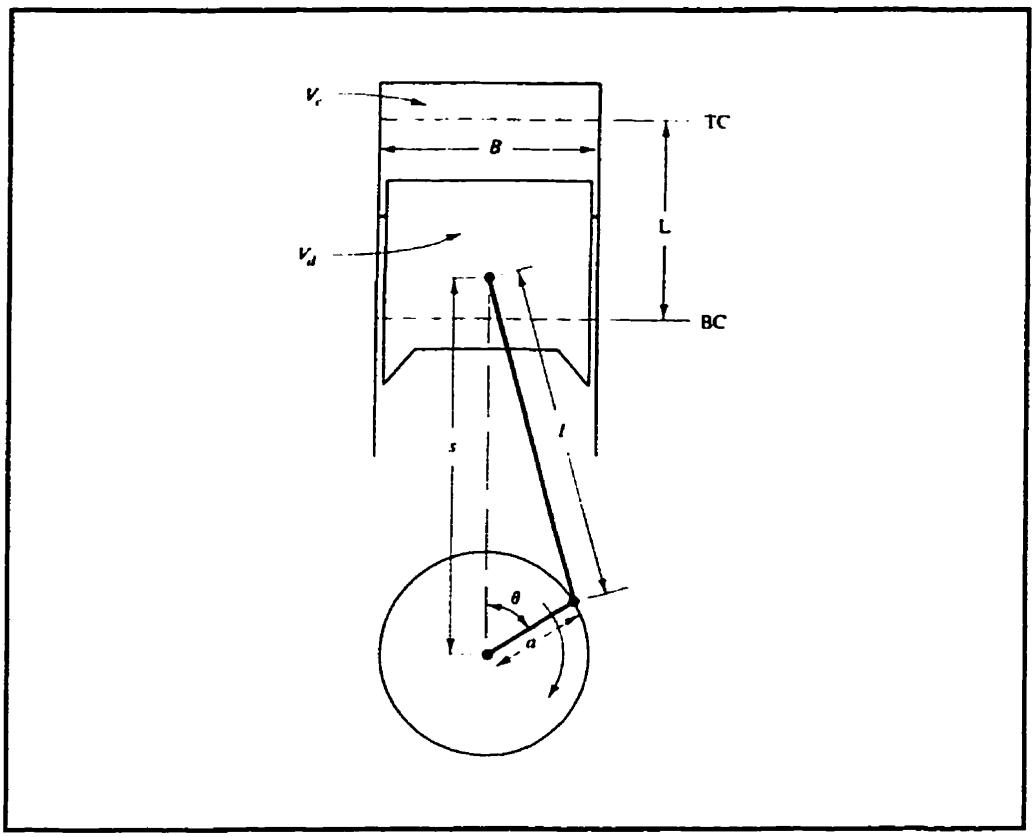

Fig B-1 Geometry of Cylinder, Piston, Connecting Rod and Crankshaft

B = 3.736 " — Bore

L = 3.48 " — Stroke

$a = L / 2 = 1.74''$ — Crank Radius

$l = 5.7''$ — Connecting Rod Length

Generally, for a natural gas fueled SI engine, the compression ratio (r_c) ranges from 9 to 12, and the spark timing can be set at crank angle $\theta = 30°$ BTDC (before top dead center).

For a 4-stroke SI engine, the compression stroke can be assumed as an isentropic process which can be expressed by the following equation,

$$Pv^{\gamma} = \text{Constant},$$

choosing $\gamma = 1.32$, hence

$$\frac{P_1}{P_2} = (\frac{V_2}{V_1})^{1.32},$$

where P_1 and V_1 are the pressure and volume when the cylinder has freshly charged mixture (P_1=1atm), and P_2 and V_2 are the pressure and volume of the cylinder at the time of the spark ($\theta = 30°$ BTDC).

Normally, the ratio of the cylinder volume V at any crank position θ to the cylinder clearance volume is:

$$\frac{V}{V_c} = 1 + \frac{1}{2}(r_c - 1)[R + 1 - \cos\theta - (R^2 - \sin^2\theta)^{\frac{1}{2}}]$$

where $R = \frac{l}{a}$, the ratio of the connecting rod length to crank radius, here R = 3.27586.

a) When $r_c = 9$, $\theta = 30$ °BTDC, $V_2/V_c = 1.6894$, and $V_2/V_1 = 0.1877$, and from $P_1V_1^{\gamma} = P_2V_2^{\gamma}$, $P_2 = 132$ psia.

b) When $r_c = 12$, $\theta = 30$ °BTDC, $P_2 = 159.8$ psia.

Taking into account of other practical factors, such as the variations of the temperature and spark timing, 150 psig and 180 psig were chosen as the monitored pressure inside the simulated combustion chamber before spark ignition in the experiments of testing the effects of CO_2 and CH_4 on the breakdown voltage. For the combustible mixtures experiments, in the sake of safety, also for the simplification, only 150 psia was chosen as the final filling pressure of air in producing the combustible mixtures.

Appendix C: Partial Pressure Method for Producing Combustible Mixtures

For the combustible mixtures, in order to evaluate the spark spectroscopy method in diagnosing the gas compositions, it is desirable to know the fuel-air ratio, as well as the fraction of the residual gas accurately. Thus, an easy to control method of preparing mixtures — the partial pressure method — was applied after a study of its feasibility.

Since in the present work, the pressure and the temperature of the combustion chamber were monitored at constant values (P = 150 psia, T = 277 °F), the amount of each component can be calculated according to the fuel-air ratio while the gases were regarded as ideal gases.

Theoretically, when the gases are assumed to behave as ideal gases, the concentration of the gas mixture can be calculated straightforwardly as following [Nelson, 1992],

$$P = p_a + p_b + \cdots + p_n$$

where P is the total pressure and $p_{a,b,\ldots,n}$ are the contributing partial pressures of the component gases. The concentration in percent by volume of each component at one temperature is

$$C_{\%} = \frac{10^2 p_n}{P}$$

In general, at room temperature and pressure, most gases conform to the perfect gas law. However, when the pressure and temperature change, the deviations are pronounced and sometimes can be corrected by the compressibility, κ, which is given by

$$\kappa = \frac{PV}{RT}$$

where P, V, and T are measured experimentally to yield κ, a correction factor for nonideality. Thus corrected, the concentration on the nth component can be expressed by

$$C_n = \frac{\frac{10^2 p_n}{\kappa_n}}{\frac{p_a}{\kappa_a} + \frac{p_b}{\kappa_b} + \bullet\bullet\bullet + \frac{p_n}{\kappa_n}}$$

where κ_n is the compressibility of the pure components at the filling pressure and $\kappa'_{a,b,\ldots,n}$ are the compressibility of the gas mixtures at the final pressure. It must be remember that as each component is added to the system under pressure, any temperature rise must be accounted for. Either an appropriate calculation correction must be made or the system must be allowed to return to the initial temperature before a pressure reading is made and the next component of the mixture. In general, it is best to add the most compressible gas first, unless it happens to be the major components of the mixture. If the compressible gas is admitted last, it is in the most compressed state and will usually introduce the greatest error.

In the present work, methane (CH_4) is the most compressible gas when the pressure increases. Hence, it is the first gas to be added when there is no residual gas. When doing the experiments with residual gas, in order to keep the real residual gas present in the chamber, CH_4 was added secondly. As listed in Table C-1, within the experimental conditions, the compressibility of those important gases is very close to units, indicating that the gases conform to the perfect gas law. The deviations of the concentrations caused

by the compressibility is not very significant, as shown in Table C-2 and Table C-3. Thus, this partial pressure method is feasible in the present work.

Table C-1: Compressibility of the Important Gases in the Mixing Process (T = 400 K) [The Matheson Unabridged Gas Data Book, 1974]

Pressure (atm) / Species (gaseous)	0.4	1.0	4.0	10.0
Air	/	/	/	1.00205
CH_4	/	0.9996	/	0.995
CO_2	0.99927	0.99817	0.99267	0.9185
N_2	/	1.0001	1.0005	1.0024

Table C-2: Deviation of the Fuel-Air Equivalence Ratio Caused by the Compressibility Error

Fuel-air Equivalence Ratio (ϕ)			Concentration of CH_4 (volumetric %)	
Theory	Partial pressure method	Error (%)	Theory	Partial pressure method
0.7	0.701842	0.263118	6.831934	6.8487
0.8	0.802126	0.265693	7.732457	7.7514
0.9	0.902414	0.268268	8.615738	8.6369
1.0	1.002708	0.270843	9.482268	9.5055
1.1	1.103008	0.273418	10.33252	10.3578

Table C-3: Deviation of the Fraction of the Residual Gas Caused by the Compressibility Error

Fraction of Residual Gas (Volumetric %)		
Theory	Partial pressure method	Error (%)
5	5.040548	0.811
10	10.0811	0.811
15	15.12164	0.811
20	20.16219	0.811
25	25.20274	0.811

Appendix D Calibration of the Schaevitz P1081 220 psig Pressure Transducer

The Schaevitz P1801 220 psi V.G. pressure sensor was used to monitor the final filling pressure of air in the mixing procedure for the combustible mixtures. It was calibrated by a Dead Weight Tester from 5 psig to 200 psig at 25 °C with the atmospheric pressure at 14.76 psia. Figure D-1 gives the calibration curve which shows that the output* is a linear function of the pressure (psia). When the pressure is 150 psia, the output is 3.400 V.

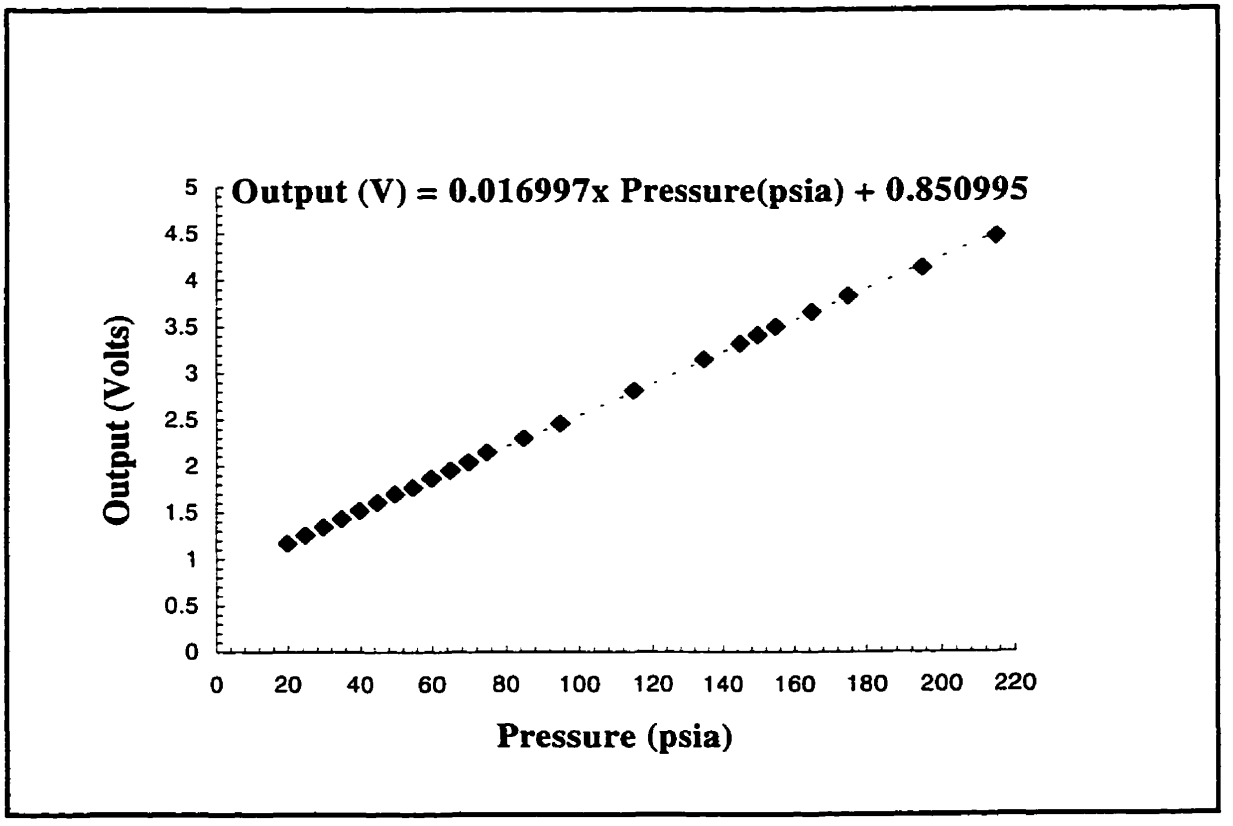

Fig. D-1 Calibration of the 220 psig Pressure Tranducer

* The output of the pressure transducer was measured by a Fluke 87 true RMS multimeter.

Appendix E Calibration of theViatran Model 118 75 psia Pressure Transducer

The Viatran Model 118 75 psia pressure transducer was used to monitor the filling pressure of CH_4 (without residual gas), as well as the filling pressure of the residual gas and CH_4 in the residual gas tests. It was calibrated by the a Dead Weight Tester from 5 psig to 60 psig at 25°C and with the atmospheric pressure at 14.803 psia. Figure E-1 gives the calibration curve which shows clearly that the output is a linear function of the pressure (psia). This pressure transducer was powered by a full bridge amplifier

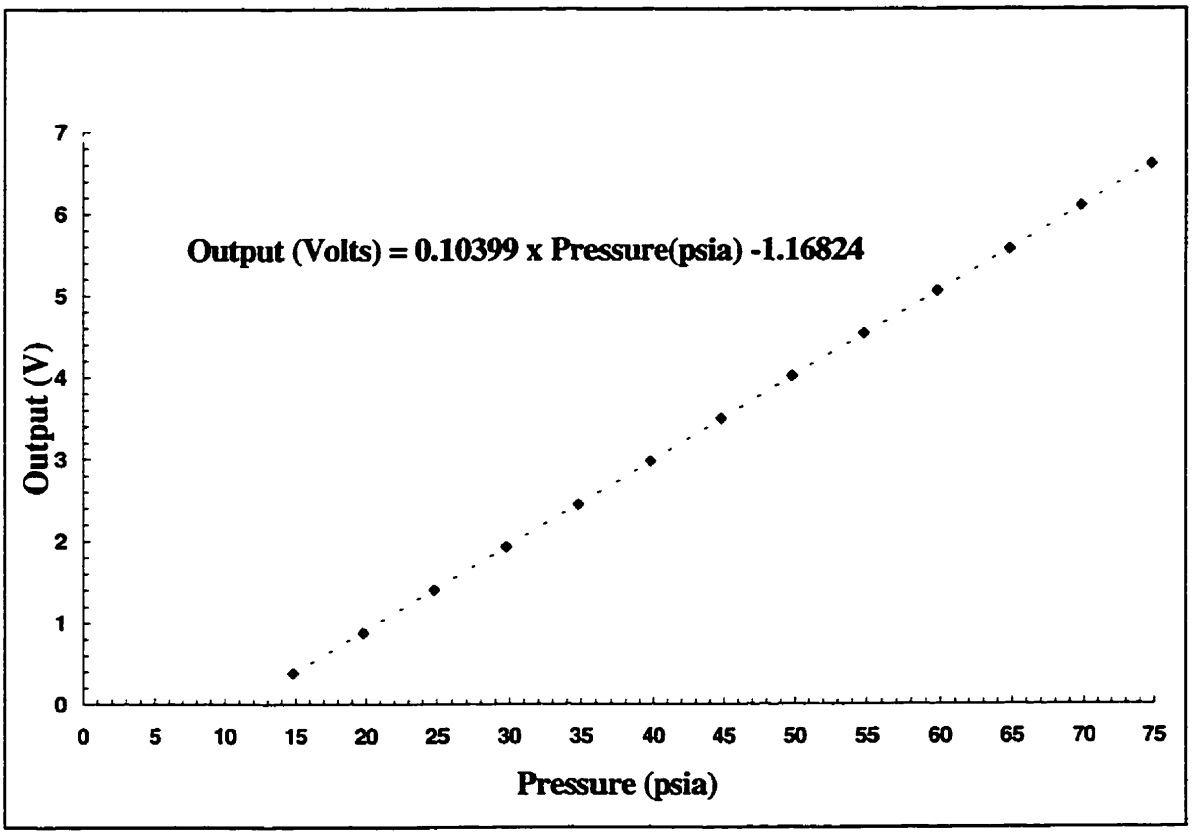

Fig. E-1 Calibration of the 75 psia Pressure Transducer

which has an offset adjust. This will cause the intersection of the curve to drift with time, but the slope will not change. During the experiments, the recalibration was done from time to time.

Appendix F Homogeneity of the Combustible Mixtures Tested by the means of HFR400 Fast FID

For the tests in combustible mixtures, the mixtures were produced by the partial pressure method, using the high accuracy pressure transducers. Since homogenous mixtures are desirable for all the tests, it is necessary to check the homogeneity of the mixture achieved for different fuel-air equivalence ratios by the experimental methods. Hence the HFR400 Fast FID was used to check the hydrocarbon concentrations of the mixture inside the combustion chamber at three fuel-air equivalence ratios (ϕ = 0.7, 0.8 and 0.9). At each ratio, the mixture was produced at least five times by using the partial pressure method as used in the other experiments. A metering valve was used to control the transmission of the mixture to the FFID. The mixing time (the period between the final filling of air and the start of the test — when the metering valve was open) was chosen at 80 s*. The values of the platform of the output of FFID was measured as the relative† concentrations of the hydrocarbon. Figure F-1 presents the results of the measurements of the relative hydrocarbon concentrations inside the combustion chamber at different fuel-air equivalence ratios which shows that at each ϕ, the outputs of the FFID — relative hydrocarbon concentrations — stay as a constant, indicating that the mixture is very homogenous and the mixing procedure is repeatable. Also Fig. F-1 shows that the relative hydrocarbon concentrations is a quite linear function of the fuel-air equivalence

* Several periods were tried during the tests. Finally 80 s was chosen because the output of the FFID has a very stable platform when choosing this mixing time, indicating that mixtures inside the chamber is homogenous. Hence, The same length of mixing time 80 s was used in all the other combustible tests.

† Since the FFID was not calibrated before doing these tests, hence the hydrocarbon concentrations measured by this FFID were relative values.

ratio from 0.7 to 0.9. indicating that the HC concentration increased when the fuel-air equivalence ratio was increased by adjusting the partial pressure of different gases.

Clearly, the combustible mixtures produced by this partial pressure method are quite homogeneous and the mixing procedures are very repeatable. Hence, the mixing method is acceptable.

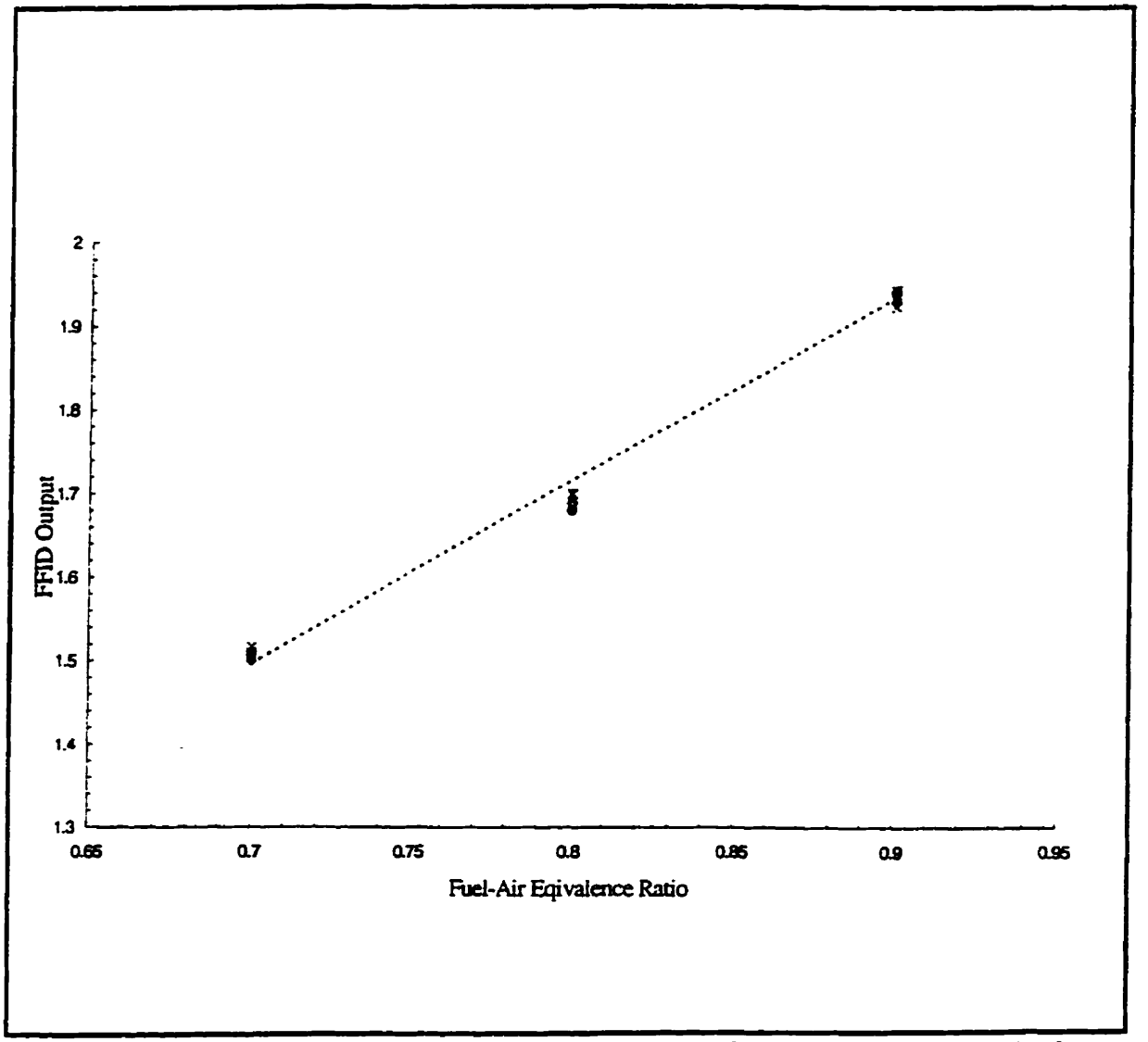

Fig. F-1 Relative Hydrocarbon Concentrations at Different Fuel-Air Equivalence Ratios (Measured by FFID)

Appendix G Design Concepts — Two Alternative Optical Probes

In order to detect the spark light emission, an efficient and replaceable optical probe is required. Three designs have been studied and the most economical on was chosen for the experiments. The following paragraphs describe in detail the other two feasible designs which can be refered to in later study.

Figure G -1 shows the first design of the new optical spark plug. This plug has a shifted center electrode which allows more space for the optical parts. A 3 mm diameter quartz rod which has two mirror aluminum coated 45° faces at the two ends could be inserted inside the spark plug body. The two mirror faces will provide good reflection in order to transmit the spark light emission out of the chamber.

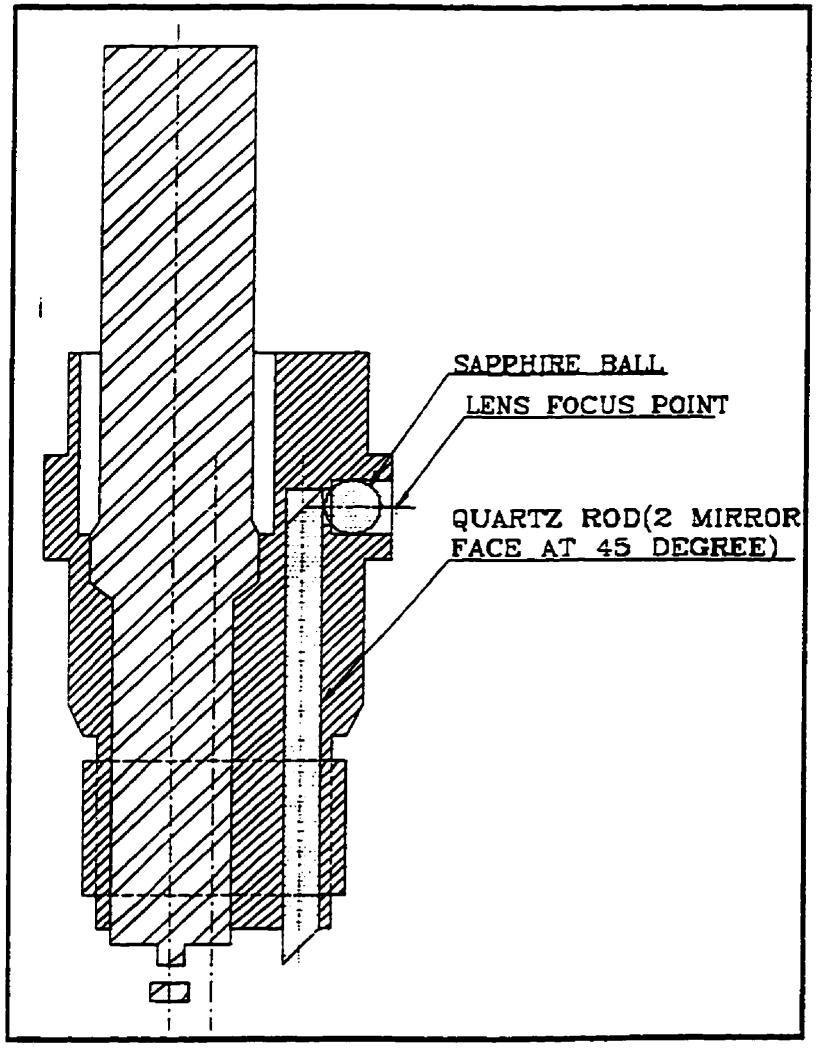

Fig. G-1 Schematic of the Optical Spark Plug

Before the light goes into the transmitting optical fibre, a sapphire ball is used as a collimator. This design will help to increase the view area of the spark emission as well as increasing the strength of the optical access parts. However, the expense of manufacturing a new spark plug body of this design is relatively high, and the double reflection and collimating will also cause significant light emission loss.

Compared to the first design, the second design is more economical since it is half ready. A FFID (Fast Flame Ionization Detector) offset sampling spark plug has been modified to be used for this application. Since a FFID sampling spark plug already has a modified body which includes a shifted center electrode as well as a partially threaded hole which allows access to the spark gap, it could be converted to an optical spark plug

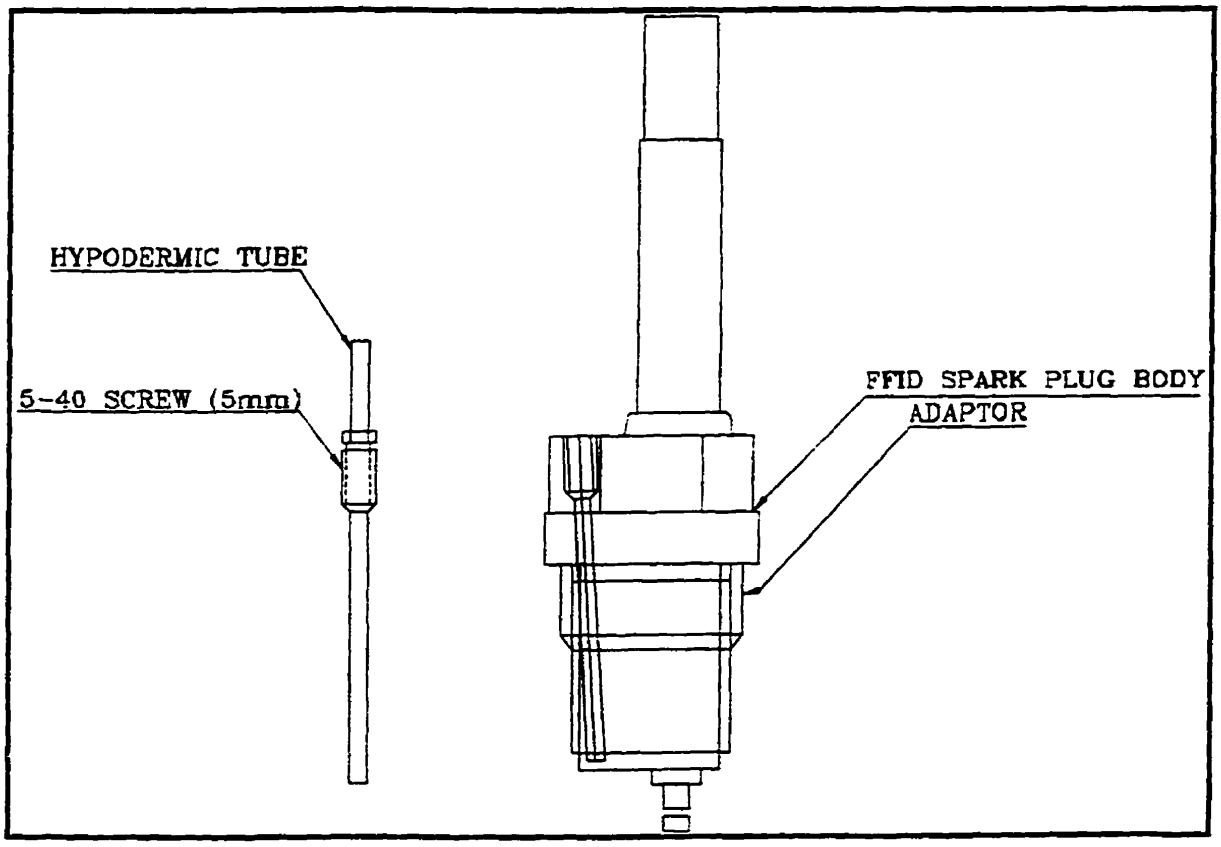

Fig. G-2 Modified FFID Spark Plug as an Optical Probe

body easily. As shown in Fig. G-2, an adapter was used to convert the Beru-Kistler FFID spark plug (D14F-7D2) to have the tapered seat of an AC R43TS (GM) spark plug which is specified for the spark plug hole of the same cylinder head as used in the breakdown voltage measurements in non-combustible mixtures.

The optical probe consists of a 750 μm diameter stripped Diaguide ST-U600F-FV optical fibre with enhanced UV characteristics enclosed in a stainless steel hypodermic tube (0.042" OD, 0.032" ID) which maintains the strength of the stripped optical fibre. The optical probe was inserted inside another wider hypodermic tube (0.058" OD, 0.042" ID) which is shown in Fig. G-2 with a drilled out screw soldered on it. The stripped optical fibre and the two hypodermic steel tubes were fixed together by Metal-Set epoxy and then were threaded inside the modified FFID spark plug with the end of the optical fibre exposed to the spark gap in order to detect the spark light emission. Since a tiny scratch on the end of the optical fibre may cause much loss of light emission, the end of the optical fibre has been polished very carefully under a microscope by a series of polishing papers of increasing fineness before being assembled to the spark plug to keep the fibre end well polished without any tiny scratches on it.

This design has been used in the combustible mixture tests to study the light emission. After sets of experiments, it was found that the central electrode wasn't insulated very well. There were arcs occurring around the bottom of the ceramic insulator. The unexpected arcs caused a loss of energy from the spark discharge, precluding the repeatability of the tests of the breakdown voltage and the intensity of the

spark light emission. Therefore, the third design (described in Section 3.3.1) was used eventurally.

Appendix H Newport (Klinger) P10-390-A Bandpass Filter

After the beam splitter, the light from the spark emission was divided into two light beams with roughly equal intensity. One beam goes directly into a photomultiplier tube for measurement of the shot intensity, while the other beam should go through a narrow band pass optical apparatus before entering the second photomultiplier tube for measurement of the spectral intensity.

At the beginning, a Newport (Klinger) P10-390-A, 0.5" diameter narrow bandpass filter was tried, which has 10 nm bandwidth with the center wavelength at 390 nm. In order to well isolate the spectral light emission from the CN radical which is centered at 385 nm, an angled filter mount was utilized. In theory, a small tilt in collimated incident light will cause the center wavelength of a thin film bandpass filter to shift to a shorter wavelength. From the formula stated below, the required tilt angle for the incident light can be calculated for the specified center wavelength (with a restriction of $\theta_i \leq 15°$).

$$\lambda_{\theta i} = \lambda_0 (n_\theta^2 - \mathrm{Sin}^2\theta_i)^{1/2} (n_\theta)^{-1}$$

where $\lambda_{\theta i}$ = center wavelength at $\theta_i°$ angle of incidence

λ_0 = center wavelength at 0° angle of incidence

θ_i = angle of incident light from normal

n_θ = effective index; specified as a numerical value derived for the indices of the thin film layers of the bandpass filter.

In our case, $\lambda_{\theta i}$ = 385 nm, λ_0 = 390 nm, and n_θ = 1.5, so we get θ_i = **13.85°** which is smaller than 15°.

Finally, an angle-adjustable assembly was designed to house the filter at ~13.85° inside the side-on photomultiplier housing before the photomultiplier tube. Also the center wavelength of the tilted filter has been tested by a professional spectrometer with high resolution in OLLRC (Ontario Laser and Lightwave Research Center). The two transmittance plots shown in Fig. H-1 (untilted) and Fig. H-2 (tilted) show the clear center wavelength shift of the tilted filter. As shown in Fig. H-2, the tilted filter has central wavelength at 385nm with a 10 nm bandwidth. However, even if the light emission intensity is measured near the center of the wavelength of CN radical, it is still impossible to avoid the effects of other radicals (e.g. CH radical) on the measured results. Thus, it would be virtually impossible to differentiate quantitatively the radicals to be measured from other radicals that might affect the measurements. In the present work, since the light intensity from the other radicals is relatively lower comparing to the light intensity from CN for a very short instant of time after the spark discharge, such effect was assumed to be negligibly small. Therefore, the light intensity measurement obtained after this filter is assumed to present the behavior of the radical of CN.

After several sets of experiments were done with this filter, it showed that the results had some unexpected variations from the measurements of the spectral light emission. Hence, it was replaced by the monochromator which has higher resolution (5 nm bandwidth). However, there are still some benefits in looking for an appropriate filter

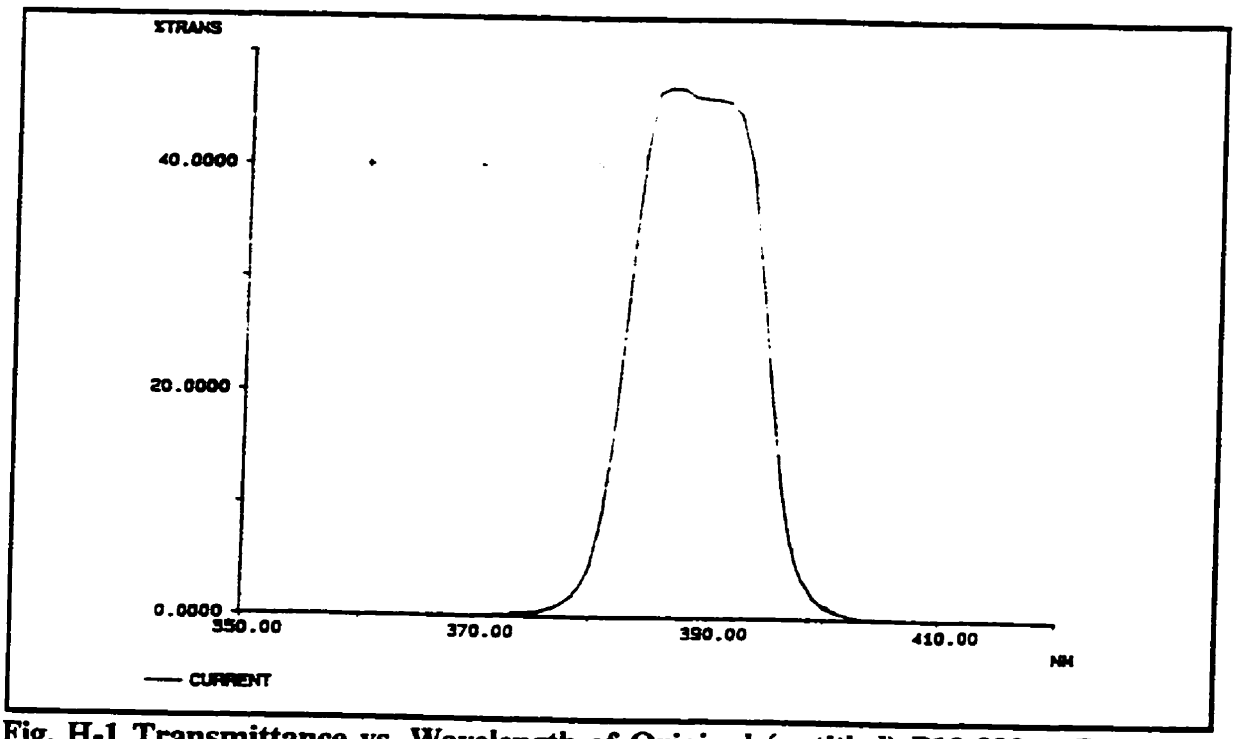

Fig. H-1 Transmittance vs. Wavelength of Original (untitled) P10-390-A Bandpass Filter (Tested By OLLRC)

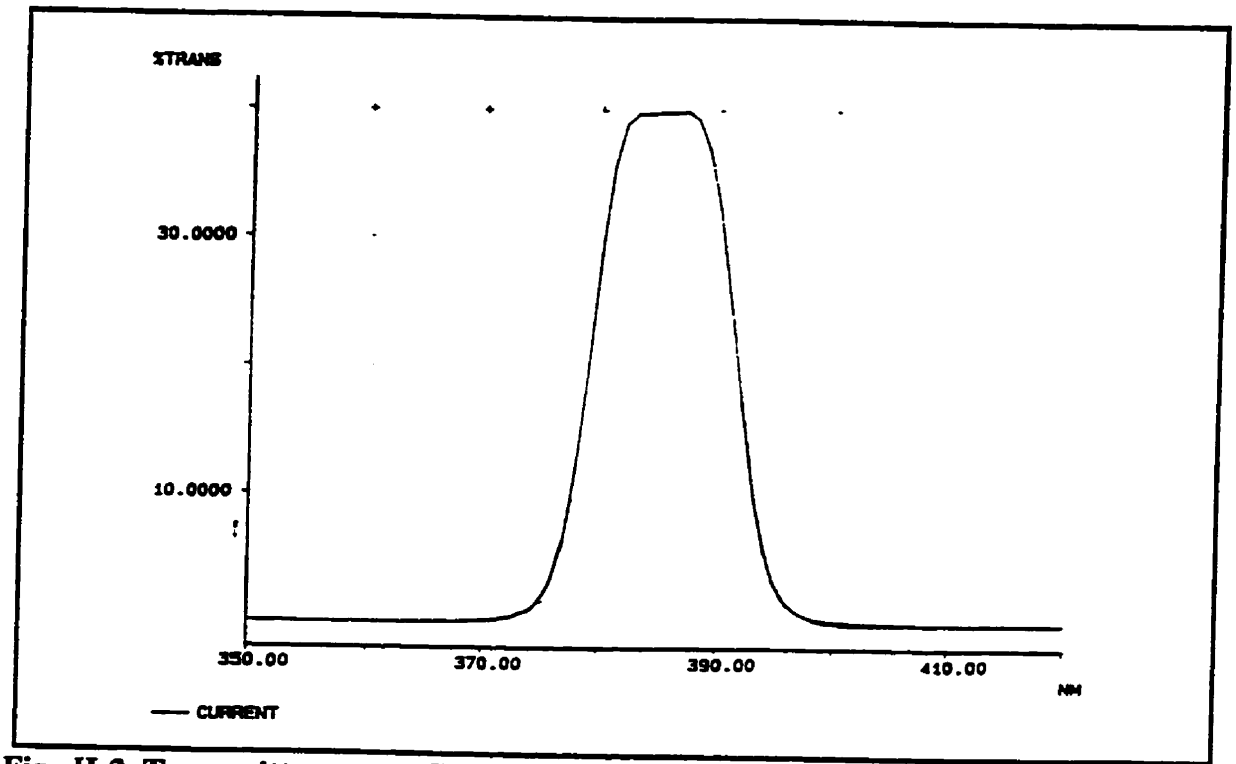

Fig. H-2 Transmittance vs. Wavelength of P10-390-A Bandpass Filter (tilted at 13.85°) (Tested By OLLRC)

in the further research, which will help not only to simplify the apparatus but also to reduce the light loss of the spark emission caused by the monochromator, especially when applying the other two designs of the optical probes which will detect less light emission from the spark compared to the present probe.

Appendix I Comparability of the Spectral Intensity and the Shot Intensity

In the combustible mixtures tests, the spark light emission was channeled out of the high pressure combustion chamber by inserting an optical fibre inside the steel plate, facing the gap of the spark plug perpendicularly. This beam was split into two equal channels, each of which was tested separately as broadband intensity (total or shot intensity) and spectral intensity (considered as the intensity of CN) respectively. The shot intensity was used to normalize the spectral intensity to reduce the effect of the variation of the spark initiation which in turn causes variations in the light detection of the optical fibre. In order to keep these two channels of light comparable, the intensity of the spark light was attenuated before it enters the PMT to keep the detector within the linear response range. However, it is important to analyze the comparability of the light intensity of these two channels.

As shown in Fig. I-1, the light intensity of the two channels was detected and converted to two voltage signals by the two PMTs and a dual-channel amplifier, and then were recorded by an oscilloscope.

In theory, it can be assumed that for the same mixture under the same condition, the spark emits the same numbers of photons across the wavelength range of interest (300 nm to 600 nm), contributing to the total intensity of I (λ), and the ratio of the spectral intensity (total energy of the photons radiated around 385 nm) to the shot intensity (total energy of the photons radiated from 300 nm to 600 nm) will be a constant. Since the optical probe position is fixed, the variations of the initiation of the spark will affect the

numbers of the detectable photons, and hence affect the detectable light intensity I (λ) of the spark, resulting in variations of the output voltage recorded after the optical detectors. The effect of the changing position of the spark on the detectable intensity can be expressed by a view factor k. When the spark occurs at different positions, the light intensity detected by the optical probe can be expressed as k• I (λ). The following is the comparison of the spectral light intensity and the shot intensity in terms of the output voltage.

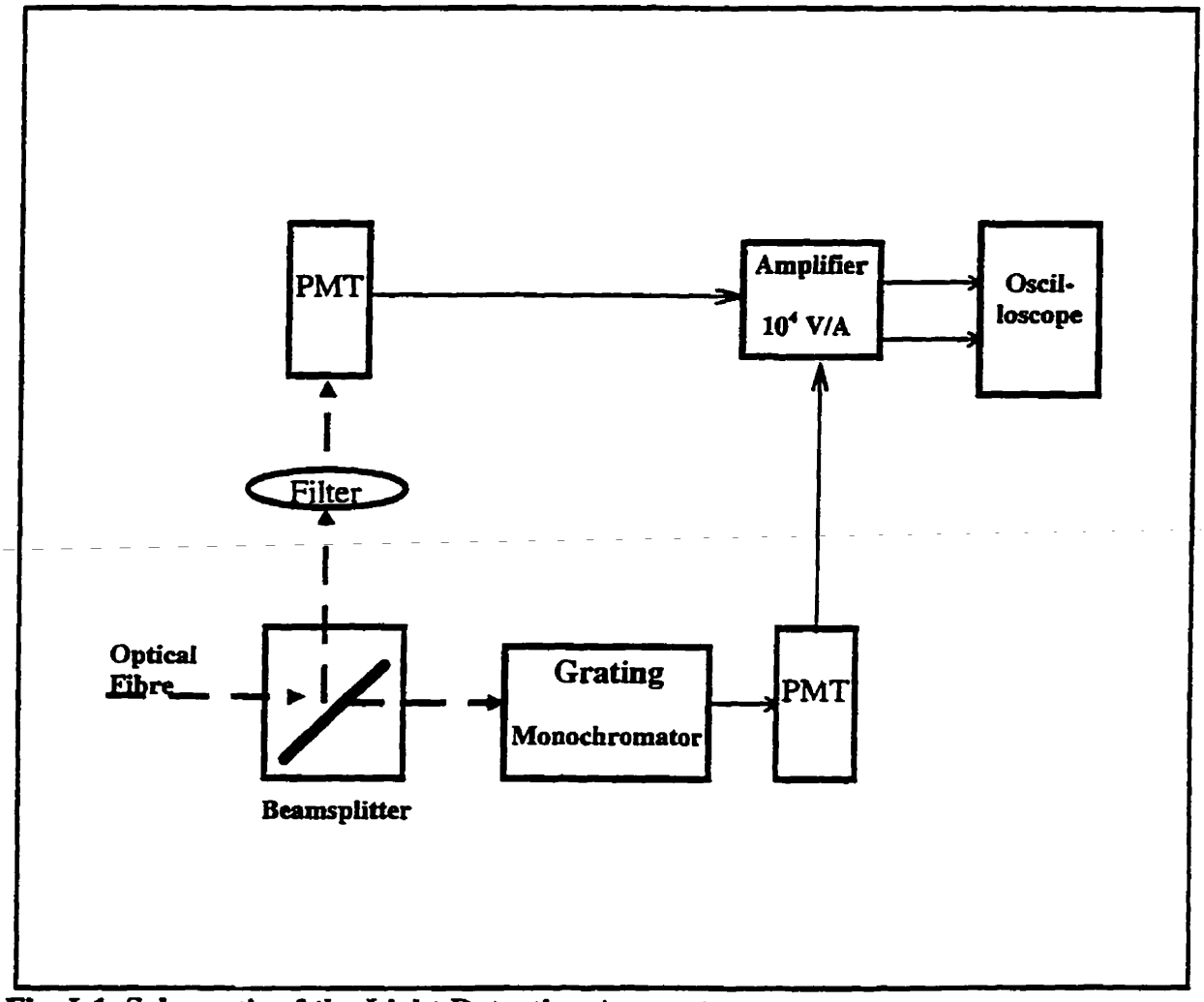

Fig. I-1 Schematic of the Light Detection Apparatus

$$V_{spec} = \frac{1}{2}\int_{\lambda_1}^{\lambda_2} k \bullet \alpha(\lambda) \bullet I(\lambda) \bullet \beta(\lambda) \bullet \delta \bullet d\lambda$$

$$V_{shot} = \frac{1}{2}\chi \bullet \int_{\lambda_0}^{\lambda_n} k \bullet I(\lambda) \bullet \beta(\lambda) \bullet \delta \bullet d\lambda$$

where, k is the view factor of the optical probe to the spark;

$I(\lambda)$ is the spark light intensity, a function of the wavelength λ;

$\alpha(\lambda)$ is the transmittance of the monochromator, a function of λ;

$\beta(\lambda)$ is the response of the photomultiplier, also a function of λ;

χ is the transmittance factor of the neutral density filter (constant);

δ is the gain factor of the dual-channel amplifier (constant);

$\lambda_1 = 382$ nm, $\lambda_2 = 387$ nm, $\lambda_0 = 300$ nm, and $\lambda_n = 600$ nm.

Therefore, the ratio of the V_{spec} to the V_{shot} is,

$$\frac{V_{spec}}{V_{shot}} = \frac{\int_{\lambda_1}^{\lambda_2} \alpha(\lambda) \bullet I(\lambda) \bullet \beta(\lambda) \bullet d\lambda}{\chi \bullet \int_{\lambda_0}^{\lambda_n} I(\lambda) \bullet \beta(\lambda) \bullet d\lambda},$$

Clearly, since the view factor k is a constant for a particular spark, it may be canceled from the numerator and denominator, then the relative intensity (expressed by $\frac{V_{spec}}{V_{shot}}$) will only be affected by the actuarial spark light emission, $I(\lambda)$, and not affected by the variations of the spark position.

Therefore, the relative intensity used in the analysis of the present work does represent the characteristics of the light emission from the CN (at 385 ± 2.5 nm) no matter where the spark was viewed. It can be referred to Fig. 6-2 which shows the similar results tested by different optical probes at different location.

Appendix J Mixing Procedure with the Outputs of the Pressure Sensors

For the combustible mixtures tests with and without residual gas, the mixing procedure was achieved by using three high accuracy pressure transducers (discussed in Chapter 3). The partial pressure and the outputs of those pressure transducers during the mixing procedures without residual gas and with residual gas are shown in Table J-1 and Table J-2 respectively.

Table J-1: Mixing Procedure with Pressure Sensor Outputs (without residual gas)

Fuel-air equivalence ratio (ϕ)	Fuel (Methane CH_4)		Air	
	partial pressure (psia)	output (Volts) (#1 sensor)	partial pressure (psia)	output (Volts) (#3 sensor)
1.10	15.500	5.1663	150	3.407
1.05	14.840	4.9547	150	3.407
1.00	14.220	4.7411	150	3.407
0.98	13.942	4.6551	150	3.407
0.95	13.553	4.5255	150	3.407
0.90	12.901	4.3079	150	3.407
0.85	12.243	4.0881	150	3.407
0.80	11.579	3.8662	150	3.407
0.75	10.927	3.6422	150	3.407
0.70	10.248	3.4160	150	3.407

Table J-2: Mixing Procedure with Pressure Sensor Outputs (with residual gas)

Fuel-air equivalence ratio (ϕ)	10% Residual gases (xCO_2+ yH_2O+ zN_2)		Fuel (Methane CH_4)	
	partial pressure (psia)	output (V) (#1 sensor)	partial pressure (psia)	output (V) (#2 sensor)
1.10	15	5.0	28.949	1.842
1.05	15	5.0	28.378	1.783
1.00	15	5.0	27.801	1.723
0.95	15	5.0	27.219	1.662
0.90	15	5.0	26.631	1.601
0.85	15	5.0	26.038	1.539
0.80	15	5.0	25.439	1.477
0.75	15	5.0	24.834	1.414
0.70	15	5.0	24.223	1.351

Appendix K Repeatability of the Measurements of the Breakdown Voltage and the Spark Light Emission in Combustible Mixtures

For the combustible mixtures tests, although changing the fuel-air equivalence ratio as well as the residual gas fraction will change the mixture compositions, this change is not very significant within the engine operating range. Thus, it is very important to check the influence on the testing results of the experimental errors. In order to verify that the variations of the results of the experiments are only caused by the change of the mixture compositions, the repeatability tests were done at a constant composition (stoichiometry) and under the same operating conditions as those of the other experiments.

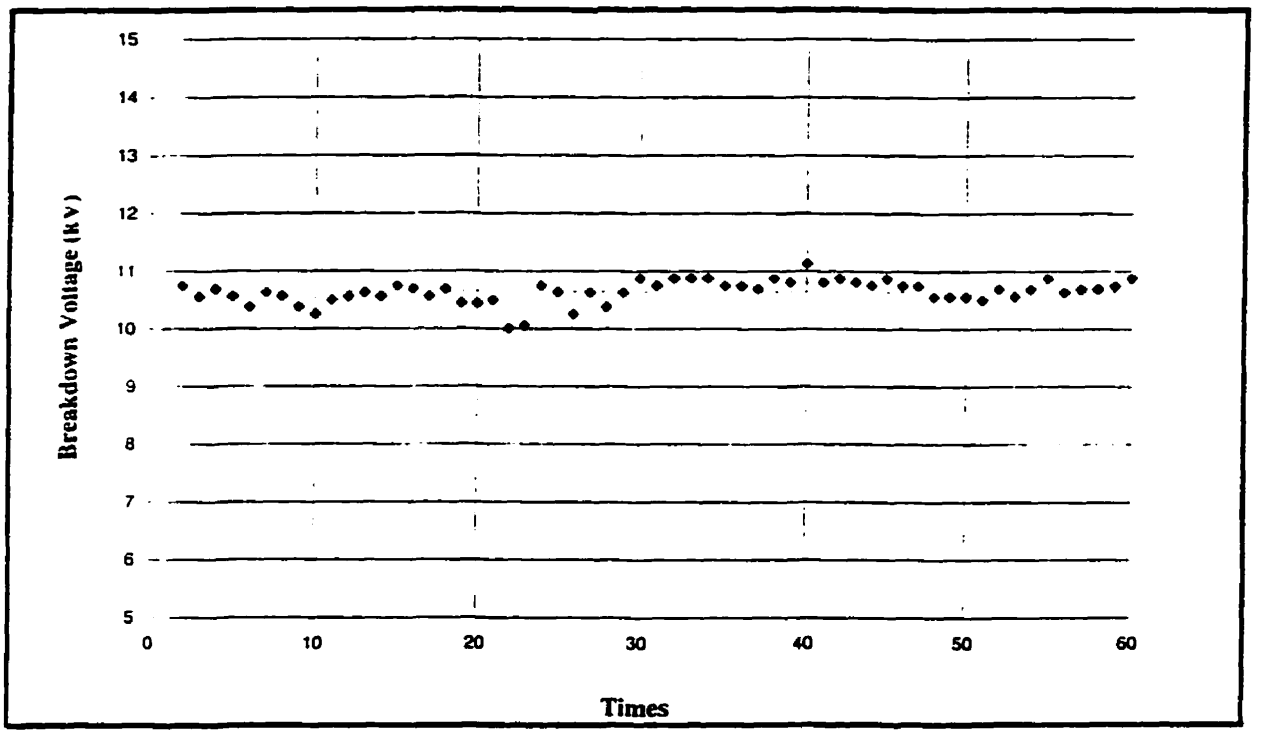

Fig. K-1 Repeatability of the Breakdown Voltage Measurements (ϕ = 1, T = 275 °F, P = 150 psia)

Figure K-1 shows the results of sixty times measurements of the breakdown voltage, while Fig. K-2 presents the result of the sixty times measurements of the relative intensity of the spark light emission. From those results, it can be conclude that the experiments are quite repeatable and the variations caused by the experimental error is insignificant. Thus the experiments are acceptable.

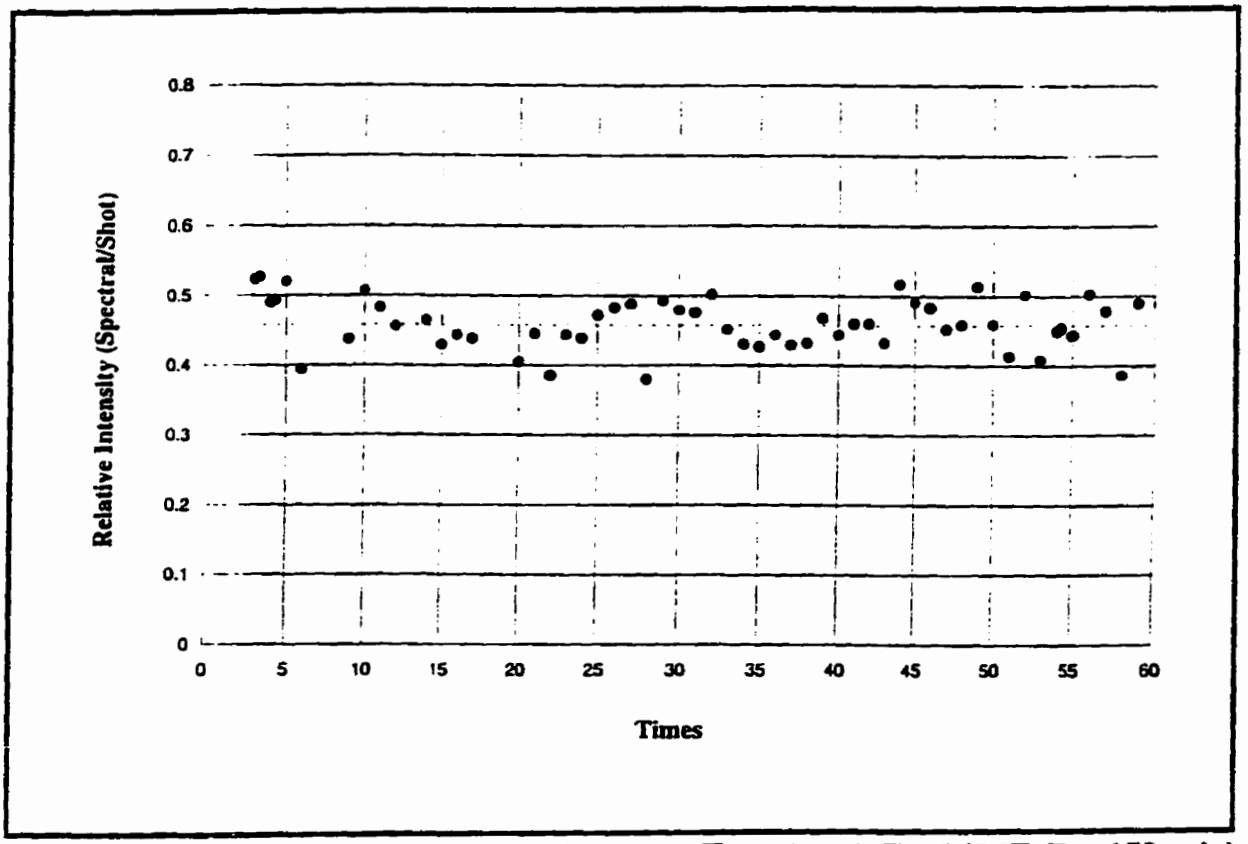

Fig. K-2 Repeatability of the Relative Intensity Tests (ϕ = 1, T = 275 °F, P = 150 psia)

IMAGE EVALUATION TEST TARGET (QA-3)

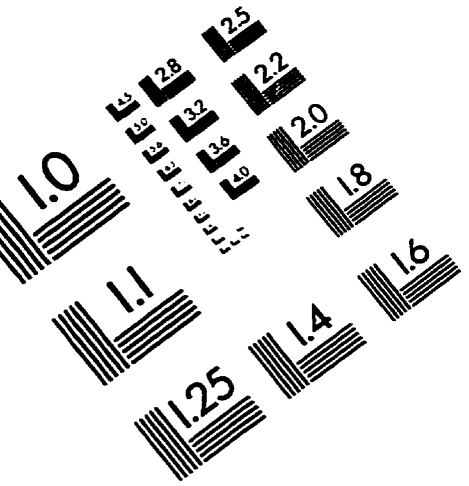

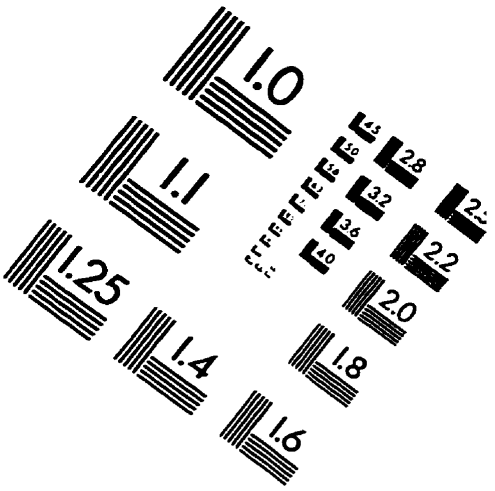

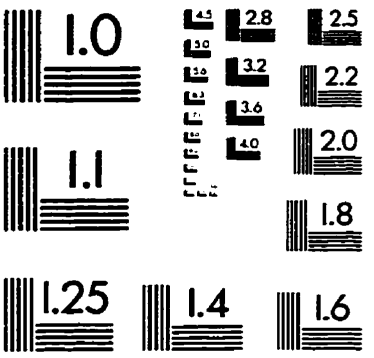

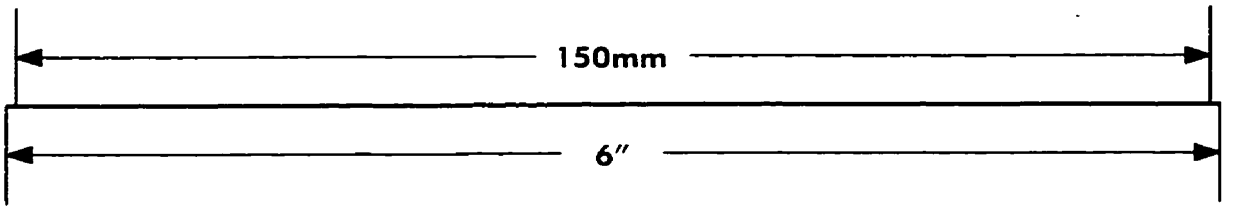

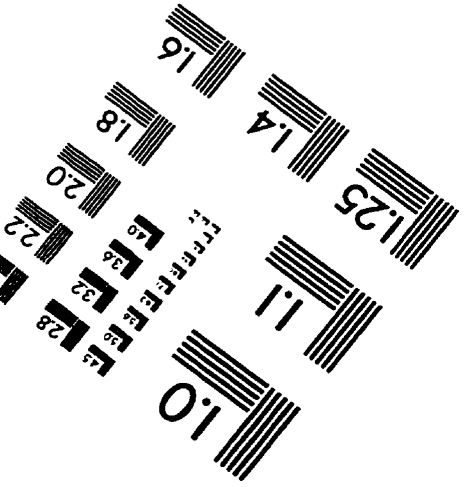

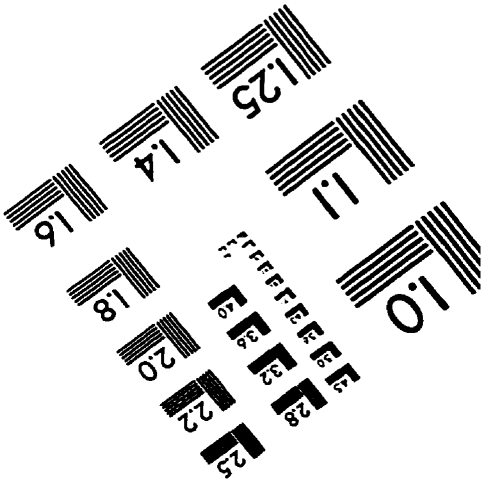

APPLIED IMAGE, Inc
1653 East Main Street
Rochester, NY 14609 USA
Phone: 716/482-0300
Fax: 716/288-5989